

**ROLE OF ARID1A ON EPITHELIAL-MESENCHYMAL TRANSITION  
IN RENAL CELL CARCINOMA**



**A Thesis Submitted to the Graduate School of Naresuan University  
in Partial Fulfillment of the Requirements  
for the Doctor of Philosophy Degree in Anatomy**

**February 2021**

**Copyright 2021 by Naresuan University**

Thesis entitled “Role of ARID1A on epithelial-mesenchymal transition in renal cell carcinoma”

By Keerakarn Somsuan

has been approved by the Graduate School as partial fulfillment of the requirements for the Doctor of Philosophy Degree in Anatomy of Naresuan University

**Oral Defense Committee**

*Wisuit Pradidarcheep* ..... Chair  
(Associate Professor Wisuit Pradidarcheep, Ph.D.)

*Natthiya Sakulsak* ..... Advisor  
(Assistant Professor Natthiya Sakulsak, Ph.D.)

*Visith Thongboonkerd* ..... Co – Advisor  
(Professor Visith Thongboonkerd, M.D., F.R.C.P.T.)

*Sutatip Pongcharoen* ..... Internal Examiner  
(Associate Professor Sutatip Pongcharoen, M.D., Ph.D.)

*Sukanya H.* ..... Internal Examiner  
(Assistant Professor Sukanya Horpaopan, Ph.D.)

**Approved**

*Paisarn Muneesawang* .....  
(Professor Paisarn Muneesawang, Ph.D.)

Dean of the Graduate School

- 8 FEB 2021

## ACKNOWLEDGEMENT

According to the collaboration between the Faculty of Medical Science, Naresuan University and the Medical Proteomics Unit, Mahidol University, the author gratefully thanks Assistant Professor Dr.Natthiya Sakulsak, advisor and Professor Dr.Visith Thongboongerd, MD., co-advisor for constant inspiration, supervision, and arranging a research grant throughout the study. The author received a valuable opportunity to learn and to improve knowledge, research skills, and scientific thinking from both of them. For a good experience during three months of training at the Medical Proteomics Unit, Office for Research and Development, Faculty of Medicine Siriraj Hospital, Mahidol University, the author would especially like to thank Dr.Paleerath Peerapen, PhD., postdoctoral staff for her kind helps on this study as well as MPU staff. The author expresses thankfulness to Dr.Ratirath Samon, MD., pathologist at the Unit of Pathology, Sawanpracharak Hospital, Nakornsawan for kindly assisting and giving supervision on the part of the histopathological study. The author gratefully acknowledges all staff at the Unit of Pathology for providing tissue samples and patient data. The author is sincerely grateful to Prof. Dr.Oshima Masanobu, at the Division of Genetics, Cancer Research Institute, Kanazawa University (DG staff and friends) and the foundation of Mae Fah Luang University for six months of research training in Japan. The author expresses her gratitude to anatomy staff, NS research group and friends at the Faculty of Medical Science, Naresuan University, especially Assistant Professor Rachanee Chanasong and Miss Yupa Srithongchai, for their kind helps.

Unforgettably, Mrs.Amphar Somsuan, Mr.Phusak Somsuan, and Pimkhan Sangprajak, they are the most influential person. The author gratefully thanks for their encouragement and fully stands on any moments throughout the PhD course.

Keerakarn Somsuan

**Title** ROLE OF ARID1A ON EPITHELIAL-MESENCHYMAL  
TRANSITION IN RENAL CELL CARCINOMA

**Author** Keerakarn Somsuan

**Advisor** Assistant Professor Natthiya Sakulsak, Ph.D.

**Co - Advisor** Professor Visith Thongboonkerd, MD., F.R.C.P.T.

**Academic Paper** Thesis Ph.D. in Anatomy, Naresuan University, 2020

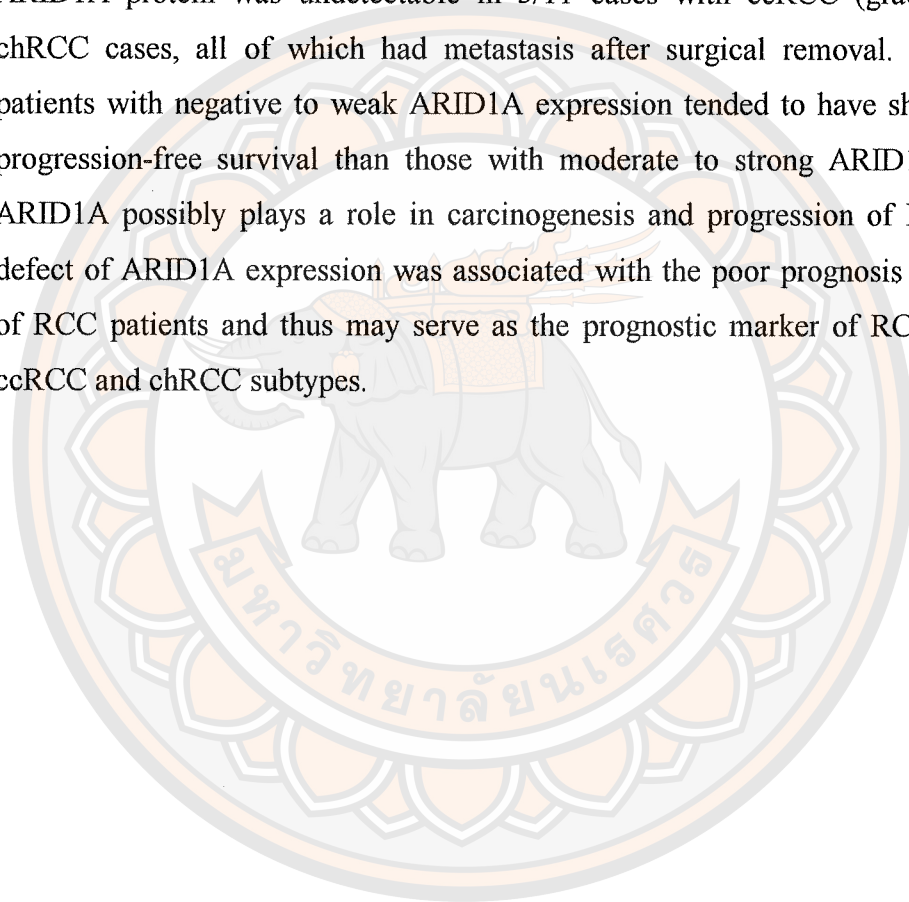
**Keywords** ARID1A, Clinical pathology, EMT, Prognosis, Renal cell  
carcinoma

### ABSTRACT

*AT-rich interactive domain-containing protein 1A (ARID1A)* is a novel tumor suppressor gene, which is involved in development and progression of several cancers. A previous study in human gastric cell lines showed that decreased expression of *ARID1A* gene increased proliferation and migration of cancer cells by triggering the epithelial-mesenchymal transition (EMT) process. Loss of ARID1A expression in human clear cell renal cell carcinoma (ccRCC) tissues was associated with poor prognosis. However, roles of ARID1A in the regulation of RCC and its prognosis significance are still poorly understood. In this study, the possible roles of ARID1A on carcinogenesis and EMT in nonmalignant Madin-Darby canine kidney (MDCK) renal cells using small interfering RNA (siRNA) against ARID1A (siARID1A).were investigated. The results showed that the siARID1A group had a significant decreased cell death, increased cell proliferation, increased migratory activity, increased nuclear size and spheroid size when compared with the siControl group ( $p < 0.05$ ). Moreover, the siARID1A group exhibited mesenchymal features including greater spindle index, increased mesenchymal markers (fibronectin/vimentin), increased Snail-1 transcription factor, and decreased epithelial markers (E-cadherin/zonula occludens-1). Decreased ARID1A expression can trigger the EMT and carcinogenesis of non-malignant renal cells. The association of *ARID1A* mutation and ARID1A protein expression with pathological outcomes and prognosis of the patients were also investigated. The Genomic Data Commons (GDC) database showed that *ARID1A* was



one of the top-ten mutated genes found in kidney cancers and its mutations were found along crucial sequences. Patients with *ARID1A* mutations had significantly lower survival (38%; n=68) as compared to the non-mutated patients (58%; n=192). By immunohistochemistry, the result revealed markedly decreased ARID1A protein expression in the RCC tissues (n=26) as compared to the adjacent non-cancer tissues (n=26), particularly in clear cell RCC (ccRCC) and chromophobe RCC (chRCC). ARID1A protein was undetectable in 3/11 cases with ccRCC (grade II) and 2/6 chRCC cases, all of which had metastasis after surgical removal. Finally, RCC patients with negative to weak ARID1A expression tended to have shorter five-year progression-free survival than those with moderate to strong ARID1A expression. ARID1A possibly plays a role in carcinogenesis and progression of RCC. Loss or defect of ARID1A expression was associated with the poor prognosis and metastasis of RCC patients and thus may serve as the prognostic marker of RCC, particularly ccRCC and chRCC subtypes.



## LIST OF CONTENT

Chapter	Page
<b>I INTRODUCTION.....</b>	<b>1</b>
Rationale for the study.....	1
Objectives of the study.....	2
Hypothesis.....	3
Significance of the study.....	3
Scope of the study.....	3
Conceptual framework.....	5
<b>II LITERATURE REVIEW.....</b>	<b>8</b>
Renal cell carcinoma (RCC).....	8
Incidence of renal cell carcinoma.....	8
Signs and symptoms of renal cell carcinoma.....	9
Risk factors of renal cell carcinoma.....	9
Histological subtypes of renal cell carcinoma.....	14
Pathological parameters for renal cell carcinoma.....	23
TMN classification and staging of RCC.....	25
Diagnosis.....	27
The immunohistochemical landscape of RCC.....	29
Application of IHC in the diagnosis of RCC.....	31
Treatment of renal cell carcinoma.....	33
Prognosis factors for RCC patients.....	37
Epithelial-mesenchymal transition (EMT).....	38
The different subtypes of EMT.....	38
EMT in renal cell carcinoma.....	44

## LIST OF CONTENT (CONT.)

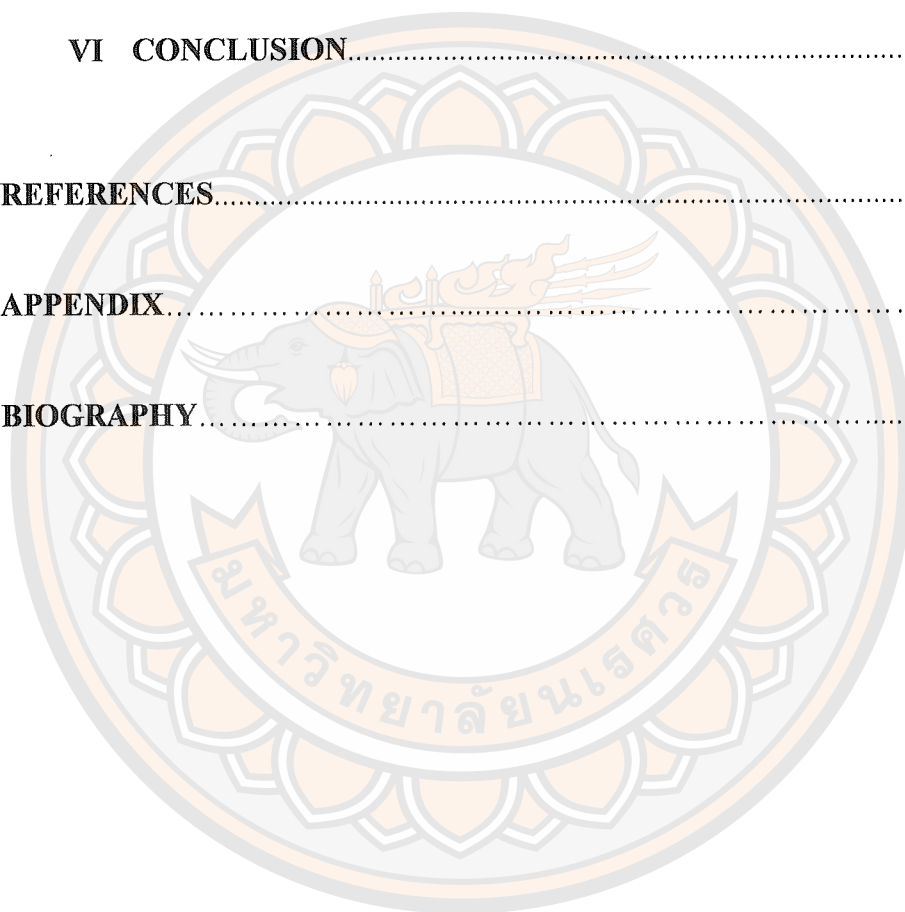
Chapter	Page
AT-rich interactive domain-containing protein 1A (ARID1A).....	46
SWI/SNF complexes.....	46
Structure of ARID1A domain.....	47
The evidence of ARID1A in cancers.....	51
The evidence of ARID1A in RCC.....	53
<b>III RESEARCH METHODOLOGY.....</b>	<b>54</b>
Cell culture.....	54
siRNA transfection.....	54
Assessment of cell viability by trypan blue staining.....	55
Immunofluorescence (IF) staining and antibodies.....	55
Assessment of cell morphology and nuclear size.....	57
Scratch wound assay.....	57
Measurement of aggregated cells by hanging drop assay.....	58
Bioinformatics analysis.....	58
Human ethic approval.....	59
Inclusion and exclusion criteria.....	59
Exclusion criteria.....	60
Storage and data collection.....	60
Patient tissue samples and the clinicopathological information.....	62
Histological study.....	62
Immunohistochemistry.....	63
Quantitative analysis of ARID1A protein expression.....	64
Association of ARID1A protein expression with clinicopathology and progression-free survival.....	66
Statistical analysis.....	66

## LIST OF CONTENT (CONT.)

Chapter	Page
<b>IV RESULTS .....</b>	<b>67</b>
Determination of optimal does of siARID1A.....	67
Efficacy of ARID1A knockdown by siRNA transfection.....	70
Effects of ARID1A knockdown on total cell number, cell death and cell viability.....	72
Effects of ARID1A knockdown on cell morphology and nuclear size.....	74
Effects of ARID1A knockdown on expression of EMT-related proteins.....	77
Effect of ARID1A knockdown on the expression of SNAI1 transcription factor protein.....	82
Effects of ARID1A knockdown on cell migrating activity and cell aggregation.....	82
<i>ARID1A</i> was one of the top-ten mutated genes most frequently found in kidney cancers and its mutations were found along its sequence.....	89
Histopathology and ARID1A protein expression in cancer vs. adjacent non-cancer areas.....	94
ARID1A protein expression in adjacent non-cancer area in ccRCC (grade I) vs. ccRCC (grade II).....	99
Association of ARID1A protein expression with clinicopathology and progression-free survival.....	99

## LIST OF CONTENT (CONT.)

Chapter	Page
V DISCUSSION.....	105
VI CONCLUSION.....	111
REFERENCES.....	112
APPENDIX.....	130
BIOGRAPHY.....	144



## LIST OF TABLES

Table	Page
1 Summary of risk factors and hypothesized mechanisms for RCC.....	10
2 Summary of hereditary syndromes associated with renal neoplasia.....	13
3 Summary of characteristics of ccRCC.....	16
4 Summary of characteristics of pRCC.....	20
5 Summary of characteristics of chRCC.....	23
6 Furhman nuclear grading for assessing renal cell carcinoma.....	24
7 TMN classification of renal cell carcinoma.....	26
8 Stages of renal cell carcinoma.....	27
9 Summary of IHC results of RCC.....	29
10 Targeted drug treatment for metastatic RCC.....	36
11 The details of primary and secondary antibodies used in the <i>in vitro</i> study.....	56
12 Total cell number, cell death and cell viability of MDCK cells after transfection with various doses of siARID1A.....	70
13 The number and percentage of MDCK nuclei in different nuclear sizes.....	77
14 The wound width ( $\mu\text{M}$ ) at each timepoint in all three groups.....	85
15 The percentage of cell migrating activity at each timepoint in all three groups.....	86
16 Frequent somatic mutations of ARID1A in kidney cancers.....	91
17 The details of Allred score and four grading of ARID1A expression in normal and cancer areas of all patients.....	98
18 Clinical data of RCC patients.....	101
19 Association of ARID1A expression with clinicopathology of RCC patients.....	102
20 The clinicopathology and outcome of patients with negative ARID1A expression.....	103



## LIST OF FIGURES

Figures	Page
1 Conceptual framework of this study.....	5
2 Conceptual framework of <i>in vitro</i> study.....	6
3 Conceptual framework of human tissue study study).....	7
4 Gross and histological structures of ccRCC.....	15
5 Molecular events and targeted therapy blocking components of VHL pathway of ccRCC.....	17
6 Gross and histological structures of pRCC.....	19
7 Gross and histological structures of chRCC.....	22
8 Sarcomatoid differentiations in RCC.....	25
9 CT scan of ccRCC.....	28
10 Application of immunohistochemical stains in the diagnosis of an oncocytic renal neoplasm.....	31
11 Partial and radical nephrectomy for management of localized renal cell carcinoma.....	34
12 Recommended surgical treatment strategy for renal cell carcinoma.....	35
13 Three subtypes of EMT.....	39
14 Type 2 of EMT associated with fibrosis.....	40
15 Type 3 of EMT associated with cancer metastasis.....	41
16 Two set of distinct protein markers in EMT.....	42
17 List of protein markers for the different types of EMT.....	43
18 Signaling pathway of EMT in RCC.....	45
19 Protein components of BAF complexes.....	46
20 Genome sequences of human ARID family.....	48
21 Location for ARID1A gene on chromosome (red line).....	49
22 Protein and mRNA expressions of ARID1A in human organs..	49
23 Six main classes of co-worker proteins with ARID1A.....	50

## LIST OF FIGURES (CONT.)

Figures		Page
24	Flowchart of the patient tissue's recruitment and collection.....	61
25	The details of Allred score.....	65
26	Morphology and total cell number of MDCK cells after transfection with various doses of siARID1A.....	68
27	Percentage of cell death and cell viability of MDCK cells after transfection with various doses of siARID1A.....	69
28	Immunofluorescent staining of nuclear ARID1A protein.....	71
29	The quantitative data of fluorescence intensity of the ARID1A expression.....	72
30	The quantitative data of total cell number, cell death, and cell viability of MDCK cells after transfection with 40 pmol of siARID1A.....	73
31	Effect of ARID1A knockdown on cell morphology.....	75
32	Effect of ARID1A knockdown on nuclear size.....	76
33	Effect of ARID1A knockdown on expression of E-cadherin protein.....	78
34	Effect of ARID1A knockdown on expression of ZO-1 protein.	79
35	Effect of ARID1A knockdown on expression of vimentin protein.....	80
36	Effect of ARID1A knockdown on expression of fibronectin protein.....	81
37	Effect of ARID1A knockdown on expression of SNAIL protein.....	83
38	Effect of ARID1A knockdown on enhancing of migrating activity by using scratch wound assay.....	84
39	The quantitative data of wound width as compared among three groups.....	85

## LIST OF FIGURES (CONT.)

Figures		Page
40	The quantitative data of cell migrating activity (%) as compared among three groups.....	86
41	Effect of ARID1A knockdown on cell aggregation.....	87
42	The quantitative data of ARID1A knockdown on cell aggregation as compared among three groups.....	88
43	List of top twenty mutated genes and ARID1A mutation profiles in kidney cancers (data from GDC database).....	90
44	Overall survival (OS) of patients.....	93
45	Histopathology of renal tissues from RCC patients.....	95
46	Expression of ARID1A protein in RCC tissues.....	96
47	Quantitative analysis of expression of ARID1A protein.....	97
48	Expression of ARID1A protein in adjacent non-cancer area in ccRCC grade I (GI) versus ccRCC grade II (GII).....	100
49	The 5-year progression-free survival of patients.....	104

## ABBREVIATIONS

AJCC	=	American joint committee on cancer
Akt	=	Protein kinase B
AMACR	=	Alpha ( $\alpha$ )-methylacyl-coenzyme A racemase
APC	=	APC regulator of WNT signaling pathway
ARID1A	=	AT-rich interactive domain-containing protein 1A
BAF	=	BRG1-associated factor
BAP1	=	BRCA1-associated protein 1
BHD	=	Birt-Hogg-Dube
BRAF250a	=	BRG1-associated factor 250a
BRD7	=	Bromodomain containing 7
CAIX	=	Carbonic anhydrase IX
ccRCC	=	Clear cell renal cell carcinoma
CD10	=	Cluster of differentiation 10
CD117	=	Cluster of differentiation 117
CD57	=	Cluster of differentiation 57
CDH-1	=	Cadherin-1
CDKN2A	=	Cyclin dependent kinase inhibitor 2A
CDX2	=	Caudal-type homeobox transcription factor 2
chRCC	=	Chromophobe renal cell carcinoma
CK7	=	Cytokeratin 7
CMEM	=	Complete growth medium
CNT	=	Connective tissue
CT	=	Collecting duct
CTC	=	Circulating tumor cells
CTs	=	Collecting tubules

## ABBREVIATIONS (CONT.)

CUP	=	Cancer of unknown primary
DCT	=	Distal convoluted tubule
EMT	=	Epithelial-mesenchymal transition
ER	=	Estrogen receptor
ERK	=	Extracellular signal-regulated kinases
Fas	=	Fas cell surface death receptor
FBS	=	Fetal bovine serum
FFPE	=	Formalin-fixed paraffin-embedded tissue
FH	=	Fumarate hydratase
FLCN	=	Folliculin
FOXO3A	=	Forkhead box O3
FSP1	=	Fibroblast-specific protein 1
GC	=	Gastric cancer
GDCs	=	The genomic data commons
Glom	=	Glomerulus
GLUT-1	=	Glucose transporters-1
GR	=	Glucocorticoid receptor
H&E	=	Hematoxylin and Eosin
HIER	=	Heat-induced epitope retrieval
HIF- $\alpha$	=	Hypoxia-inducible factor- $\alpha$
HMB-45	=	Human melanoma black 45
HPF	=	High power field
IHC	=	Immunohistochemistry
INF- $\alpha$	=	Interferon-alpha
INI1	=	Integrase interactor 1
IS	=	Intensity score
KDM5C	=	Lysine demethylase 5C
KDM6A	=	Lysine demethylase 6A

## ABBREVIATIONS (CONT.)

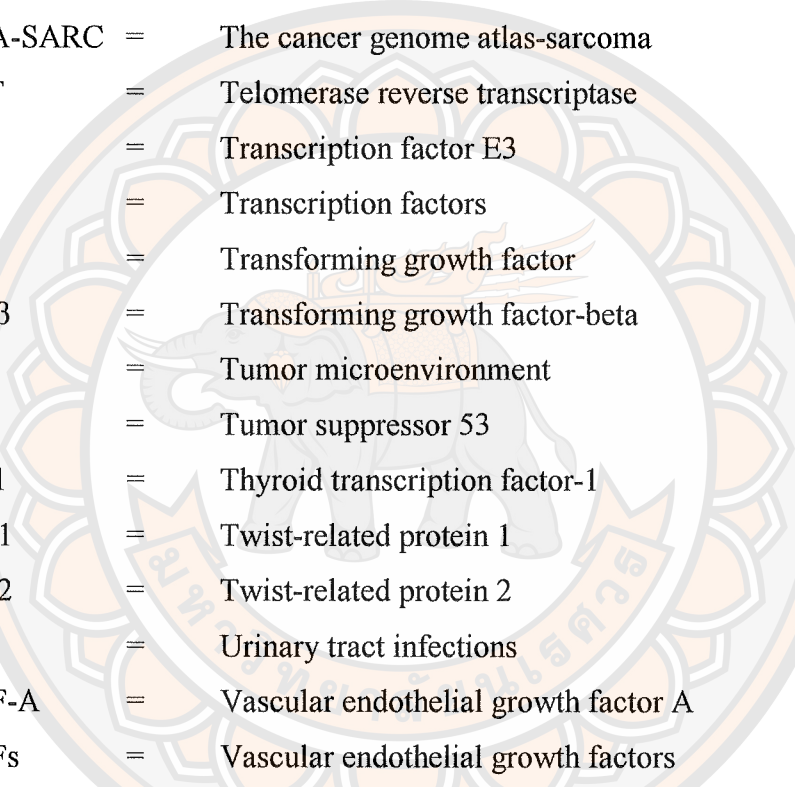
Ki-67	=	Marker Of proliferation Ki-67
LEF	=	Lymphoid enhancer binding factor
MAPK	=	Mitogen activated kinase-like protein
MDCK	=	Madin-Darby Canine Kidney
MEM	=	Minimum essential medium
MET	=	Mesenchymal-epithelial transition
MET	=	MET proto-oncogene
MMP2	=	Matrix metalloproteinase 2
MMP9	=	Matrix metalloproteinase 9
mRCC	=	Metastatic renal cell carcinoma
mTOR	=	Mammalian target of rapamycin
MUC1	=	Mucin 1, cell surface associated
NF1	=	Neurofibromin 1
NLS	=	Nuclear localization sequence
OVCA	=	Ovarian clear cell adenocarcinomas
Oct4	=	Octamer-binding transcription factor 4
OD	=	Optical density
p63	=	Tumor protein p63
PAX2	=	Paired box gene 2
PAX8	=	Paired box gene 8
PBAF	=	Polybromo-associated BAF
PBRM	=	Polybromo
PBS	=	Phosphate buffered saline
PBS-T	=	Phosphate buffered saline-Tween
PCT	=	Proximal convoluted tubule
PDGF	=	Platelet-derived growth factor
Pfam	=	Protein family
PGCC	=	Polyploid giant cancer cell



## ABBREVIATIONS (CONT.)

PI	=	Propidium iodide
PI3K	=	Phosphoinositide 3-kinase;
PIK3CA	=	Phosphatidylinositol-4, 5-bisphosphate 3-kinase catalytic subunit alpha
pRCC	=	Papillary renal cell carcinoma
PS	=	Proportional score
PSM	=	Positive surgical margins
PTEN	=	Phosphatase and tensin homolog
pTNM	=	Pathological tumor-node-metastasis
RAF	=	Rapidly accelerated fibrosarcoma
RAS	=	Rat sarcoma virus
RCC	=	Renal cell carcinoma
SEM	=	Standard error of the mean
SETD2	=	SET domain-containing protein 2
shRNA	=	Short hairpin RNA
siRNA	=	Small interfering RNA
SMAD2	=	SMAD family member 2
SMAD3	=	SMAD family member 3
SMARCA	=	SWI/SNF related, matrix associated, actin dependent regulator of chromatin, subfamily A, member
SNAIL	=	Zinc finger protein SNAIL or Snail
SNPs	=	Single nucleotide polymorphisms
sRCC	=	Sarcomatoid renal cell carcinoma
SRX	=	Sex determining region Y
SSEA-1	=	Stage-specific embryonic antigen-1
SWI/SNF	=	SWITCH/Sucrose non-fermentable
TCF	=	T-cell specific transcription factor

## ABBREVIATIONS (CONT.)



TCGA	=	The cancer genome atlas
TCGA-KICH	=	The cancer genome atlas-kidney chromophobe
TCGA-KIRC	=	The cancer genome atlas-kidney renal clear cell carcinoma
TCGA-KIRP	=	The cancer genome atlas-kidney renal papillary cell carcinoma
TCGA-SARC	=	The cancer genome atlas-sarcoma
TERT	=	Telomerase reverse transcriptase
TFE3	=	Transcription factor E3
TFs	=	Transcription factors
TGF	=	Transforming growth factor
TGF- $\beta$	=	Transforming growth factor-beta
TME	=	Tumor microenvironment
TP53	=	Tumor suppressor 53
TTF-1	=	Thyroid transcription factor-1
Twist1	=	Twist-related protein 1
Twist2	=	Twist-related protein 2
UTIs	=	Urinary tract infections
VEGF-A	=	Vascular endothelial growth factor A
VEGFs	=	Vascular endothelial growth factors
VHL	=	Von Hippel-Lindau
Wnt	=	Wingless-related integration site
ZEB	=	Zinc finger E-box binding homeobox
ZO-1	=	Zona occludin-1
$\alpha$ -SMA	=	Alpha-smooth muscle actin

# CHAPTER I

## INTRODUCTION

### **Rationale for the study**

Renal cell carcinoma (RCC) is the ninth most common cancer ranked according to age-adjusted invasive cancer incidence rates in the US, with an increasing incidence rate at 16.2 per 100,000 persons in 2014 (Group, 2017). Among RCC patients, 20-30% have an incidence of metastatic disease, which commonly spreads to the lung, liver and brain. Moreover, approximately 20-40% of RCC patients die from the disease every year. Therefore, RCC is considered as a very aggressive and often fatal disease (Bianchi et al., 2012; Protzel, Maruschke, & Hakenberg, 2012).

Epithelial-mesenchymal transition (EMT) is involved in several biological processes including embryogenesis and organ fibrosis, especially renal fibrosis (Kalluri, & Weinberg, 2009; Kanlaya, Khamchun, Kapincharanon, & Thongboonkerd, 2016). In particular, EMT is the prime mover in the invasion-metastasis cascade of cancer cells. Patterns of EMT encompass several biological changes including the acquisition of mesenchymal morphology and loss of cell polarity resulting in detachment from their basement membrane. Transformed cells exhibit down-regulation of epithelial proteins: i.e. E-cadherin, Zonula occludens-1 (ZO-1), claudins and cytokeratins. Conversely, up-regulation of mesenchymal proteins: N-cadherin, vimentin,  $\alpha$ -smooth muscle actin and activation of specific transcription factors (TF) such as Snail, Slug, ZEB1/2 and Twist1/2 can be found in those cells (Lee, Dedhar, Kalluri, & Thompson, 2006; Zhu, Gao, Wu, & Qin, 2013). Clinically, the expression of Snail has strong correlations with tumor recurrence, metastasis, and even resistance to immunosuppressants (Chen et al., 2017).

Recently, *AT-rich interactive domain-containing protein 1A (ARID1A)*, a tumor suppressor gene has been reported as a novel gene required for the proliferation and metastasis in several cancers, particularly in RCC. ARID1A is a key component of the SWI/SNF chromatin remodeling complex (Kadoch, & Crabtree, 2015). In clear cell RCC (ccRCC), HotNet model has identified the second most

frequently mutated gene network in ccRCC including *PBRM1*, *ARID1A* and *SMARCA4* (The Cancer Genome Atlas Research, 2013; Vandin, Upfal, & Raphael, 2011). Previous studies have revealed that the expression of BRAF250a, the protein product of *ARID1A*, is significantly reduced exclusively in ccRCC cases by approximately 67% compared with its normal expression in kidney (Lichner et al., 2013). In addition, low expression of BRAF250a shows a strong association with tumor progression leading to a shorter cancer specific survival and progressive free survival (Park et al., 2015). Study in gastric cancer has found interrelation of ARID1A and EMT; ARID1A silencing facilitates the migration and invasion in GC cells by suppression of E-cadherin and  $\beta$ -catenin levels. Decreased ARID1A expression is associated with lymph node metastasis and tumor infiltration of patients (Yan et al., 2014).

All of the above provide the potential involvement of ARID1A in carcinogenesis of RCC and regulation of EMT in cancer metastasis. Nevertheless, role of ARID1A on carcinogenesis by triggering the processes of epithelial-mesenchymal transition (EMT) remains unknown, particularly in RCC. Therefore, the possible role of ARID1A on carcinogenesis and EMT of RCC *in vitro* was investigated. In addition, the association of ARID1A gene mutation and ARID1A protein expression with pathological outcomes and prognosis in RCC patients was evaluated in order to clarify clinical significance of ARID1A expression in humans.

### **Objectives of the study**

#### **1. *In vitro* study**

1.1 To investigate effects of ARID1A silencing on carcinogenic features in MDCK cells

1.2 To investigate effects of ARID1A silencing on alteration of the EMT protein markers in MDCK cells

#### **2. Human tissue study**

2.1 To study mutation of ARID1A in kidney cancers on the Genomic Data Commons (GDC) database

2.2 To determine the expression of ARID1A in the normal tissue compared to the cancer tissue in RCC subtypes

2.3 To explore the association of ARID1A expression with pathological outcome of patients

### **Hypothesis**

#### **1. Hypothesis of *in vitro* study**

1.1 ARID1A silencing may increase carcinogenesis features: cell proliferation, migration and aggregation of RCC.

1.2 ARID1A silencing may trigger EMT by increasing mesenchymal proteins: fibronectin, vimentin, and SNAIL (Zinc finger protein SNAIL or Snail).

#### **2. Hypothesis of human tissue study**

2.1 Mutation of ARID1A in kidney cancers may be associated with short survival of patients.

2.2 Expression of ARID1A may decrease in human RCC tissues as compared with normal kidney tissues.

2.3 Expression of ARID1A may be associated with a worse pathological outcome of patients.

### **Significance of the study**

The scientific data from this study will provide the novel understanding of ARID1A in regulation of RCC by triggering a process of EMT, which is an important process that regulates cancer metastasis. The result will confirm patterns of ARID1A expression in various types of RCC and association of ARID1A with pathological outcomes of patients, which can be applied to the routine laboratory investigation for this disease.

### **Scope of the study**

#### **1. *In vitro* study**

*In vitro* study was performed in the MDCK cell lines which were the physiological cell lines. Cells were transfected with siRNA specific for ARID1A mRNA to silence the expression of ARID1A mRNA. Effects of ARID1A knockdown were investigated in term of carcinogenesis features: cell apoptosis, proliferation, migration and aggregation among the wild-type, siRNA control and siRNA ARID1A



groups. The expression of EMT proteins and SNAIL transcription factor protein was investigated by immunofluorescence assay. The conceptual frameworks of this study and of *in vitro* study were showed in the Figure 1 and 2.

## 2. Human tissue study

This study was approved by the Human Ethic Review Board of Sawan Pracharak hospital, Nakhon Sawan, Thailand in 2017 (No. 47/2560) and by Naresuan University Ethics Committee for Human Research (NU-IRB) (No. 0489/61), COE No. 115/2018. In a retrospective design, the formalin-fixed, paraffin embedded (FFPE) blocks of patients who were diagnosed with RCC were included during 2013-2017. Demographic data were accessed by maintaining privacy and confidentiality provisions to protect information of patients. Immunohistochemistry was performed to detect expression of ARID1A in RCC tissues compared with normal control. Moreover, the association of ARID1A expression, demographic and pathological outcomes was analyzed. The conceptual framework of human tissue study was showed in the Figure 3.



## Conceptual framework

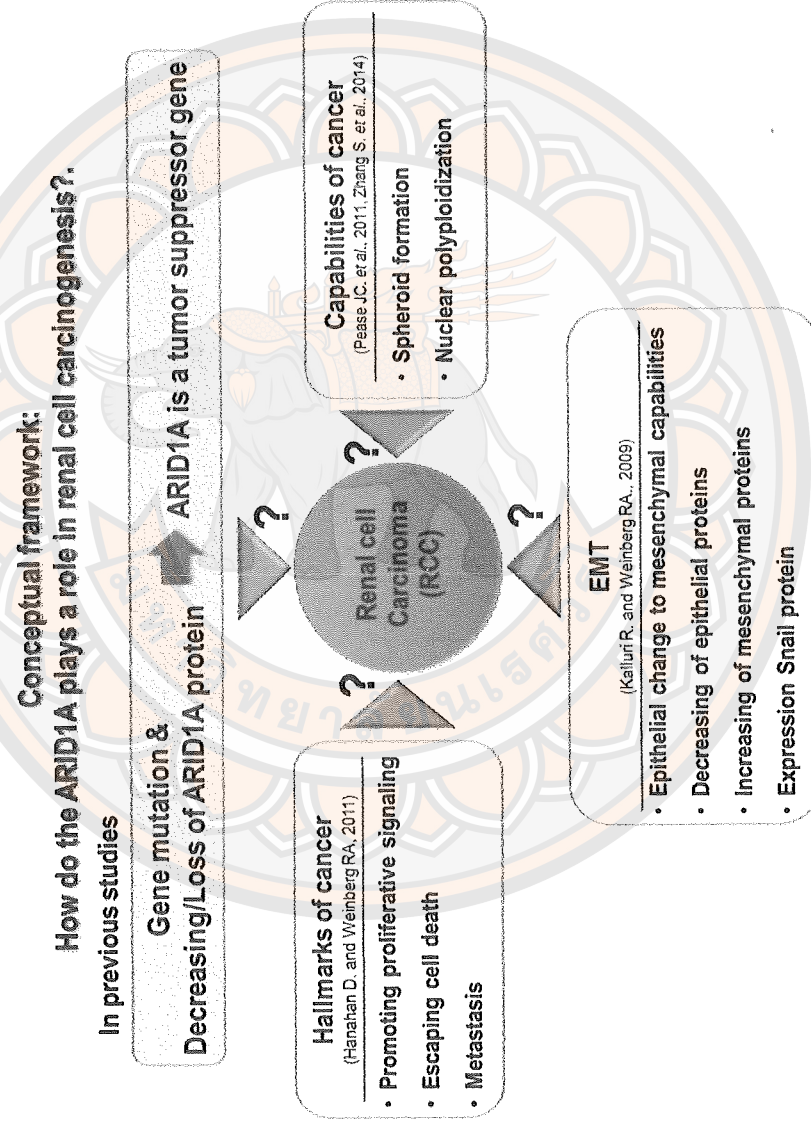


Figure 1 Conceptual framework of this study

## Conceptual framework: *In vitro* study

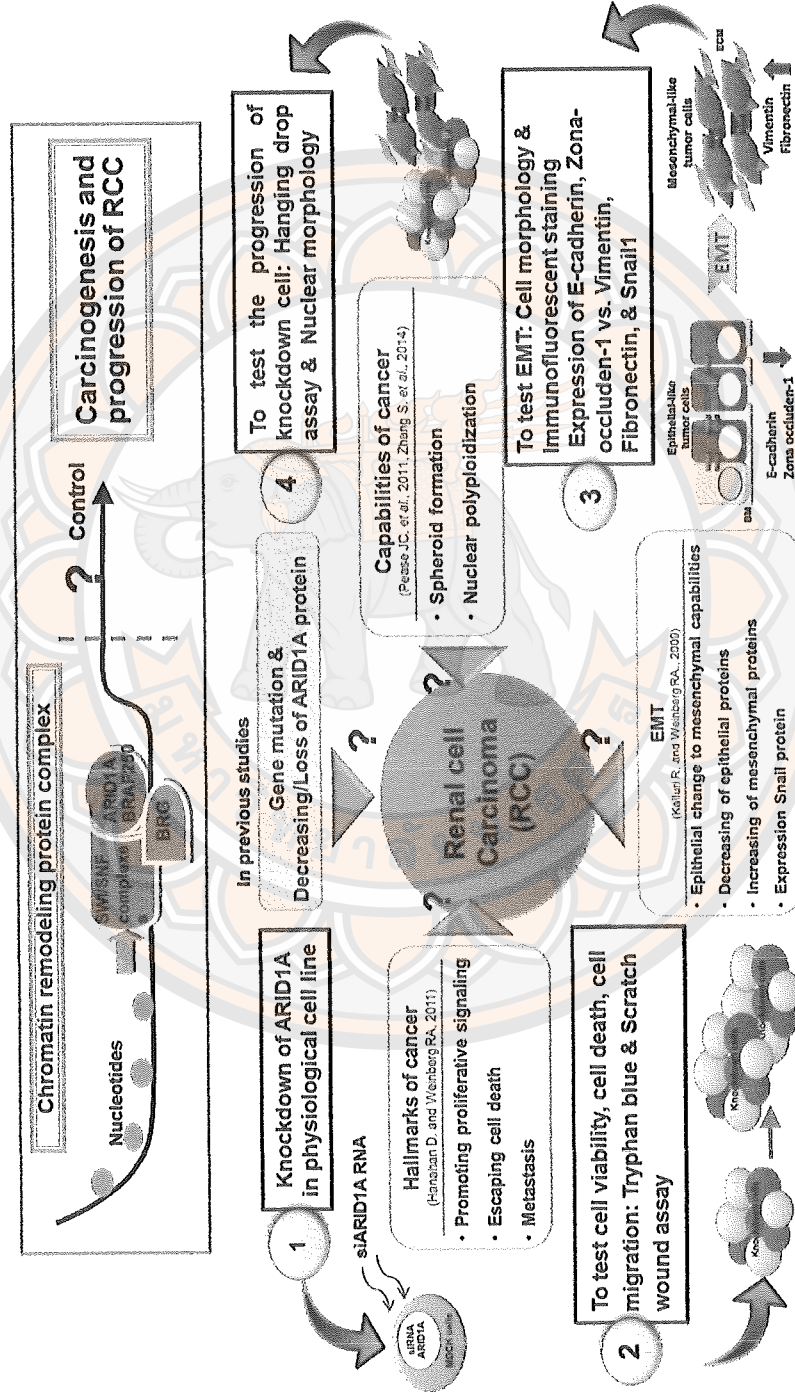
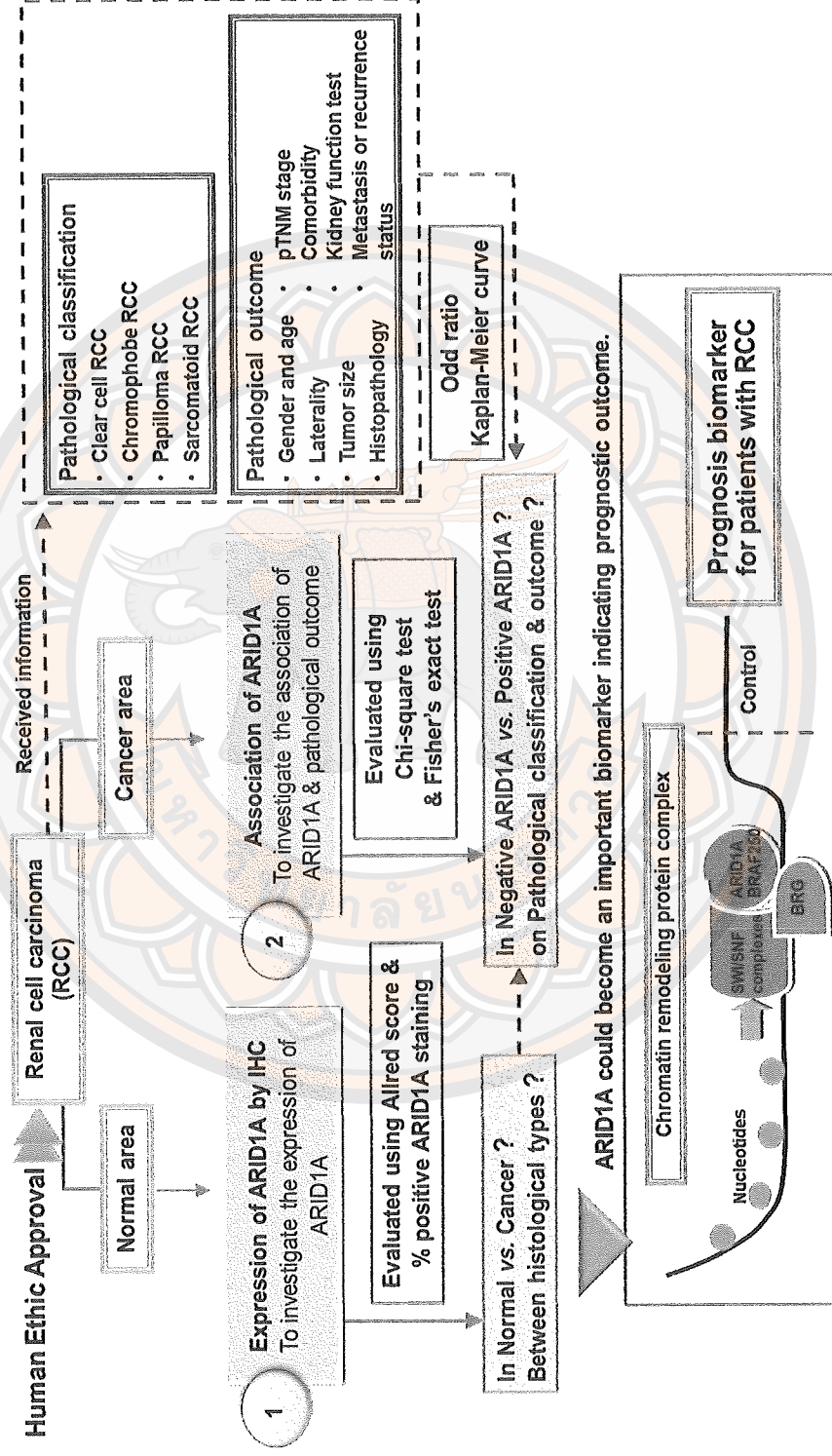


Figure 2 Conceptual framework of *in vitro* study

# **Conceptual framework: Human tissue study**



**Figure 3 Conceptual framework of human tissue study study)**

## CHAPTER II

### LITERATURE REVIEW

#### **Renal cell carcinoma (RCC)**

##### **1. Incidence of renal cell carcinoma**

Estimates of the worldwide incidence and mortality for all cancers in 2012 are now available in the GLOBOCAN series of the International Agency for Research on Cancer. Kidney cancer was the twelfth most common malignancy, with 338,000 new cases diagnosed and 144,000 deaths in the world (Ferlay et al., 2015). Incidence of kidney cancer was higher for men (214,000 cases) than for women (124,000 cases). Mortality of kidney cancer was also common for men (91,000 cases) than for women (53,000 cases) (Ferlay et al., 2015). Percentage of death for men was 91% and for women was 53%. The highest rates of incidence for kidney cancer are found in Northern America, Australia/New Zealand and Europe, while the lowest rates are found in Africa and Pacific Islands. Incidence of kidney cancer in South-Eastern Asia accounted 3.8 per 100,000 for men and 1.7 per 100,000 for women. Mortality of kidney cancer in South-Eastern Asia accounted 3.4 per 100,000 for men and 1.9 per 100,000 for women (Ferlay et al., 2015). Incidence rate of kidney cancer in Thailand are increasing. The highest rise of incidence and mortality trends in 2020 and 2030 included Brazil (911%), Ecuador (437%), Thailand (230%), Bulgaria (186%), and Malta (131%) (Wong et al., 2017). Trends of incidence and mortality of kidney cancer in Thailand were increasing because of rapid changes in lifestyle, behavior, and dietary. Food consumption pattern shifted from Asian-diet to a more westernized-diet characterized by increased proportion of fat and meat (Lojanapiwat, 2015).



## **2. Signs and symptoms of renal cell carcinoma**

Renal cell carcinoma (RCC) is the most common kidney cancers that accounts for 80-85% of kidney cancers (Petejova, & Martinek, 2016). Common signs and symptoms of RCC included gross hematuria (66%), flank pain (48%), a lump or mass at the kidney area (20%). Ten percent of patients presented systemic symptoms such as fever, weight loss, and loss of appetite (Ata-ur-Rehman et al., 2015). Other symptoms of RCC may include urinary tract infection, abdominal pain, back pain, nausea, fatigue, constipation, increased inflammatory markers, increased leukocytes, low hemoglobin, increased blood sugar, thrombocytosis, abnormal liver function, and increased creatinine (Shephard, Neal, Rose, Walter, & Hamilton, 2013).

## **3. Risk factors of renal cell carcinoma**

Smoking, obesity, physical inactivity and hypertension are well-established risk factors for RCC. Possible contributing factors included certain occupational and environmental exposures to industrial agents, such as trichloroethylene, cadmium, arsenic, radon and nitrate. A summary of risk factors and hypothesized mechanisms for RCC is showed in Table 1 (W.-H. Chow, Dong, & Devesa, 2010). Moreover, genetic susceptibility or hereditary factors may be effector on incidence rates. Multifocal and bilateral renal tumors are commonly found in RCC associated with hereditary syndromes (Von Hippel–Lindau disease), and extra-renal symptoms of disease, such as uterine tumors, pancreatic cysts, tumors and adrenal pheochromocytomas. A summary of hereditary syndromes associated with renal neoplasia is shown in Table 1

Table 1 Summary of risk factors and hypothesized mechanisms for RCC

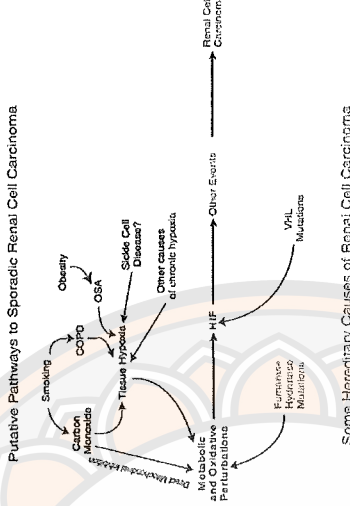
Risk factors		Hypothesized mechanisms
1. Cigarette smoking - N-nitrosamine - Benzo (α) pyrene diol epoxide	↑ level of DNA damage in peripheral blood lymphocytes.	 <p>Putative Pathways to Sporadic Renal Cell Carcinoma</p> <p>Some Hereditary Causes of Renal Cell Carcinoma</p>
	↑ chronic tissue hypoxia due to carbon monoxide exposure	
	↑ genetic alterations, deletions in chromosome 3p	
	↑ chronic obstructive pulmonary disease	
	(Clague et al., 2009; Sharifi & Farrar, 2006; Zhu et al., 2008)	
2. Obesity	- obesity with a BMI > 30 kg/m <sup>2</sup> : ↑ cardiovascular and renal diseases.	<p>↑ mitosis, migration, angiogenesis</p> <p>↑ cell apoptosis, proliferation and invasion</p> <p>(Hoeben et al., 2004; Li &amp; Kalantar-Zadeh, 2013; Renehan, Tyson, Egger, Heller, &amp; Zwahlen, 2008; Zhang, Zhu, &amp; Ye, 2014)</p>
	- insulin resistance (IR): ↑ tumor development and progression.	
	- PI3K & MAP kinase, insulin-like growth factor (IGF-1):	
	- ROS & inflammatory mediators (NF-κB):	



Table 1 (cont.)

Risk factors	Hypothesized mechanisms
3. Hypertension	<ul style="list-style-type: none"> <li>- obese associated long-term hypertension: ↑ levels of blood pressure</li> <li>- diuretics and other anti-hypertensive medications: ↑ chronic renal hypoxia and lipid peroxidation with formation of ROS &amp; risk of RCC</li> </ul> <p>(W. H. Chow, Gridley, Fraumeni, &amp; Jarvholm, 2000; Gago-Dominguez, Castela, Yuan, Ross, &amp; Yu, 2002; Weikert et al., 2008)</p>
4. Other pre-existing conditions	<ul style="list-style-type: none"> <li>- kidney transplant patients: ↑ RCC diagnosed in the native kidney &gt; the transplanted kidney</li> <li>- patients with acquired renal cystic disease: ↑ RCC risk</li> </ul> <p>(Bassal et al., 2006; Bonsib, 2009; Klatte et al., 2010; Wiklund et al., 2009)</p>
5. Reproductive and hormonal factors	<ul style="list-style-type: none"> <li>- women who gave multiple births at a relatively young: ↑ risk RCC 40% to 90%</li> <li>- use of oral contraceptives &amp; hormone replacement therapy</li> <li>- pregnancy-induced hypertension, and renal stress</li> </ul> <p>(Kabat, Silvera, Miller, &amp; Rohan, 2007; Lambe, Lindblad, Wu, Remler, &amp; Hsieh, 2002; Jung Eun Lee, Susan E. Hankinson, &amp; Eunyoung Cho, 2009; J. E. Lee, S. E. Hankinson, &amp; E. Cho, 2009)</p>

Table 1 (cont.)

Etiologic factor	Hypothesized mechanisms
6. Physical activity	<p>- exercise and routine physical activity: ↓ body weight and blood pressure, ↓ reduce chronic inflammation, ↓ oxidative stress, ↑ insulin sensitivity: ↓ risk of RCC (Pialoux, Brown, Leigh, Friedenreich, &amp; Poulin, 2009; Richardson et al., 2008; Solomon et al., 2009))</p>
7. Diet and beverages	<p>- acrylamide (Group 2A “probable” human carcinogen) by the IARC: ↑ in consumed fried &amp; baked foods, ↑ RCC risk</p> <p>- alcohol consumption: ↓ 28% in RCC risk among those who drank ≥15 gram/day (Lee et al., 2007; Tornqvist, 2005; Virk-Baker, Nagy, Barnes, &amp; Groopman, 2014)</p>
8. Occupation and environment	<p>- trichloroethylene (TCE) (Group 2A “probable” human carcinogen) by IARC: ↑ in metal degreaser &amp; chemical additive: ↑ RCC risk</p> <p>- ochratoxins (OTA) and citrinin (CIT): ↑ nephrotoxic, genotoxic and carcinogenic effects</p> <p>- OTA (genotoxic carcinogen): ↑ covalent adducts at carbon level 8 (C8) guanine C8-dG-OTA</p> <p>- co-exposure to CIT and OTA: ↑ DNA adduct formation of C-C8dG-OTA (W.-H. Chow, Liao, &amp; Devesa, 2010; Malir, Ostry, Pfohl-Leszkowicz, &amp; Novotna, 2013; Pfohl-Leszkowicz, 2009)</p>

Source: Modified from Chow et al., 2010

**Table 2 Summary of hereditary syndromes associated with renal neoplasia**

Type of RCC	Syndrome / Inheritance pattern	Gene / Locus / Type / Protein
ccRCC	Von Hippel-Lindau / AD	VHL / 3p25 / Tumor suppressor / (pVHL)
	Hereditary nonpolyposis colon cancer (Lynch Syndrome) / AD	MLH1, MSH2, MSH6, PMS2 / 2p22, 3p22, 2q31, 2p16 / mismatch repair / –
	PTEN hamartoma tumor syndrome (Cowden disease) / AD	PTEN / – / tumor suppressor / phosphatase
	BAP1 (BRCA-associated Protein 1) Mutations and familial kidney cancer / –	BAP1 / 3p21.1 / tumor suppressor / deubiquitinase
	Familial nonsyndromic clear cell RCC / AD	– / – / – / –
Angiomyolipomas, ccRCC	Tuberous sclerosis complex / AD	TSC1, TSC2 / 9q34, 16p13.3 / Tumor suppressor / (mTOR pathway, hamartin, tuberin)
Non-specified, ccRCC	Autosomal recessive renal cancer/AR	– / – / – / –
Oncocytoma, ccRCC, chRCC, pRCC	Familial paraganglioma syndrome / AD	SDHA, B, C, D / 5p15, 11q13.1, 1p36, 1q21, 11q23 / tumor suppressor / –
oncocytic/chRCC/pRCC	Birt-Hogg-Dubé / AD	FLCN / 17p12q11.2 / Tumor suppressor / (folliculin)
pRCC (HLRCC)	Hereditary leiomyomatosis/renal cell cancer / AD	FH / 1q42.1 / Tumor suppressor / (fumarate hydratase)
pRCC	Hereditary papillary renal cancer / AD	MET / 7q31, 1q21 / Proto-oncogene / c-MET
	Familial papillary thyroid and renal cancer syndrome / AD	fPTC / PRN / 1q21 / – / –
Oncocytoma	Familial oncocytoma / AD	Partial loss of chromosome 1, FLCN/t(9:11) 11q13, p23:q23 t(8:9), (q24.1; q34.3), recipro-caltranslocation / –

**Source:** Modified from Petejova and Martinek, 2016

#### 4. Histological subtypes of renal cell carcinoma

According to the WHO classification in 2004, histological subtypes of RCC are recognized underlying on morphological and histopathological characteristics to provide relevant prognostic information and therapeutic guidance (Eble JN, 2004). Histological subtypes of RCC are: 1) Clear cell renal cell carcinoma (ccRCC), 2) Multilocular clear cell renal cell carcinoma, 3) Papillary renal cell carcinoma (pRCC), 4) Chromophobe renal cell carcinoma (chRCC), 5) Carcinoma of the collecting ducts of Bellini, 6) Renal medullary carcinoma, 7) Xp11 translocation carcinomas, 8) Carcinoma associated with neuroblastoma, 9) Mucinous tubular and spindle cell carcinoma, and 10) Unclassified renal cell carcinoma.

Three main histological subtypes are clear cell renal cell carcinoma (ccRCC) is account about 75% of sporadic renal carcinoma, papillary renal cell carcinoma (pRCC) is account about 15% of all RCC, and chromophobe renal cell carcinoma (chRCC) is account about 5% of all RCC. Sarcomatoid dedifferentiation has been described in about 5% of papillary RCC (Corti et al., 2006).

##### 4.1 Clear cell renal cell carcinoma (ccRCC)

###### 4.1.1 Characteristics of ccRCC

Ninety five percent of clear cell renal cell carcinomas are sporadic, and the remaining 5% are associated with Von Hippel–Lindau (VHL) disease. Clear cell RCC originates from epithelial cells of the proximal convoluted tubules in renal cortex. Macroscopically, ccRCC represents a solid, yellowish lesion with variable degrees of internal necrosis, hemorrhage, and cystic degeneration (Figure 4A). Histologically, cancer cells show clear cells because of their lipid- and glycogen-rich cytoplasmic content (Figure 4B). In high-grade and poorly differentiated tumors, cancer cells lose their cytoplasmic clearing and also present granular eosinophilic cytoplasm (Figure 4C) (Zhou, & He, 2003). A summary of characteristics of ccRCC is shown in Table 3.



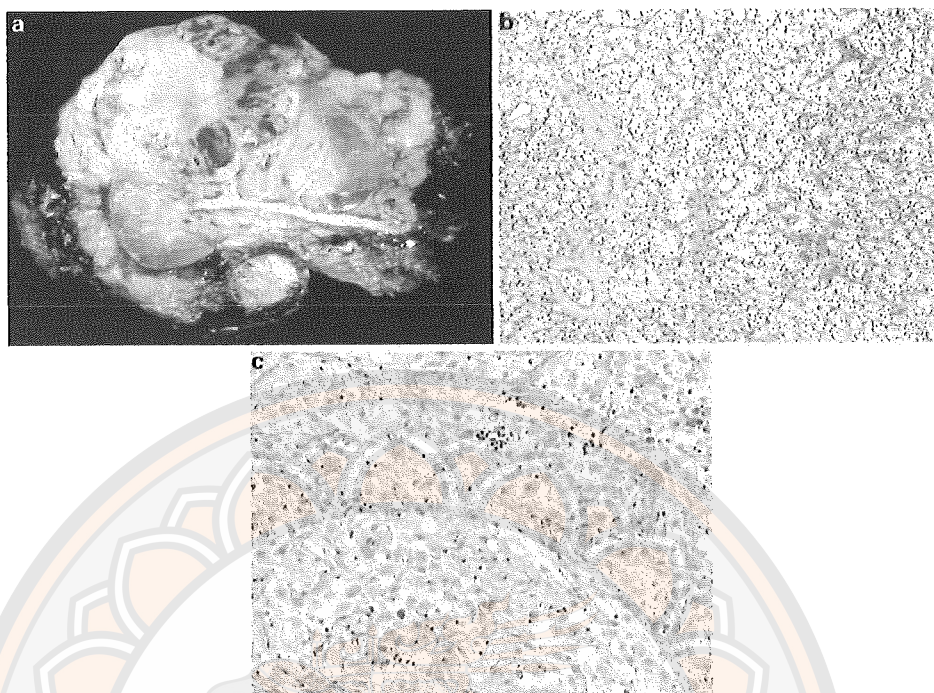


**Figure 4 Gross and histological structures of ccRCC (A) Gross structure of large ccRCC presents golden yellow color extending into perinephric fat and sinus. Adrenal metastasis is also seen on the bottom of the image. B) Microscopic structure presents compact nests of tumor cells with clear cytoplasm. C) Microscopic structure of high grade presents eosinophilic and granular cytoplasm)**

**Source:** Zhou et al., 2013



**Table 3 Summary of characteristics of ccRCC**

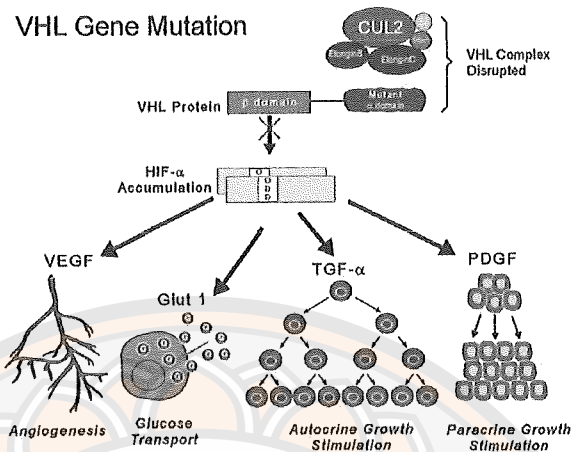
Clinical features	Pathological features	
	Gross structure	Microscopic structure
<ul style="list-style-type: none"> <li>– 60–70% of ccRCC presents in all age groups.</li> <li>– 5% of the patient shows an inherited syndrome.</li> <li>– Familial ccRCC often represents multifocal and bilateral renal tumors in young patients.</li> </ul>	<ul style="list-style-type: none"> <li>– Presents unilateral and unicentric, round and well-demarcated mass with a fibrous capsule</li> <li>– Cut surface often shows golden yellow color, hemorrhage, necrosis, cystic degeneration, and calcification.</li> </ul>	<ul style="list-style-type: none"> <li>– Presents as compact nests, sheets, alveolar, or acinar structures</li> <li>– Shows high lipid and glycogen content in the cytoplasm</li> <li>– Tumor cells have clear cytoplasm.</li> <li>– In high, tumor cells mostly present granular eosinophilic cytoplasm.</li> </ul>

**Source:** Modified from Zhou et al., 2013

#### 4.1.2 Molecular events of ccRCC

The fundamental biology of ccRCC development and progression are associated with *VHL* mutation. A mutation in the *VHL* gene disrupts binding of elongin B and C leading to an E3 ubiquitin ligase complex, resulting in accumulation of hypoxia-inducible factor- $\alpha$  (HIF- $\alpha$ ) in an intracellular component. The stabilization of HIF- $\alpha$  subunits activate of downstream targets, including vascular endothelial growth factors (VEGFs), glucose transporters (GLUT-1), transforming growth factor (TGF), and platelet-derived growth factor (PDGF) (Figure 2A) (Rini, Campbell, & Escudier, 2009). Molecularly targeted therapy blocking components of VHL pathway of ccRCC has been developed and successfully introduced to inhibit protein translation cell growth, cell proliferation, cell survival, and differentiation pathways (Figure 2B) (Protzel, Maruschke, & Hakenberg, 2012).

A



B

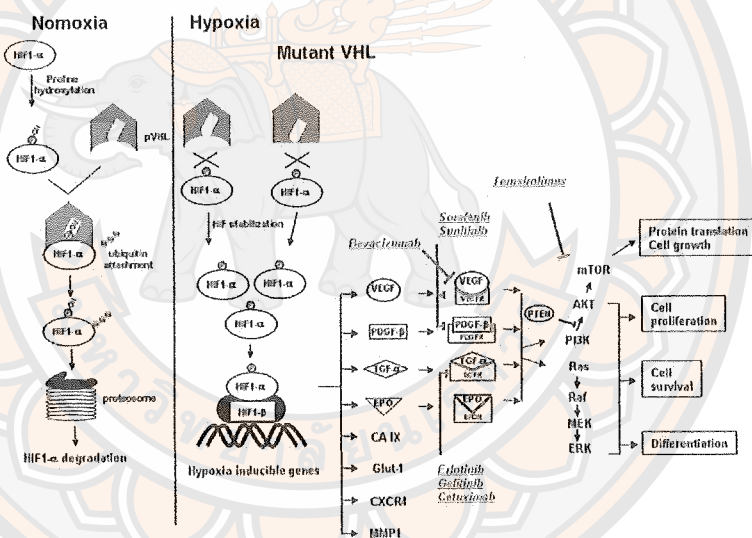


**Figure 5 Molecular events and targeted therapy blocking components of VHL pathway of ccRCC (A) *VHL* gene mutation of ccRCC promotes angiogenesis, glucose transpotation, autocrine and paracrine growth stimulations by activating of VEGF, GLUT 1, TGF- $\alpha$ , and PDGF. B) Targeting drugs of VHL pathway of ccRCC has been developed to inhibit these pathways)**

Source: Rini et al., 2009; Protzel et al., 2012

## 4.2 Papillary renal cell carcinoma (pRCC)

### 4.2.1 Characteristics of pRCC

Papillary RCC (pRCC) is the most second type of RCC, and accounts for 10–15% of renal cell carcinomas. Papillary RCC are histologically divided into two types: type 1 pRCC and type 2 pRCC. However, prognosis in patients with type I pRCC have a better than those with type II pRCC. Macroscopically, pRCC represents as a well-circumscribed mass enclosed within pseudocapsule. Most of pRCC may be found bilateral and multifocal tumors. Some tumor area presents necrotic and friable (Figure 6A). Histologically, pRCC is composed of tightly packed of papillae, tubulopapillae, and tubules with fibrovascular cores (Figure 6B). Type I pRCC contains papillae are delicate and short, lined with single cell layer with scant cytoplasm and low-grade nuclei (Figure 6B). Type II pRCC, carcinogenic cells represent large, eosinophilic cytoplasm, and large pseudostratified nuclei with prominent nucleoli (Figure 6C) (Zhou, & He, 2003). A summary of characteristics of pRCC is shown in Table 4.

### 4.2.2 Molecular events of pRCC

Cytogenetic changes comprising of trisomy or tetrasomy of chromosome 7, trisomy of chromosome 17, and loss of Y chromosome in males are common in pRCC. The gain of chromosome 7p and 17p is more common in type I tumors, while deletion of heterozygosity at 9p13 is typically found in type II tumors (Zhou, & He, 2003). Mutation of *MET* oncogene on chromosome 7, encodes for a receptor tyrosine kinase, plays a role in cell proliferation and immortalization, motility, and invasion (Corti et al., 2006).

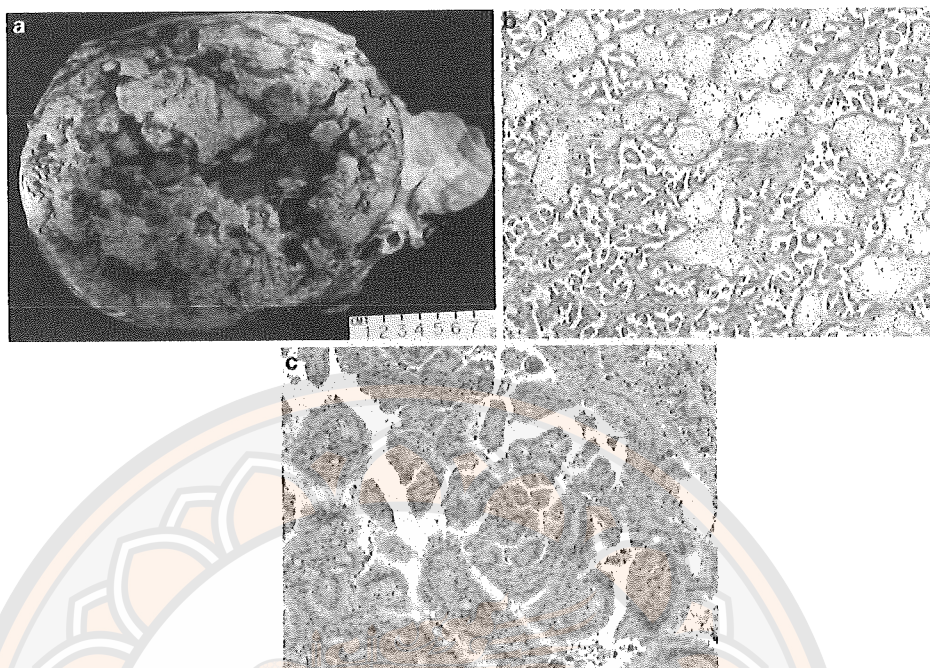


**Figure 6 Gross and histological structures of pRCC (A) Gross structure of pRCC contains a thick tumor capsule and extensive necrosis. B) Microscopic structure of type I pRCC shows papillae and single layer of cancer cells. C) Microscopic structure of type II pRCC presents eosinophilic cytoplasm of cancer cells with pseudostratified nucleus with prominent nucleoli)**

**Source:** Zhou et al., 2013



**Table 4 Summary of characteristics of pRCC**

Clinical features	Pathological features	
	Gross structure	Microscopic structure
<ul style="list-style-type: none"> <li>– 90% of patients with pRCC have better prognosis with 5-year survival.</li> <li>– Type I (2/3 of pRCC) and Type II (1/3 of pRCC)</li> <li>– Prognosis of patients with type I pRCC have a better than those with type II tumor.</li> </ul>	<ul style="list-style-type: none"> <li>– Presents as a well-circumscribed mass enclosed within a pseudocapsule</li> <li>– Appears necrotic and friable mass</li> <li>– Often occurs bilateral and multifocal tumors</li> </ul>	<ul style="list-style-type: none"> <li>– Presents as various size of papillae, tubulopapillae, and tubules with delicate fibrovascular cores</li> <li>– Shows necrosis, hemorrhage, hemosiderin deposition</li> <li>– pRCC type I contains delicate and short papillae.</li> <li>– pRCC type II contains large cells having eosinophilic cytoplasm, large pseudostratified nuclei with prominent nucleoli.</li> </ul>

**Source:** Modified from Zhou et al., 2013



### 4.3 Chromophobe renal cell carcinoma (chRCC)

#### 4.3.1 Characteristics of chRCC

Chromophobe RCC (chRCC) is rare type and accounts for 5% of renal cell carcinomas. Macroscopically, chRCC are well-circumscribed solid mass, non-encapsulated, and highly lobulated mass. The surface appears homogeneously beige, light tan, brown or yellow (Figure 7A). Histologically, the tumor cells are usually arranged in solid sheets with tubulocystic architecture. Tumor cells might be present in varying proportions. Most of tumor cells are large-pale and polygonal cells. Population of smaller cells are small granular cells with eosinophilic cytoplasm. The nuclei of both are irregular shape (Figure 7B) (Zhou, & He, 2003). A summary of characteristics of chRCC is shown in Table 5.

#### 4.3.2 Molecular events of chRCC

The genetics of chRCC have not been clearly explained. Chromophobe RCC is associated with loss of chromosomes 1, 2, 6, 10, 13, 17, and 21. Familial chRCC is associated with Birt–Hogg–Dube (BHD) syndrome, which encodes the protein folliculin (FLCN). However, *BHD* mutations are rarely found in sporadic chRCC (Zhou, & He, 2003).

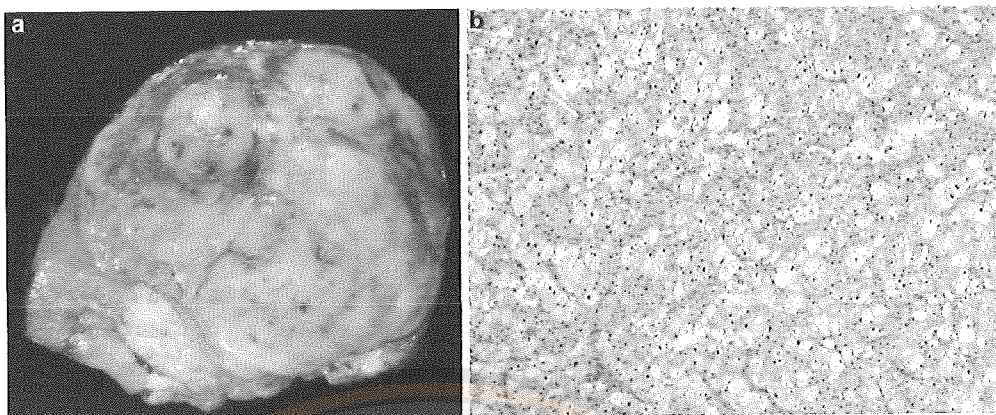


**Figure 7 Gross and histological structures of chRCC (A) Gross structure of chRCC presents circumscribed mass with light brown cut surface. B) Microscopic structure of chRCC shows large and polygonal tumor cells with irregular nuclei and perinuclear clearing)**

Source: Zhou et al., 2013

**Table 5 Summary of characteristics of chRCC**

Clinical features	Pathological features	
	Gross structure	Microscopic structure
<ul style="list-style-type: none"> <li>– 5% of RCCs can occur in all age range.</li> <li>– chRCC occurs equally in males and females.</li> <li>– The prognosis of chRCC is better than ccRCC.</li> </ul>	<ul style="list-style-type: none"> <li>– Presents a solitary, well-circumscribed and nonencapsulated mass with homogenous light brown solid cut surface</li> </ul>	<ul style="list-style-type: none"> <li>– Presents solid sheets with tubulocystic structure</li> <li>– Consists of large polygonal cells with finely reticulated cytoplasm</li> <li>– The nuclei are typically irregular, hyperchromatic with perinuclear haloes</li> </ul>

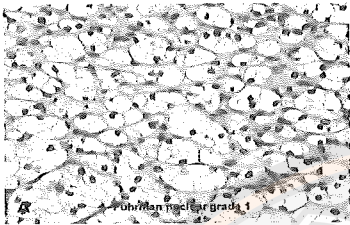
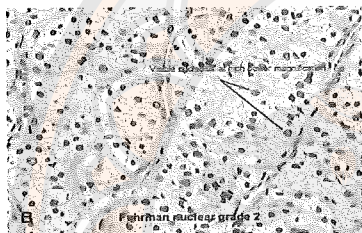
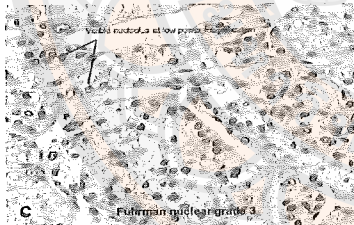
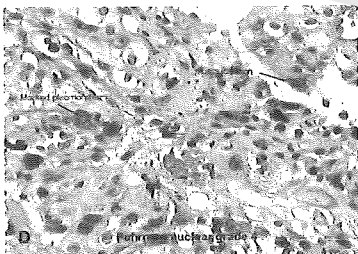
Source: Modified from Zhou et al., 2013

## 5. Pathological parameters for renal cell carcinoma

5.1 Fuhrman nuclear grading is the most widely used grading system for grading renal cell carcinoma. Fuhrman nuclear grading is classified based on the microscopic morphology of nuclear size, nuclear shape, and nucleolar prominence. The Fuhrman nuclear grading system divides RCC into one of four grades as described in Table 6 (Corti et al., 2006; Fuhrman, Lasky, & Limas, 1982).

5.2 Sarcomatoid differentiation accounts for five percent of RCCs that can be observed in high grade and poorly differentiated RCCs. The incidence of sarcomatoid differentiation was found in collecting duct carcinoma (29%), unclassified RCC (11%), chRCC (9%), ccRCC (8%), and pRCC (3%). Microscopically, sarcomatoid differentiation consists of abundant spindle elements that resemble leiomyosarcoma, fibrosarcoma, angiosarcoma, rhabdomyosarcoma, and other sarcomas (Figure 11). Sarcomatoid change in RCC associated with a worse prognosis (de Peralta-Venturina et al., 2001; Zhou, & He, 2003).

**Table 6** Fuhman nuclear grading for assessing renal cell carcinoma

Fuhrman nuclear grade	Microscopic features of nucleus
<b>Grade I</b> 	<ol style="list-style-type: none"> <li>1. Nuclei are small (10 <math>\mu</math>M)</li> <li>2. Hyperchromatic nuclei</li> <li>3. Round (resembling mature lymphocytes)</li> <li>4. Indistinct nucleoli</li> <li>5. little detail chromatin</li> </ol>
<b>Grade II</b> 	<ol style="list-style-type: none"> <li>1. Nuclei are slightly large (15 <math>\mu</math>M)</li> <li>2. Finely granular chromatin</li> <li>3. Inconspicuous nucleoli</li> </ol>
<b>Grade III</b> 	<ol style="list-style-type: none"> <li>1. Nuclei are large (20 <math>\mu</math>M)</li> <li>2. Oval shape nuclei</li> <li>3. Coarsely granule chromatin (open chromatin)</li> <li>4. Prominent nucleoli</li> </ol>
<b>Grade IV</b> 	<ol style="list-style-type: none"> <li>1. Polymorphic nuclei</li> <li>2. Hyperchromasia</li> <li>3. Single or multiple macronucleoli</li> </ol>

**Source:** Modified from Qayyum T. et al., 2013; Corti B. et al., 2006;  
Zhang Y. et al., 2017



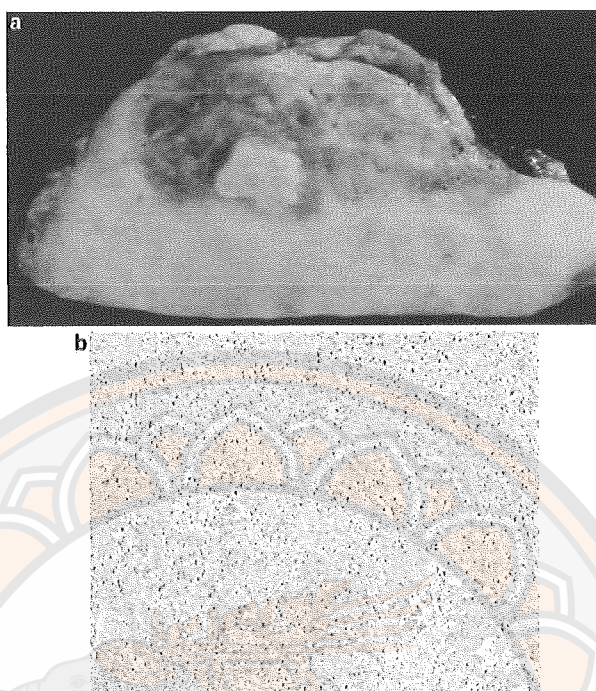


**Figure 8 Sarcomatoid differentiations in RCC (A) The lower a fleshy appearance are suggested as sarcomatoid differentiation. B) Microscopically, the sarcomatoid feature shows abundant spindle cancer cells)**

**Source:** Zhou et al., 2013

## **6. TMN classification and staging of RCC**

The American Joint Committee on Cancer (AJCC) tumor-node-metastasis (TNM) staging is the most commonly used and universally accepted staging system for cancer. TMN classification is classified according to the primary tumor site; the regional lymph node involvement; and the presence or otherwise of distant metastatic spread (Table 7). The RCC has been classified with the TNM system, and then an overall stage is assigned (Table 8) (Edge, & Compton, 2010; Petejova, & Martinek, 2016).



**Table 7 TMN classification of renal cell carcinoma**

<b>Classification</b>	<b>Definition</b>
Primary tumor (T)	Tx Primary tumor cannot be assessed
	T0 No evidence of primary tumor
	T1 Tumor $\leq 7$ cm in greatest dimension and limited to kidney
	T1a Tumor $\leq 4$ cm
	T1b Tumor $> 4$ cm but $\leq 7$ cm
	T2 Tumor $>7$ cm in greatest dimension and limited to kidney
	T2a Tumor $>7$ cm but $\leq 10$ cm
	T2b Tumor $>10$ cm
	T3 Tumor extends into major veins or perinephric tissues, but not beyond Gerota's fascia
	T3a Tumor extends into the renal vein or directly invades perinephric tissues, but not beyond Gerota's fascia
	T3b Tumor grossly extends into vena cava below the diaphragm
	T3c Tumor grossly extends into vena cava above diaphragm or invades wall of the vena cava
	T4 Tumor invades beyond Gerota's fascia (including contiguous extension into the ipsilateral adrenal gland)
Regional lymph nodes (N)	Nx Regional lymph nodes cannot be assessed
	N0 No regional lymph node metastasis
	N1 Metastasis in regional lymph node
Distant metastasis (M)	Mx Distant metastasis cannot be assessed
	M0 No distant metastasis
	M1 Distant metastasis

**Source:** Modified from Petejova, & Martinek, 2016

**Table 8 Stages of renal cell carcinoma**

Stage	TNM classification
Stage I	T1, N0, M0
Stage II	T2, N0, M0
Stage III	T1, N1, M0
	T2, N1, M0
	T3, N1, M0
	T3, Any N, M0
Stage IV	T4, Any N, M0
	Any T, Any N, M1

**Source:** Modified from Petejova and Martinek, 2016

## 7. Diagnosis

Diagnostic techniques are commonly used for RCC, including computed tomography scanning (CT-scan), or abdominal ultrasound (US), or magnetic resonance imaging (MRI). Computed tomography is the key detection of renal masses. Sensitivity of CT-scan is ranging from 88% to 100%. To confirm the diagnosis of RCC should include CT imaging and intravenous contrast because it provided information of the tumor extension such as extrarenal spread or venous involvement. Ultrasound is not considered for detection and characterization of small renal tumors, it is common to distinguish between cystic and solid renal masses. Abdominal ultrasound and/or magnetic resonance imaging should be an alternative to CT-scan (Patard et al., 2003) (B. Ljungberg et al., 2010; Petejova, & Martinek, 2016). CT-scan for ccRCC is presented in Figure 9.

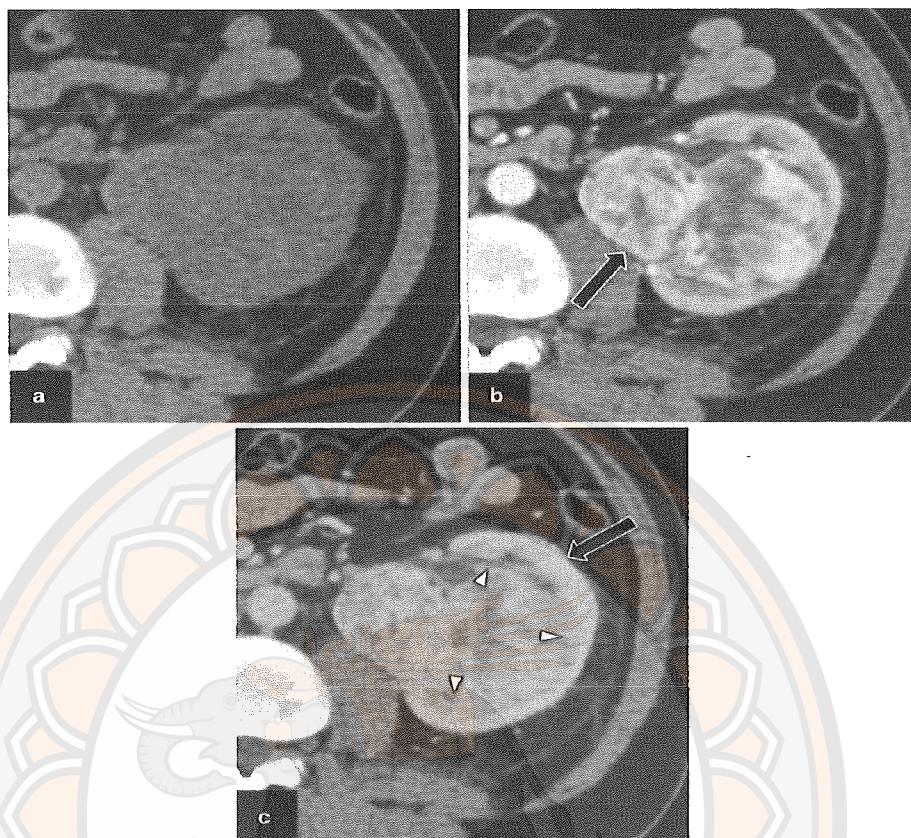


**Figure 9 CT scan of ccRCC (A) Precontrast phase shows the area of kidney. B) Corticomedullary phase shows large central renal mass extending into the renal sinus (black arrow), with intense and heterogeneous contrast enhancement. C) Nephrographic phase shows the renal parenchyma with hyperdense (black arrow), compared to the tumor outlining mass (arrowheads))**

**Source:** Purysko et al., 2009

### 8. The immunohistochemical landscape of RCC

For RCC diagnosis, immunohistochemistry (IHC) results serve as valuable diagnostic tools when staining is positive or negative. Each segment of renal tubules has a specific IHC expression profile. Therefore, IHC expression for each subtypes of RCC should be different immunoreactivity (Shen, Truong, Scarpelli, & Lopez-Beltran, 2012). The most common markers used in diagnostic strategies of RCC are described in Table 9.

**Table 9 Summary of IHC results of RCC**

RCC subtypes	Detectable immuoreactivity	Undetectable immunoreactivity	Ref.
ccRCC	<ul style="list-style-type: none"> <li>- EMA: epithelial membrane antigen</li> <li>- Low molecular weight cytokeratins (CK8, CK18, CK19)</li> <li>- AE1/AE3</li> <li>- Cam 5.2</li> <li>- Vimentin</li> <li>- MUC-1, MUC-3</li> <li>- CD10 ( Most in ccRCC)</li> <li>- Placental alkaline phosphatase (PLAP)</li> <li>- Renal cell carcinoma marker</li> <li>- PAX2, PAX8</li> <li>- CAIX (carbonic anhydrase IX)</li> </ul>	<ul style="list-style-type: none"> <li>- High-molecular-weight cytokeratins</li> <li>- <math>\beta</math>-Defensin-1</li> <li>- Parvalbumin</li> <li>- Kidney-specific cadherin</li> <li>- CK7, CK20, CD117</li> </ul>	(Murphy WM, 2004; Shen et al., 2012)



Table 9 (cont.)

RCC subtypes	Detectable Immuoreactivity	Undetectable immunoreactivity	Ref.
pRCC	<ul style="list-style-type: none"> <li>- Pancytokeratin</li> <li>- Low molecular weight cytokeratins</li> <li>- AE1/AE3</li> <li>- Cam 5.2</li> <li>- CK7</li> <li>- CD10</li> <li>- <math>\beta</math>-Defensin-1</li> <li>- Parvalbumin</li> <li>- Vimentin</li> <li>- PAX2, PAX8</li> <li>- AMACR, <math>\alpha</math>-methylacyl-coenzyme A racemase</li> </ul>	<ul style="list-style-type: none"> <li>- CD117</li> <li>- Kidney-specific cadherin</li> <li>- Parvalbumin</li> </ul>	(Corti et al., 2006; Shen et al., 2012)
chRCC	<ul style="list-style-type: none"> <li>- Pancytokeratin &amp; EMA Ab</li> <li>- CD10 (50%)</li> <li>- RON</li> <li>- Parvalbumin</li> <li>- <math>\beta</math>-Defensin-1</li> <li>- E-cadherin</li> <li>- Kidney-specific cadherin</li> <li>- CD117</li> <li>- AE1/AE3</li> <li>- CK7 strong/diffuse for chromophobe RCC</li> </ul>	<ul style="list-style-type: none"> <li>- Vimentin</li> <li>- CK7 (or weak for oncocytoma)</li> <li>- CAIX</li> <li>- AMACR</li> </ul>	(Corti et al., 2006; Shen et al., 2012)



## 9. Application of IHC in the diagnosis of RCC

### 9.1 Diagnosis of an oncocytic renal neoplasm and pRCC

The hematoxylin-eosin image showed a tumor arranged of solid growth of eosinophilic/oncocytic cells (Figure 16A). Differential diagnosis may include ccRCC, chRCC, oncocytoma, and type-2 pRCC. The IHC results represented strong and diffuse positive stain of vimentin (Figure 16B). RCC marker protein had unique apical membrane cellular pattern (Figure 16C). Alpha-Methylacyl coenzyme A racemase protein showed diffuse and strong cytoplasmic pattern (Figure 17D). Therefore, all IHC features could support a diagnosis of pRCC (Shen et al., 2012).

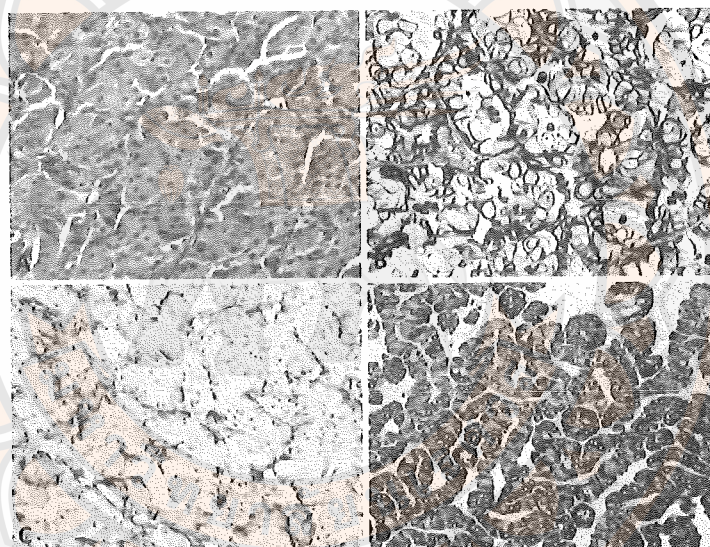


**Figure 10** Application of immunohistochemical stains in the diagnosis of an oncocytic renal neoplasm (A) Hematoxylin-eosin stain shows a solid growth of oncocytic cells. B) Vimentin staining was strong and diffuse positive stain of cancer cells. C) The RCC marker was positive staining at apical membrane of cancer cells. D) Alpha-Methylacyl coenzyme A racemase stain was diffuse and strong cytoplasmic staining of cancer cells (original magnifications X200))

Source: Shen et al., 2012

## 9.2 Diagnosis of renal cell and non-renal cell neoplasm

The key protein markers for diagnosis of RCC are PAX2, PAX8, RCC marker, CD10. Marker proteins of metastatic cancer calls from other organs are tissue-specific markers of a non-renal tumor such as TTF-1 for the lung cancer, prostate-specific antigen (for the prostate cancer), CDX2 for the colorectal cancer, hepar-1 for the liver cancer, inhibin for adrenal cortical carcinoma, S100 and HMB-45 for melanoma (Shen et al., 2012).

## 9.3 To diagnosis of histological subtypes of RCC

The useful IHC panel for diagnosis of pRCC included CK7, AMACR, CD10 or RCC marker, TFE3, and CD57. Strong and diffuse CK7 staining is the most remarkable in a diagnosis of chRCC. Differential diagnosis of chRCC from oncocytoma can choose S100A1 and CD82 to be panel markers. The panel markers to distinguish an invasive high-grade urothelial carcinoma from a high-grade RCC included RCC marker, PAX2 or PAX8, uroplakin III, thrombomodulin, and p63 (Albadine et al., 2010; Butnor, & Ordonez, 2008; Shen et al., 2012).

## 9.4 Diagnosis of RCC in small biopsy specimens

Al-Ahmadie et al. reported that the combination of five panel markers (CAIX, CD117, AMACR, CK7, and CD10) helps to improve the accuracy of medical diagnosis of needle biopsy for renal tumors after nephrectomy (Al-Ahmadie et al., 2011; Shen et al., 2012).

## 9.5 Diagnosis of metastatic RCC in distant sites

The panel markers for evaluating metastatic RCC should include PAX2 or PAX8, and RCC marker or CD10 (Shen et al., 2012).

## 10. Treatment of renal cell carcinoma

### 10.1 Treatment of localized renal cell carcinoma

Small renal masses ( $\leq 4$  cm: becoming brighter on CT with contrast) were treated surgically with radical or partial nephrectomy. Partial nephrectomy is the gold standard management of small renal masses that can now be done laparoscopically. Partial nephrectomy was preferred whenever the patient presented patients with chronic kidney disease (Rini et al., 2009). Partial and radical nephrectomy for localized renal cell carcinoma is represented in Figure 14. Recommended surgical treatment for patients with renal cell carcinoma according to clinical tumor stage is shown in Figure 15.

Large renal tumors (4–7 cm.) should be considered nephron-sparing approaches (Capitanio, & Montorsi, 2016). The best treatment for localized renal cancers at T1a-b is the partial nephrectomy rather than radical nephrectomy. Ipsilateral adrenalectomy, embolization and lymphadenectomy are considered to be additional treatments for any case with massive hematuria, flank pain, or/and tumor extended to the lymph nodes (Jonasch, Gao, & Rathmell, 2014). According to the European Association of Urology (EAU) guidelines of RCC, the standard procedure for solitary renal tumors ( $> 7$  cm.) also is nephron-sparing surgery (Borje Ljungberg et al., 2015). New therapeutic approaches are based on a clinical trial, including microwave ablation, stereotactic radiosurgery, and laser ablation (Borje Ljungberg et al., 2015).

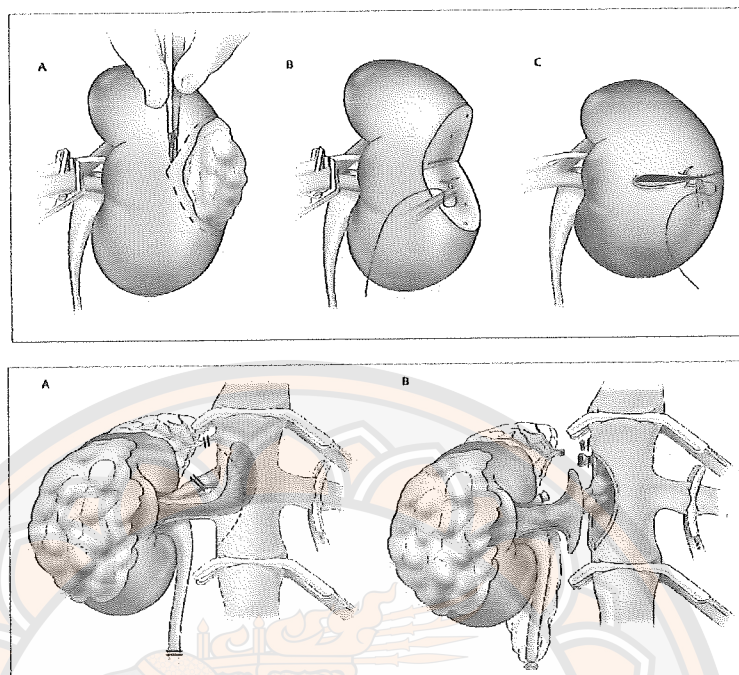


**Figure 11 Partial and radical nephrectomy for management of localized renal cell carcinoma (Upper panel includes A) Temporary occlusion of vasculature. B) Resection of tumor with a rim of normal parenchyma. C) Reconstruction of the kidney. Lower panel includes (A) After mobilisation of the kidney and ligation of the renal artery, the regional vasculature is isolated. (B) The ostium of the renal vein is then excised)**

**Source:** Modified from Rini et al., 2009



Stage	Surgery	Approach	Recommendations
T1	Nephron-sparing surgery	Open	Recommended standard
		Laparoscopic	Optional in experienced centres
	Radical nephrectomy	Laparoscopic	In patients not suitable for nephron-sparing surgery
		Open	Optional in patients not suitable for nephron-sparing surgery
T2	Radical nephrectomy	Laparoscopic	Recommended standard
		Open	Adequate and recommended but has higher morbidity
T3, T4	Nephron-sparing surgery		Recommended in selected patients in experienced centres
	Radical nephrectomy	Open	Recommended standard for most patients
		Laparoscopic	Feasible in selected patients

**Figure 12 Recommended surgical treatment strategy for renal cell carcinoma**

Source: Ljungberg et al., 2010

## 10.2 Treatment of metastatic renal cell carcinoma

Treatments of metastatic renal cell carcinoma (mRCC) were different because the patient's clinical status has changed over the last 10-15 years. The use of cytoreductive nephrectomy (CN) in the cytokine therapy era was well established by Southwest oncology group 8949 (SWOG 8949) and European Organization for Research and Treatment of Cancer (EORTC 30947) (Pantuck, Belldegrun, & Figlin, 2007). Previous study has been reported that the median survival of patients who treated by CN following given interferon (11.1 months) were longer than the patients who given interferon alone (8.1 months) ( $p = 0.05$ ) (Flanigan et al., 2001). The recommendation of ccRCC for first-line therapy were: 1) sunitinib (50 mg daily orally for a period of 4 weeks followed by 2 weeks of rest); 2) pazopanib (800 mg orally daily); 3) and the combination of INF- $\alpha$  (9 MU three times per week subcutaneously) + bevacizumab (10 mg/kg biweekly intravenously). The therapeutic agents for second-line therapy were axitinib, sorafenib, and everolimus after prior administration of tyrosine kinase inhibitors; and sorafenib, axitinib, and pazopanib after prior administration of cytokines (B. Ljungberg et al., 2010). For third-line therapy were additionally by given everolimus after VEGF and sorafenib after mTOR (B. Ljungberg et al., 2010). Targeted drugs for patients with metastatic RCC are concluded in Table 10.



**Table 10 Targeted drug treatment for metastatic RCC**

Targeting agents	Drug classification	Mechanisms of drug
5-fluorouracil	Pyrimidine analog – chemotherapeutic agent	– inhibition of DNA replication – irreversible inhibition of thymidylate synthase
Bevacizumab	Monoclonal antibody against circulating VEGF	– inhibition of angiogenesis
Temsirolimus Everolimus	Mammalian target of rapamycin (mTOR) inhibitors	– stimulates the degradation of cyclin D1, that inhibits the G1 to S-phase transition in the cell cycle, – downregulation phospho-p70 S6 kinase, is considered to be an indicator of the activated mTOR pathway
Interleukin 2 (IL-2)	Cytokine	– potent stimulator of T-cell proliferation, tumor-specific CTLs, NK cells, and possibly the subset of these that are intratumoral (tumor infiltrating lymphocytes) activated, and these leukocytes then kill the cancer cells
Interferon- $\alpha$ (IFN- $\alpha$ )	Cytokine	– binding to cell surface receptors and activating the Jak protein family. – antiproliferative activity – activation of T-cells and NK cells – inhibition of cell cycle arrest
Sorafenib Sunitinib Pazopanib Axitinib	Tyrosine kinase, VEGF, FGF, PDGF and angiogenesis inhibitor	– inhibition of tyrosine kinase which can cause increase in tumor cell proliferation and growth, induce antiapoptotic effects and promote angiogenesis and metastasis.

**Source:** Modified from Patejova, & Martinek, 2016

### 11. Prognosis factors for RCC patients

Systems of prognostic factors have been studied to improve the treatment strategies of RCC. Accurate and reliable prognostic factors should be identified to provide the highest-quality information to patients (Lang, & Jacqmin, 2003). Prognosis factors for RCC included histological subtypes, sarcomatoid differentiation, tumor necrosis, tumor size, and molecular events. Independent significant prognostic variable were pathological TNM staging and Fuhrman nuclear grade (Börje Ljungberg, 2007).

The high grade, or advanced stage, or sarcomatoid differentiation of RCC related with poor survival of patients (Tastekin, 2012). Beisland et al. reported that among mRCC patients who younger age at diagnosis, previous nephrectomy, and treatment by one or more dispensing targeted therapy had long-term overall survival (Beisland et al., 2017). Isolated lymph node (pN1) was a poor prognosis feature of patients. However, some of patients undergo long-term survival after surgical resection (Gershman et al., 2017). Positive surgical margins (PSM) for RCC are the presenting of malignant cells at the edge of tumor resection under the microscope. Ten percent of PSM (10%) were significantly associated with recurrence, metastasis, high grade, and stage of RCC (Bansal et al., 2017). Immunohistochemical staining of protein markers: VEGF-A, HIF-1 $\alpha$ , CD34 and Ki67 was performed to indicate the relationship with conventional prognostic markers. The expression of HIF-1 $\alpha$  was positively correlated to Fuhrman grade, invasion of the renal vein, and tumor stage. The expression of Ki67 was positively correlated to the presence of necrosis, capsular invasion, and advanced tumor stage. The expression of CD34 was negatively correlated to tumor necrosis and overall survival (Bürgesser et al., 2014).

## Epithelial-mesenchymal transition (EMT)

### 1. The different subtypes of EMT

The entire epithelial cells are polarized cells, which their basal surface interacts with the basement membrane. The biological process is called epithelial-mesenchymal transition (EMT) involving in the differentiation of epithelial cells to transform mesenchymal cells and to migrate away from epithelial layer. Process of EMT usually involved the repression of two adhesive molecules, including E-cadherin and N-cadherin. Mesenchymal proteins such as  $\alpha$ -SMA, FSP1, vimentin, and desmin are expressed in the transformed cells. Reversibly, a mesenchymal-epithelial transition (MET) involves the alternation of mesenchymal cells to epithelial derivatives (Kalluri, & Weinberg, 2009). Three subtypes of EMT occur in different biological processes: 1) implantation, embryo formation and organ development; 2) tissue repair and pathological processes; and 3) cancer progression and metastasis (Kalluri, & Weinberg, 2009). Three subtypes of EMT are shown in Figure 19.

During implantation, the trophoblastic cells invade the endometrium of the uterus, which is the first stage of **type 1 EMT** and subsequently from the placenta, function in the gas and nutrient exchange. During the third week, embryo experiences gastrulation, which generates the three germ layers consisting of ectoderm, mesoderm and endoderm. These layers are formed by the differentiation of the primitive streak. The midline and dorsal structures of the embryo are formed by proliferation and migration of epiblastic cells (Moore et al., 2015). The displacing and modification of epiblastic cells to the mesenchymal cells, is generally known as EMT, resulting in the forming of embryonic mesoderm and endoderm layers. The embryonic mesoderm gives rise to the primary mesenchyme, including axial, paraxial, intermediated, and lateral plate mesoderms that generating the connective tissue cells (Aplin, Haigh, Vicovac, Church, & Jones, 1998; Hay, 2005; Thiery, & Sleeman, 2006). Previous study has been reported that Wnt signaling pathway was associated with EMT in development of gastrulation. The embryo could not undergo gastrulation when Wnt3 deficiency occurred. Wnt8c was associated with formation of primitive streak (Liu et al., 1999; Popperl et al., 1997; Skromne, & Stern, 2001; Thomas, Brickman, Popperl, Krumlauf, & Beddington, 1997).

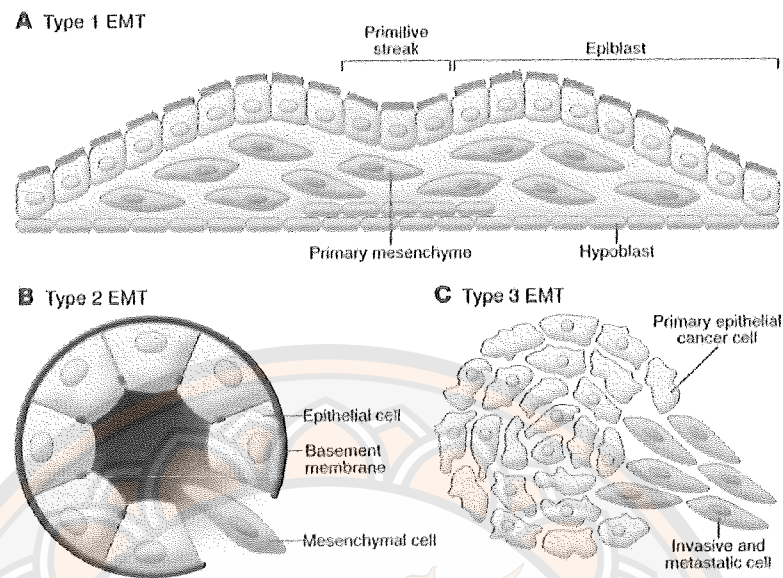


**Figure 13 Three subtypes of EMT (A) Type 1 EMT associated with implantation and embryonic gastrulation and gives rise to the mesoderm and endoderm and to mobile neural crest cells. The primitive epithelium, specifically the epiblast, gives rise to primary mesenchyme via an EMT. B) The type 2 EMT involved in the context of inflammation and fibrosis. C) Type 3 EMT associated with many organs can transform into cancer cells)**

**Source:** Kalluri, & Weinberg, 2009



**Type 2 EMT** is associated with inflammation and fibrogenesis, connective tissue and fibrous tissue comprising of fibroblast and extracellular matrix are formed. Pathophysiology of fibrosis consists of angiogenesis, accumulation of fibroblast, increase in collagen fibers, and remodeling of fibrous tissues. Type 2 EMT can destroy the affected organs such as kidney, liver, and lung caused by prolonged inflammation (Figure 20) (Kim et al., 2006; Potenta, Zeisberg, & Kalluri, 2008; E. M. Zeisberg et al., 2007; M. Zeisberg et al., 2007). The epithelium of renal tubules is derived from the intermediate mesoderm of the embryo via the MET. The inflammatory process can re-activate the EMT renal epithelial cells lead to kidney fibrosis (Aufderheide, Chiquet-Ehrismann, & Ekblom, 1987; Ivanova, Butt, & Matsell, 2008). TGF- $\beta$  is released from residual fibroblast and inflammatory cells, which are important mediators of fibrosis. These growth factors also induced the EMT via both Smad2/3-dependent pathway and MAPK-dependent pathway (Nawshad, Lagamba, Polad, & Hay, 2005; Yang, & Weinberg, 2008).

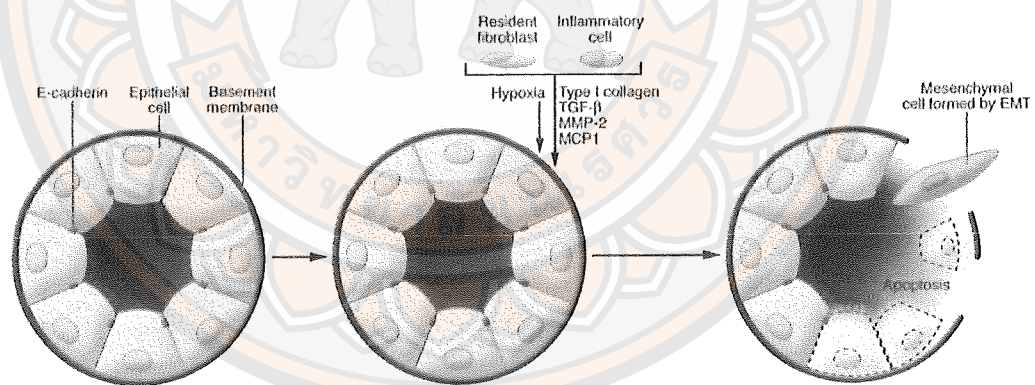


**Figure 14 Type 2 of EMT associated with fibrosis (Inflammatory cells cause disruption of the epithelial cells via degradation of the basement membrane. The epithelial cells lose polarity and undergo apoptosis or EMT)**

**Source:** Kalluri, & Weinberg, 2009



**Type 3 EMT** involved in several steps of cancer progression. Initially, alteration of genetic controls leads to the transformation of epithelial cells to carcinoma in situ (Cao, Xu, Liu, Wan, & Lai, 2015). Tumor epithelial cells lose their cell polarity and cell-cell adhesion, and gain the mesenchymal phenotype. Tumor mesenchymal cells invade their basement membrane to the extracellular matrix, processes called invasion and migration. Tumor cells can enter to blood circulation (intravasation), and travel through the bloodstream to distant organs (extravasation). Subsequently, colonization of tumor cells in distant organs involves the activation of MET process (Figure 21) (Cao et al., 2015; Zeisberg, & Neilson, 2009).

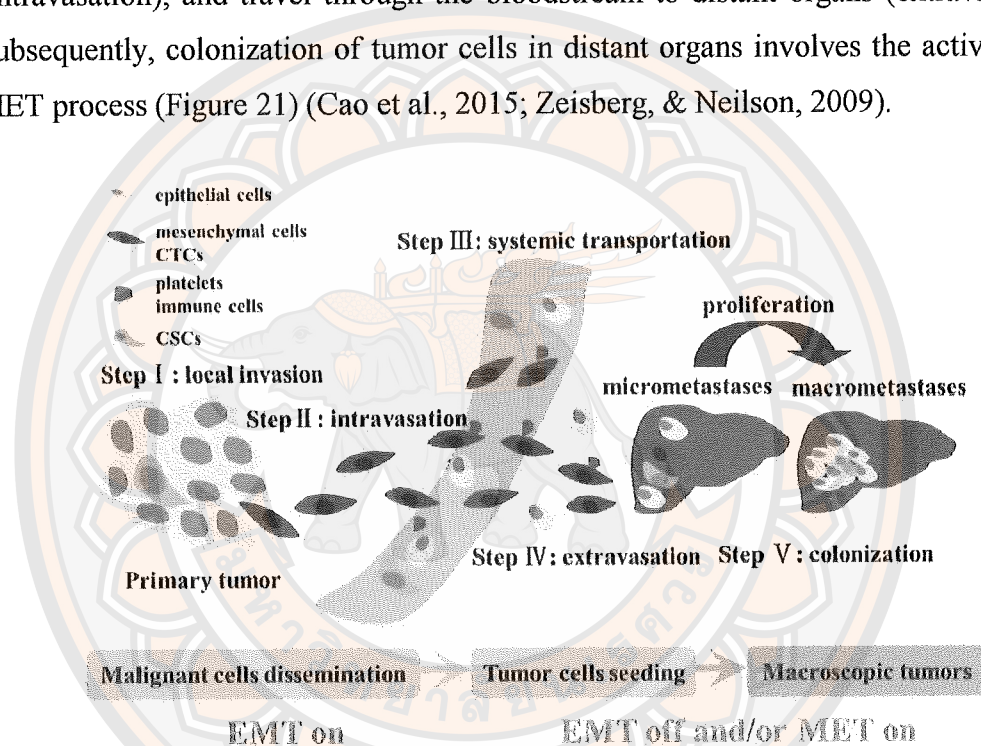


**Figure 15** Type 3 of EMT associated with cancer metastasis (Tumor cells at the invasive front may lose epithelial properties and invade the local matrix and enter into the vasculature. Circulating tumor cells (CTCs) are transported in the systemic circulation to distant organ and formed colonization)

**Source:** Cao et al., 2015

Mesenchymal biomarkers such as  $\alpha$ -SMA, FSP1, vimentin and desmin are found in cancer cells, which are acquired by the mesenchymal phenotype whereas cell-cell adhesive proteins such as E-cadherin showed a decrease in its expression. Several studies has been reported that signaling transducing proteins, including ERK, MAPK, PI3K, Akt, Smads, and  $\beta$ -catenin associated with the controlling of EMT pathway (Tse, & Kalluri, 2007; Yang, & Weinberg, 2008). The EMT biomarkers are divided into two sets of epithelial and mesenchymal proteins that are illustrated in Figure 22. Various biomarkers have been used to demonstrate all three types of EMT (Figure 23).

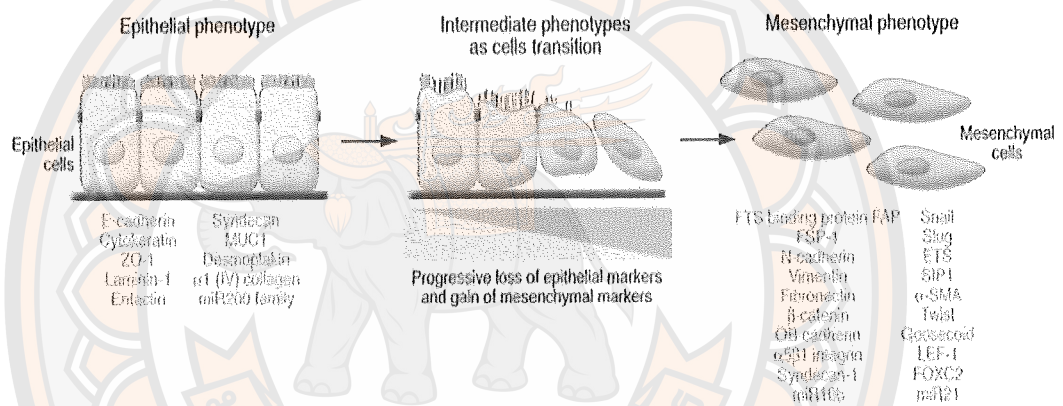


**Figure 16 Two set of distinct protein markers in EMT (Epithelial protein markers (orange) and mesenchymal protein markers (green))**

**Source:** Kalluri, & Weinberg, 2009

Acquired markers		Attenuated markers	
Name	EMT type	Name	EMT type
<b>Cell-surface proteins</b>			
N-cadherin	1, 2	E-cadherin	1, 2, 3
OB-cadherin	3	ZO-1	1, 2, 3
$\alpha 5\beta 1$ integrin	1, 3		
$\alpha V\beta 6$ integrin	1, 3		
Syndecan-1	1, 3		
<b>Cytoskeletal markers</b>			
FSP1	1, 2, 3	Cytokeratin	1, 2, 3
$\alpha$ -SMA	2, 3		
Vimentin	1, 2		
$\beta$ -Catenin	1, 2, 3		
<b>ECM proteins</b>			
$\alpha 1(I)$ collagen	1, 3	$\alpha 1(IV)$ collagen	1, 2, 3
$\alpha 1(III)$ collagen	1, 3	Laminin 1	1, 2, 3
Fibronectin	1, 2		
Laminin 5	1, 2		
<b>Transcription factors</b>			
Snail1 (Snail)	1, 2, 3		
Snail2 (Slug)	1, 2, 3		
ZEB1	1, 2, 3		
CBF-A/KAP-1 complex	2, 3		
Twist	1, 2, 3		
LEF-1	1, 2, 3		
Ets-1	1, 2, 3		
FOXC2	1, 2		
Goosecoid	1, 2		
<b>MicroRNAs</b>			
miR10b	2	Mir-200 family	2
miR-21	2, 3		
ZEB1, zinc finger E-box binding homeobox 1.			

**Figure 17 List of protein markers for the different types of EMT**

**Source:** Zeisberg, & Neilso, 2009

## 2. EMT in renal cell carcinoma

EMT plays a crucial role in development and progression of RCC. The inactivation of the *von Hippel–Lindau (VHL)* tumor suppressor gene induced EMT in ccRCC. Loss of *VHL* leads to an accumulation and translocation of HIF1 $\alpha$  transcription factor into the nucleus. It subsequently activates the transcription of HIF target genes that are involved in important oncogenic pathways (Snail/Slug, Ras/Raf, MAPK kinase, FOXO3A, MUC1, ZEP1, PI3K/AKT/mTOR pathway) (Landolt et al., 2017; Piva et al., 2016). Protein expressions of Snail, Slug, MMP2 and MMP9 were analyzed in primary RCCs by immunohistochemistry. Protein expression of Snail was positively associated with pathological tumor stage, histological grade and sarcomatoid differentiation. Knockdown of Snail expression in RCC cell line 786-O resulted in down-regulation of expressions of *vimentin*, *MMP2* and *MMP9*, but up-regulated *E-cadherin*. The invasiveness of Snail knockdown cells also inhibited. Increases of Snail, MMP2, and MMP9 protein expressions have a significantly worse prognosis of the patients (Mikami et al., 2011). A role of FOXO3A in ccRCC metastasis has been established. Loss of FOXO3A induced EMT activity by up-regulating Snail, which promoted tumor metastasis. Decreased expression of FOXO3a was an independent prognostic factor for metastasis of ccRCC (Ni et al., 2014). Previous study has demonstrated that MUC1 promoted EMT in renal carcinoma through Wnt/ $\beta$ -catenin pathway and interaction with SNAIL promoter. Results revealed that interaction of MUC1 and  $\beta$ -catenin increased SNAIL transcriptional activity. Expressions of MUC1 and SNAIL were overexpressed in sarcomatoid type of RCC (Gnemmi et al., 2014). Pathway reconstruction of EMT in RCC obtained from the previous studies is illustrated in Figure 25.

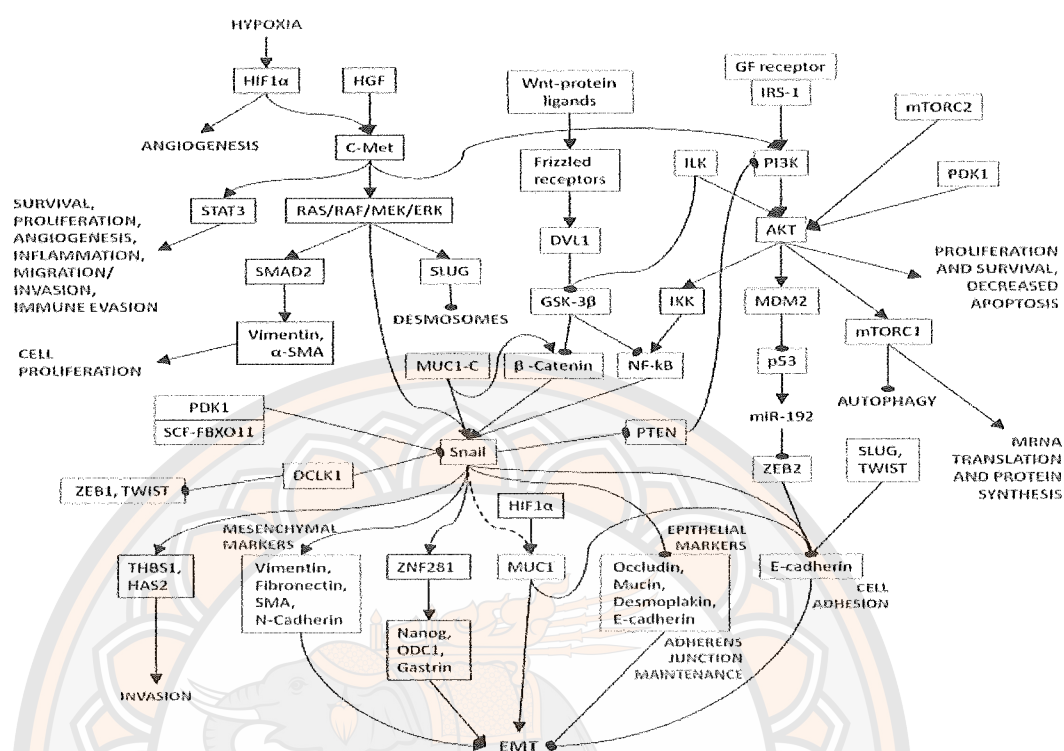


**Figure 18 Signaling pathway of EMT in RCC (Solid line means a direct interaction. Dashed line means an indirect interaction)**

Source: Piva et al. 2016



## AT-rich interactive domain-containing protein 1A (ARID1A)

### 1. SWI/SNF complexes

The human SWI/SNF chromatin remodeling complexes (Switch/Sucrose NonFermentable) are composed of 14 subunits encoded by 26 genes. They are categorized into core subunits (four proteins), accessory subunits (eight proteins), and specific subunit (one significant protein) (Figure 23). The signature subunits are mutually exclusive in different species and giving arrays, BAF (BRM/BRG1-associated factor) contained BAF250/ARID1 and PBAF (Polybromo-associated BAF) contained BAF180/PBRM, BRD7 and BAF200/ARID2 (Ruijtenberg & van den Heuvel, 2016). ARID1A (AT-rich interactive domain-containing protein 1A) is an exclusively signature subunit of the BAF complex of human SWI/SNF chromatin remodeler. The complex plays a crucial role in many cellular processes, including cell growth, differentiation-specific cell type, and cell proliferation. The emerging role of ARID1A involved in tumor suppressor has been reported by Wu et al. in 2014. In cancer, ARID1A had functions as gatekeeper and caretaker for regulating cell cycle progression, and preventing genomic instability (R.-C. Wu, Wang, & Shih, 2014).

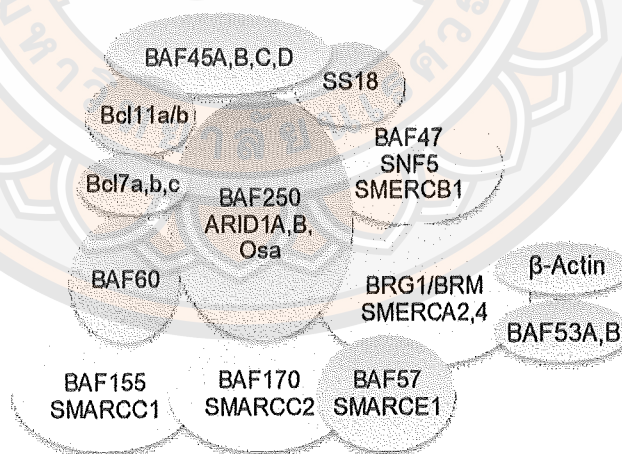


**Figure 19 Protein components of BAF complexes (BAF complexes consist of core subunits (yellow), accessory (blue), and signature subunits (red))**

**Source:** Modified from Ruijtenberg, & Van Den Heuvel, 2016

## 2. Structure of ARID1A domain

ARID (A-T Rich Interactive Domain) family comprises of five-teen isoforms in humans, that each isoform contains a 100-amino acid specific to DNA-binding ARID domain. ARID family are categorized into seven subclasses, including ARID1, ARID2, ARID3, ARID4, ARID5, JRID1, JRID2 that share variant residue on their sequences (Figure 27A) (Patsialou, Wilsker, & Moran, 2005). ARID1 consists of two distinct proteins are ARID1A and ARID1B, which share about 80% amino acid homology on the ARID domain. Function of ARID domain on ARID1A has selectively binding to AT-rich of DNA site. In addition, ARID1A contains glutamine-rich regions and several LXXLL motifs on C terminal region that generally interact with nuclear hormone receptors, particularly the glucocorticoid receptor (Figure 27B). *In vitro*, BAF250 stimulates transcriptional activation of the glucocorticoid receptor (GR), and the transcriptional activation was decreased when the C-terminal region (LXXLL motif absent) of BAF250 was deleted (Nie et al., 2000).

*AT-rich interactive domain-containing protein 1A (ARID1A)* gene is located on chromosome 1p36.11 (Figure 25), which is found frequently deleted in human cancers (Bagchi, & Mills, 2008). ARID1A gene consists of by 20 exons spanning 86,08 Mb (<http://atlasgeneticsoncology.org>) and encodes two functionally identical 2285 and 2086 amino acid isoforms, molecular weight was 250 kDa. Levels of ARID1A mRNA and protein were identified in most human tissues (<https://www.proteinatlas.org>). Expression of ARID1A protein is highly found in brain, lymph node, bone marrow, thymus, tonsil, urinary bladder, cervix, uterine, endometrium, placenta and skin. High/moderate expression of ARID1A protein was found in the glomerular cells and tubular epithelial cells of kidneys (Figure 29A). Levels of ARID1A mRNA have been reported by mean of transcripts per million (TPM) (Figure 29B).

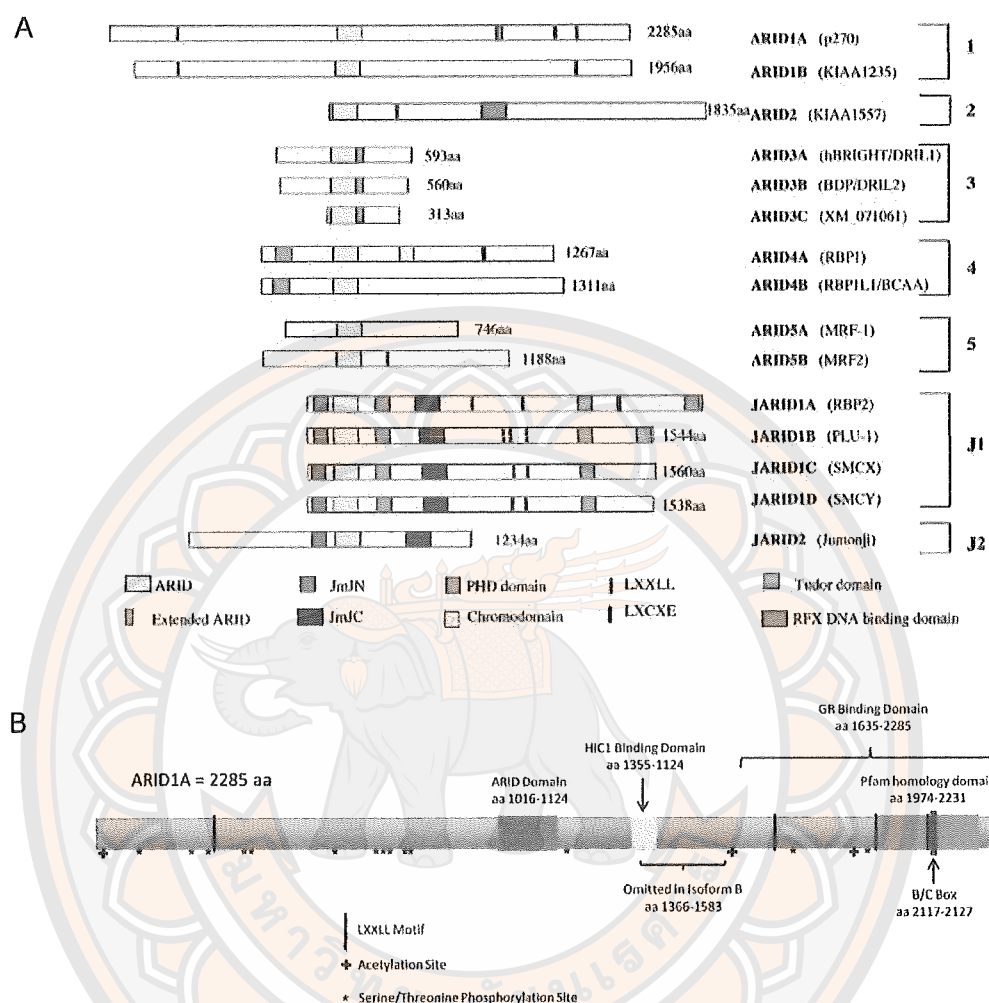


**Figure 20 Genome sequences of human ARID family (A) Genome sequences of 15 proteins in the human ARID family, B) Similar domains and the difference between ARID1A and ARID1B)**

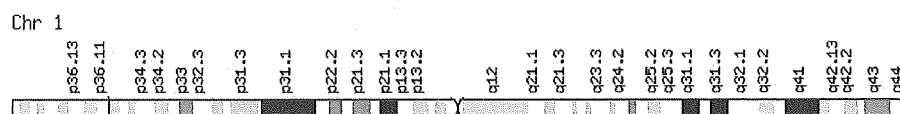


**Figure 21 Location for ARID1A gene on chromosome (red line)**

**Source:** Gene cards on human gene database. Accessed from <https://www.genecards.org/cgi-bin/carddisp.pl?gene=ARID1A> on date 10 June 2018

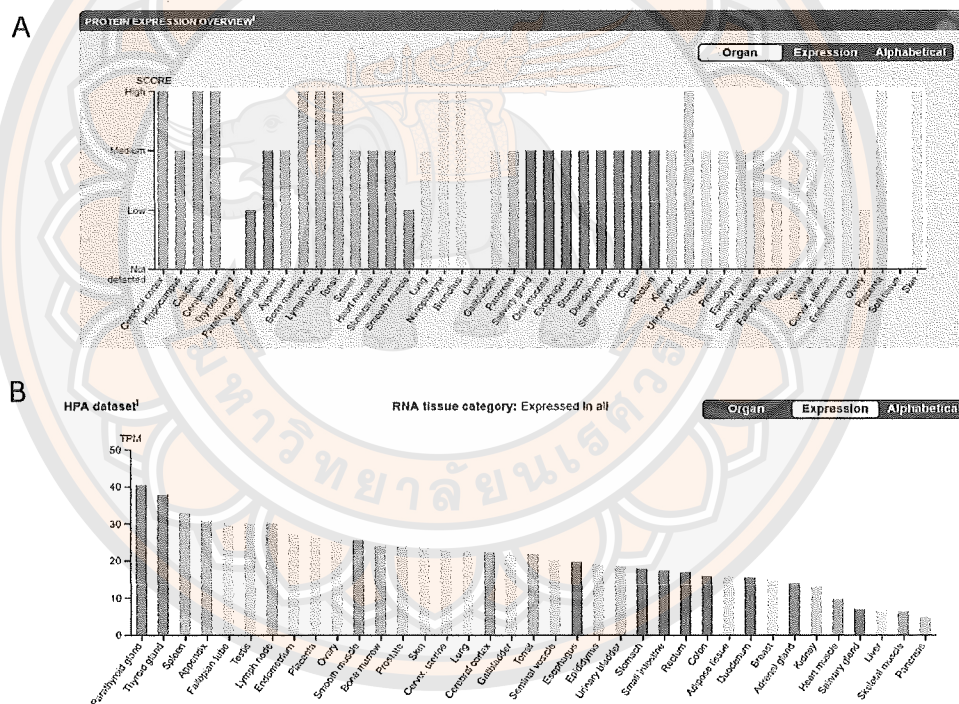


**Figure 22 Protein and mRNA expressions of ARID1A in human organs (A) Protein expressions of ARID1A. B) mRNA expressions of ARID1A)**

**Source:** The human protein atlas. Accessed from <https://www.proteinatlas.org/ENSG00000117713-ARID1A/tissue> on date 10 June 2018



ARID1A is a large nucleocytoplasmic protein and expressed in almost all tissues. Nuclear ARID1A is more unstable than its cytoplasmic counterpart because it is rapidly degraded by ubiquitin-proteasome (Guan, Gao, Wu, Wang, & Shih Ie, 2012). Expression of ARID1A protein is more fluctuated during the cell cycle than ARID1B. The accumulation of ARID1A protein is detected during the G0-G1 phase of the cell cycle, while a decrease of ARID1A occurs during the G2-S phase (Flores-Alcantar, Gonzalez-Sandoval, Escalante-Alcalde, & Lomeli, 2011). ARID1A protein interacts with numerous proteins. Six main classes of related proteins with ARID1A included 1) the SWI/SNF complex, 2) transcription factors, 3) coactivator/corepressor complexes, 4) histone-modifying enzymes, 5) ubiquitin ligase machinery, and 6) tumor suppressors (p53) (Figure 23) (J. N. Wu, & Roberts, 2013).

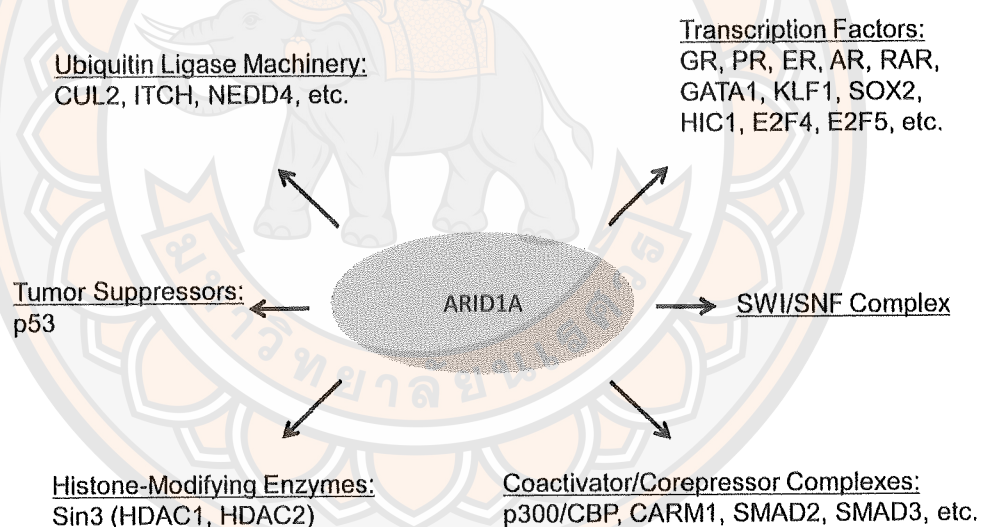


**Figure 23 Six main classes of co-worker proteins with ARID1A (1) The SWI/SNF complex; 2) Transcription factors; 3) Coactivator or corepressor complexes; 4) Histone modifying enzymes; 5) Ubiquitin ligase machinery, and 6) Tumor suppressors)**

**Source:** Wu, & Roberts, 2013



### 3. The evidence of ARID1A in cancers

Loss/decrease of ARID1A expression was frequently found in breast and kidney cancers (Wang et al., 2004). Somatic mutations of ARID1A lead to abnormal mRNA and truncated protein, which have been reported in several human cancer tissues, including ovarian clear cell carcinoma (57%) (Jones et al., 2010), uterine endometrioid carcinoma (40%) (Guan et al., 2011), and gastric carcinoma (30%) (Takeshima et al., 2015). Common mutations of *ARID1A* gene are frameshift insertions and deletions (Indels) and nonsense mutations (Jones et al., 2010). Consequently, disruptions of chromatin remodeling complexes such as *SMARCA2* and *SMARCA4* promoted cancer cell growth by these mutations (Takeshima et al., 2015).

ARID1A knockdown decreased apoptosis, but increased proliferation, invasion and migration in hepatocellular and breast cancer cells (He et al., 2015; Mamo et al., 2011). Regulation of ARID1A in apoptosis evasion remains unclear, but may involve inhibition of Fas-mediated cell death. Previous study reported that suppression of ARID1A by shRNA inhibited both Fas-Ab-induced Caspase-8 cleavage and mitochondrial potential reduction (Luo et al., 2008). Moreover, *ARID1A* mutation may lead to dysfunction of histone H2B ubiquitination. Restoration of histone H2B in the nucleus causes an aberration of chromatin remodeling proteins, which resulted in apoptosis evasion (Shigetomi et al., 2011).

Previous study in osteoblast precursor cell line (MC3T3) has been reported that ARID1A and ARID1B are counterpart proteins. ARID1A is accumulated in G0 and diminished throughout the S and G2/M phases of the cell cycle, subsequent completely diminished during mitosis, whereas ARID1B exhibited in comparative levels of all phases, even during mitosis (Flores-Alcantar et al., 2011). In addition, a cooperation of *ARID1A* and *ARID1B* can promote both cellular proliferation and cancer formation (Helming et al., 2014). Therefore, considering of ARID1A deficiency is essential for cellular proliferation. PI3K/(AKT) pathway is a particular pathway regulating cancer proliferation, which *PIK3CA* mutations more frequently harbored ARID1A-negative in ovarian clear cell adenocarcinomas (OCCC) and promotes cellular proliferation (Yamamoto, Tsuda, Takano, Tamai, & Matsubara, 2012). Previous study in gastric cancers tissues demonstrated that mRNA expression of ARID1A was significantly decreased whereas PI3KCA mRNA expression was

significantly increased in tumor area compared to normal area (Ibarrola-Villava et al., 2015). APC/ $\beta$ -catenin signaling may involve in uncontrolled proliferation of ARID1A knockdown cells. Mutation of *APC* in cancer promotes  $\beta$ -catenin translocation into the nucleus. It bound to TCF transcription factor and triggered gene controlled in cell proliferation (Kumar, 2007).

Recently, ARID1A knockdown in gastric cancer cells reduced E-cadherin expression, while vimentin and N-cadherin were strongly expressed. Loss of ARID1A leads to inhibition of SWI/SNF complexes binding to *CDH1* promoter (encoding gene of E-cadherin), resulting in reduction of E-cadherin transcription. It also contributes to  $\beta$ -catenin nuclear translocation. The complexes of  $\beta$ -catenin binding to LEF/TCF transcription factor are associated with metastatic GC cells by activation of the Wnt/ $\beta$ -catenin signaling pathway (Yan et al., 2014). On the other hand, Mathur et al. has reported that loss of ARID1A in *Mx1-cre; Arid1a<sup>fl/fl</sup>* mice exhibited invasive colon adenocarcinoma, which presented predominantly mucinous differentiation and tumor-infiltrating lymphocyte (Mathur et al., 2017).

ARID1A loss is associated with severe clinicopathological features including large nuclear size, large tumor size, higher Furman nuclear grade, higher pTNM stage (III and IV), and worse prognosis. They suggested that ARID1A IHC may serve as a prognosis marker of RCC that could be applied in laboratory practice (Lichner et al., 2013; Park et al., 2015). Molecular-targeted therapy was bringing the potential use of molecular inhibitor of the PI3K/AKT pathway in case of ARID1A mutation. The result in ovarian clear cell carcinoma (OCCC) showed that administration of sorafenib with PI3K/AKT pathway inhibitor in ARID1A mutation patients can inhibit proliferation of OCCC and endometrioid carcinoma (Bitler, Fatkhutdinov, & Zhang, 2015; Samartzis et al., 2014; Takeda et al., 2016).

#### 4. The evidence of ARID1A in RCC

Inactivation of the SWI/SNF chromatin remodeling complex has been studied in renal medullary carcinoma, clear cell RCC, rhabdoid RCC, chromophobe RCC, and papillary RCC. The promoter CpG islands of *PBRM1*, *KDM6A*, *KDM5C*, *ARID1A*, *SETD2*, and *BAP1* were unmethylated in ccRCC (Ibragimova, Maradeo, Dulaimi, & Cairns, 2013). Positive staining of BRM, PBRM1, ARID1A, CD10, vimentin, carbonic anhydrase IX (CA-IX), and AMACR were found in rhabdoid RCC, but INI1, BRG1, CK7, CD117, TFE3, and Cathepsin K were negative staining. In this study, they suggested that rhabdoid RCC may differentiate from ccRCC (Rao et al., 2014). Recently, circulating tumor DNA (ctDNA) profile of patients with metastatic RCC and changes across patients receiving first-line and later lines of therapy were assessed. First-line regimens included sunitinib, pazopanib, and bevacizumab, and postfirst-line regimens included everolimus, axitinib, cabozantinib, and nivolumab. Most frequent genes included *TP53* (35%), *VHL* (23%), *EGFR* (17%), *NF1* (16%), and *ARID1A* (12%). Difference of genomic alterations between postfirst-line and first-line were predominant in *TP53* (49% vs 24%) and *NF1* (20% vs 3%), while *ARID1A* was equivalent (13% vs 11%). Routine ctDNA assessment should be addressed during the therapeutic treatments of mRCC patients (Pal et al., 2017). The nuclear expression of ARID1A was evaluated ccRCC by immunohistochemistry. Decrease of ARID1A expression was significantly associated with the higher nuclear grade and higher pTNM stage. Patients with low expression of ARID1A had significantly shorter cancer-specific and progression-free survival. ARID1A expression was an independent prognostic factor for progression-free survival by Cox-regression model. Nuclear expression of ARID1A may serve as a new prognostic marker in ccRCC patients (Park et al., 2015). Decreased BAF250a protein were mostly found in ccRCC, but not observed in papillary RCC, chromophobe RCC, oncocytoma, and transitional cell carcinoma. Expression of BAF250a protein and ARID1A mRNA was correlated with tumor stage and grade. This study indicated that both the protein and mRNA levels of ARID1A were significant prognostic markers for ccRCC (Lichner et al., 2013).

## CHAPTER III

### RESEARCH METHODOLOGY

#### Cell culture

Madin-Darby Canine Kidney (MDCK) cell lines were cultured in complete growth medium (CMEM), which is Eagle's Minimum Essential Medium (MEM) (Gibco, Invitrogen Corp.; Grand Island, NY) supplemented with following constituents: 10% fetal bovine serum (FBS) (Gibco), 2 mM L-glutamine (Sigma; St.Louis, MO), and 1.2% penicillin G/streptomycin (Sigma). Cells were maintained in a humidified incubator at 37 °C and 5% CO<sub>2</sub> until they were approximately 80% confluent prior to subsequent siRNA transfection.

#### siRNA transfection

Cells were seeded onto six-well plates at a density of  $1 \times 10^5$  cells/mL in antibiotic-free MEM supplemented with FBS until cells were 80% confluent. The transfected solutions A and B were prepared according to Santa Cruz Biotechnology manufacture's instruction. Solution A was prepared by adding 2 µL of commercial ARID1A siRNA (sc-45942; Santa Crus Biotechnology, CA, USA) in 100 µL Opti-MEM reducing serum medium (Gibco; lifetechnologies) to make a final concentration of 20, 40, 80 pmol/ml. Solution B was prepared by adding 2 µL of Lipofectamine@ 2000 reagent (Invitrogen; Thermo Fisher Scientific, CA, USA) in 100 µL Opti-MEM. Thereafter, both solutions were mixed together in an eppendorf tube by gently pipetting and incubated at room temperature for 45 minutes. Subsequently, 800 µL of Opti-MEM were added into the mixture and transfer to target cells in six-well plates. The transfected solution was discarded after 5 hours of transfection and replaced with 2 mL CMEM. The transfected cells were maintained at 37 °C and 5% CO<sub>2</sub> for 48 hours. Control siRNA (sc-37007; Santa Crus Biotechnology, CA, USA) was added to make solution A for the siControl group.



### Assessment of cell viability by trypan blue staining

Monolayer of cells was harvested after the siRNA transfection procedure using 0.1% trypsin in 2.5 mM EDTA/PBS for 5 minutes. The dissociation of cells was observed and the trypsinization was stopped using CMEM. Thereafter, the cell suspension was placed in a conical tube and centrifuged at 300 ×g for 3 minutes and the supernatant discarded. The cell pellet was mixed with CMEM containing 0.4% trypan blue dye (Thermo Fisher Scientific). The number of total cells and non-viable cells were counted under the Olympus CKK41 inverted microscope (Olympus; Tokyo, Japan) using a hemocytometer. The percentages of cell death and cell viability were calculated using following equations (Aluksanasuwan, Sueksakit, Fong-Ngern, & Thongboonkerd, 2017):

$$\text{Cell death (\%)} = (\text{Number of dead cell} / \text{Number of total cell}) \times 100.$$

$$\text{Cell viability (\%)} = (\text{Number of dead cell} / \text{Number of total cell}) \times 100.$$

### Immunofluorescence (IF) staining and antibodies

Coverslips containing a cell monolayer were washed with PBS<sup>+</sup> and fixed in 3.7% (v/v) formaldehyde in PBS for 15 minutes and rinsed 3 times with PBS<sup>+</sup>. Cell permeability was increased by adding 0.2% Triton X-100 in PBS for 15 minutes. The primary antibodies included mouse monoclonal anti-ARID1A (PSG3) (sc-32761; Santa Cruz Biotechnology), rabbit polyclonal anti-E-cadherin (sc-7870; Santa Cruz Biotechnology), mouse monoclonal anti-ZO1 (Invitrogen), mouse monoclonal anti-vimentin (sc-73258; Santa Cruz Biotechnology), mouse monoclonal anti-fibronectin (sc-56391; Santa Cruz Biotechnology), and rabbit polyclonal anti-SNAI1 (sc-28199; Santa Cruz Biotechnology). All primary antibodies were diluted 1:250 in 1%BSA/PBS and incubated at 4 °C overnight, and then further incubated at 37 °C for 3 hours. The secondary antibodies included goat anti-mouse Alexa fluor 488 (dilution 1:500 in 1%BSA/PBS; Invitrogen; Burlington, Canada) and donkey anti-rabbit Alexa fluor 555 (dilution 1:500 in 1%BSA/PBS; Invitrogen), were applied to conjugate with the corresponding primary antibody at 37 °C for 2 hours. Hoechst dye (dilution 1:1,000 in PBS; Invitrogen; Paisley, UK) was used to stain the nucleus at 37 °C for 2 hours. Finally, the coverslips were mounted on glass slides using 50% glycerol/PBS. The immunofluorescent signals of protein staining were observed and captured under



Nikon Eclipse 80i fluorescence microscope (Nikon; Tokyo, Japan). The intensity of fluorescent dyes was measured in at least 100 cells from ten randomized images for each group using NIS-Elements D V.4.11 program (Nikon).

**Table 11 The details of primary and secondary antibodies used in the *in vitro* study**

Primary antibody	Corporation	Secondary antibody	Corporation
<b>To investigate the expression of ARID1A protein</b>			
Mouse monoclonal anti-ARID1A (PSG3)	Santa Crus Biotechnology	Goat anti-mouse Alexa fluor 488	Invitrogen
<b>To investigate the expression of epithelial proteins</b>			
Rabbit polyclonal anti-E-cadherin	Santa Crus Biotechnology	Donkey anti-rabbit Alexa fluor 555	Invitrogen
Mouse monoclonal anti-ZO1	Invitrogen	Goat anti-mouse Alexa fluor 488	Invitrogen
<b>To investigate the expression of mesenchymal proteins</b>			
Mouse monoclonal anti-vimentin	Santa Crus Biotechnology	Goat anti-mouse Alexa fluor 488	Invitrogen
Mouse monoclonal anti-fibronectin	Santa Cruz Biotechnology	Goat anti-mouse Alexa fluor 488	Invitrogen
<b>To investigate the expression of SNAIL transcription factor proteins</b>			
Rabbit polyclonal anti-SNAI1	Santa Cruz Biotechnology	Donkey anti-rabbit Alexa fluor 555	Invitrogen

### Assessment of cell morphology and nuclear size

Morphological changes in MDCK cells were observed under a Nikon Eclipse Ti inverted microscope (Nikon; Tokyo, Japan), and images captured after completed transfection. Thereafter, the spindle index and nuclear size of cells were measured and analyzed by NIS-Elements D V.4.11 (Nikon) at least 100 cells from 10 random high power field (HPF) images for each group. The Spindle index was calculated using following equation (Thanomkitti, Fong-Ngern, Sueksakit, Thuangtong, & Thongboonkerd, 2018):

$$\text{Spindle index} = \text{Length of each cell} / \text{Width of each cell}.$$

### Scratch wound assay

The scratch wound assay was performed to test the migrating activity of cells (Manissorn, Khamchun, Vinaiphat, & Thongboonkerd, 2016; Peerapen, Chaiyarit, & Thongboonkerd, 2018). Briefly, cells were plated on six-well plates by seeding  $2 \times 10^5$  cells/well. Cells were transfected using the siRNA transfection procedure as described above. A sharp and straight scratch was generated on the cell monolayer by using a 200  $\mu\text{L}$  pipette tip. After carefully aspirate the cell debris with PBS, the culture plates were placed into a Nikon BioStation CT (Nikon Corporation; Tokyo, Japan) at 37 °C with 5%  $\text{CO}_2$ . Each scratch wound was automatically captured every 3 hours after initial scratch assay (0, 3, 6, 9, 12 time points). Wound width was measured from a total of 10 points of the wound width for each group using Tarosoft@ Image framework v.0.9.6 software (Nikon Corporation; Tokyo, Japan). Cell migratory activity at each time point was calculated using the following formula:

$$\text{Migratory activity (\%)} = \frac{[\text{Wound width at T0} - \text{Wound width at Tn}]}{[\text{Wound width at T0}]} \times 100.$$

Note: Tn is the indicated time point

### Measurement of aggregated cells by hanging drop assay

The hanging drop assay was performed as a previous study (Foty, 2011; Toret, D'Ambrosio, Vale, Simon, & Nelson, 2014). After siRNA transfection, MDCK cells were harvested and counted with a hemocytometer to make a final concentration of  $2.5 \times 10^5$  cells/mL. Cell suspension was dropped, at approximately 20  $\mu$ L/drop, on the upper dish of 100-mm tissue culture dishes (30 drops/dish), and then the upper dish was inverted over 5 ml of CMEM in the bottom dish for humidification. The dishes were incubated for 24 hours. A total of 100 drops for each group were harvested by 1,000  $\mu$ L pipette tip and mixed with 5 mL CMEM. The spheroid formation was observed under a Nikon Eclipse Ti inverted microscope (Nikon; Tokyo, Japan). The size of aggregated cells was measured using NIS-Elements D V.4.11 program (Nikon).

### Bioinformatics analysis

The mutated genes commonly found in kidney cancers were analyzed through the Genomic Data Commons (GDC) database (<http://portal.gdc.cancer.gov/>). The Cancer Genome Atlas (TCGA) projects related to kidney cancers were TCGA-KIRC (kidney renal clear cell carcinoma), TCGA-KIRP (kidney renal papillary cell carcinoma), TCGA-KICH (kidney chromophobe) and TCGA-SARC (sarcoma), which was accessed on October 11, 2019. Top twenty mutated genes of RCC were recorded. Additionally, the profile of *ARID1A* mutations along the protein-coding regions and their frequency were investigated. Moreover, Kaplan-Meier curve and the log-rank test were conducted to estimate the overall survival of patients with *ARID1A* mutation compared to those without *ARID1A* mutation.

### **Human ethic approval**

The study protocol involving human subjects was approved by the Human Ethic Review Board of Sawanpracharak Hospital (approval no. 47/2560) and by Naresuan University Ethical Committee for Human Research (NU-IRB) (approval no. 0489/61; COE no. 115/2018) and was conducted in accordance with the Declaration of Helsinki Principles (see Appendix). Twenty-six tissue FFPE samples were used in this study. All patients were diagnosed with RCC and submitted of their tissue biopsy to the unit of pathology, Sawan Pracharak hospital during 2013 - 2017.

### **Inclusion and exclusion criteria**

1. FFPE blocks must obtain from RCC patients who submitted their biopsy during 2013 – 2017 because long-term storage of FFPE blocks may affect by proteolysis. Protein expression may be unexpectedly reduced (Nuovo et al., 2013).
2. FFPE blocks must obtain from RCC patients whose ages are ranging from 45 – 95 years old. Young age onset of RCC provides a clue to a possible hereditary etiology of RCC. Previous study showed that the mean and median of age at diagnostic time of hereditary RCC syndromes were 39.9 and 37 years (Shuch et al., 2014).
3. Relevant demographic and pathological information of patients could be prompt to access.
4. There should have one more available FFPE blocks to prevent any possible problem of inadequate samples for further diagnosis and investigation.
5. Each FFPE block must be sufficient for section at least 10-15 sections of 5- $\mu$ m-thick section.

**Exclusion criteria**

1. Patients diagnosed with hereditary RCC syndromes and age were less than 45 years old were excluded.
2. Patients diagnosed with cancer of unknown primary (CUP) were excluded.
3. Patient who was diagnosed with RCC during pregnancy was excluded.
4. Histological and/or immunohistochemical investigation cannot be clarified by pathologist or researcher.

**Storage and data collection**

RCC pathological subtypes for each case were diagnosed by pathologist. Representative H&E slides, demographic and pathological information for each were provided. All slides were labeled using research code, corresponding with of the FFPE blocks. The confidential data of patient e.g. name, identification number, and hospital number were blinded to protect the information of patients. FFPE blocks were transferred under control temperature at 4 °C, and then collected at -20 °C until performing experiments. H&E slides were stored in the RCC slide boxes. All of information were scanned and recorded securely on password protected computer of researcher. Flowchart of the patient tissue's recruitment and collection was represented in Figure 24



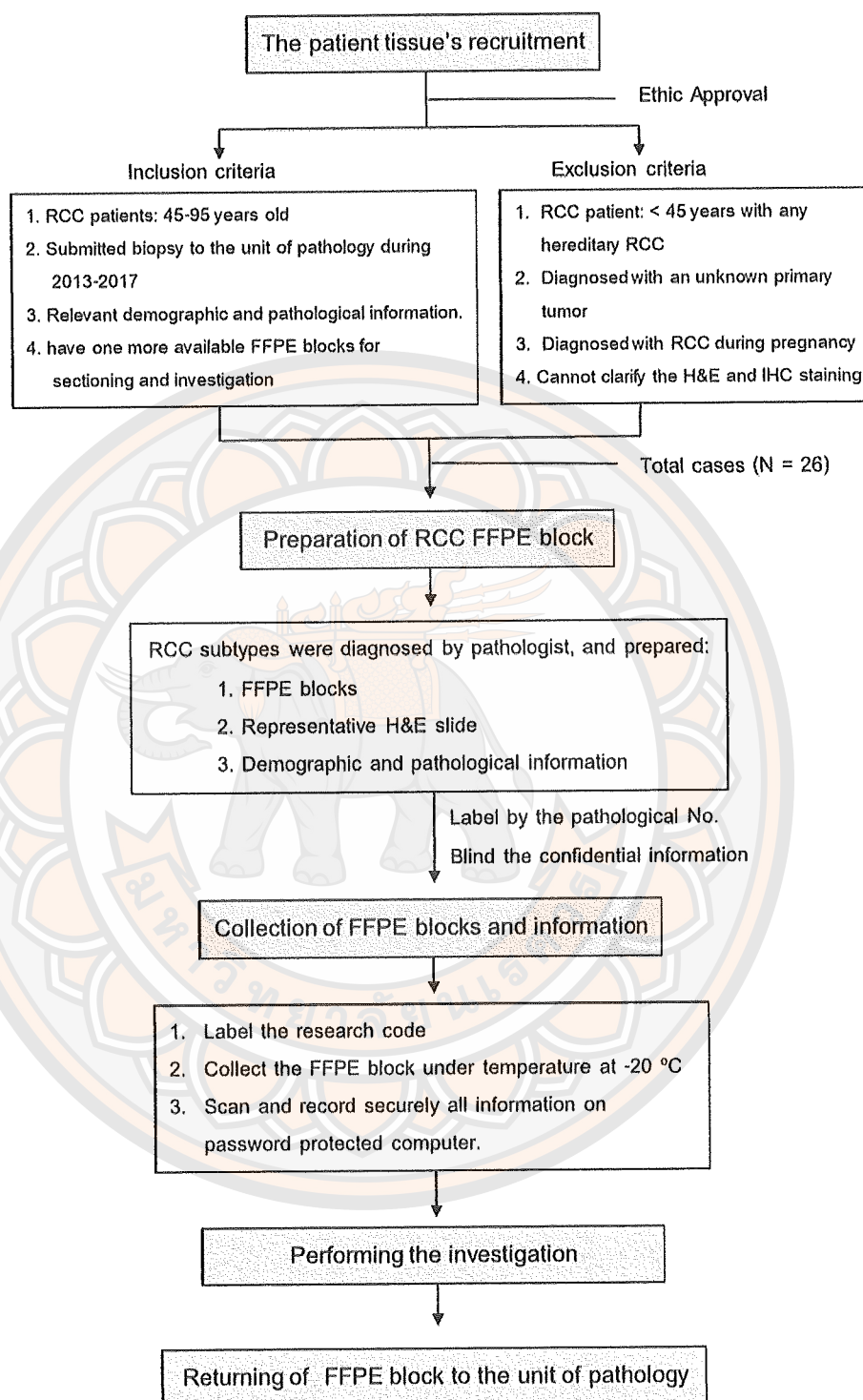


**Figure 24 Flowchart of the patient tissue's recruitment and collection**

### **Patient tissue samples and the clinicopathological information**

Twenty-six samples of formalin fixed, paraffin embedding (FFPE) of cancer and adjacent non-cancer areas were collected. The specimens included 6 clear cell RCC, Fuhrman nuclear grade I (ccRCC, GI), 11 clear cell RCC, Fuhrman nuclear grade II (ccRCC, GII), 6 chromophobe RCC (chRCC), 2 papillary RCC (pRCC), and 1 sarcomatoid RCC (sRCC). Clinical data, i.e., age, gender, cancer laterality, pathological subtype and staging (TNM and AJCC systems), tumor mass diameter, tumor invasion, metastasis, recurrence and other complications, were extracted and analyzed.

### **Histological study**

Hematoxylin and eosin (H&E) staining was performed using the standardized protocol. Adjacent non-cancer and cancer FFPE blocks were sectioned at 4- $\mu$ m-thick section. Tissue slides were deparaffinized in xylene (RCI labscan) and rehydrated in serial alcohols for 5 minutes per each. Next, hematoxylin and eosin dye (C.V. Laboratories CO., LTD.) were applied, and then dehydrated by serial alcohols and cleared in xylene (RCI labscan) for 5 minutes per each. Finally, tissue slides were covered by cover-slip and Permount (Fisher Scientific). Histology of adjacent non-cancer and cancer areas were observed and photographed the using the Olympus BX50 microscope (Olympus; Tokyo, Japan). RCC subtypes and Fuhrman nuclear grading were confirmed (Corti et al., 2006; Fuhrman, Lasky, & Limas, 1982).

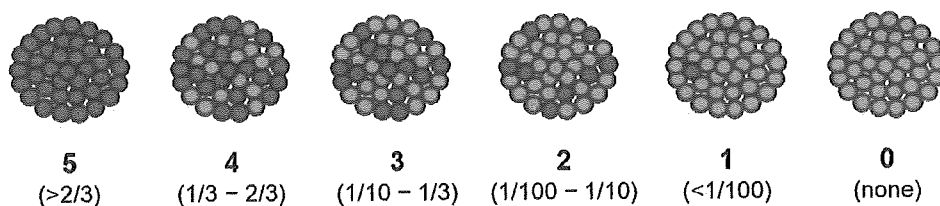
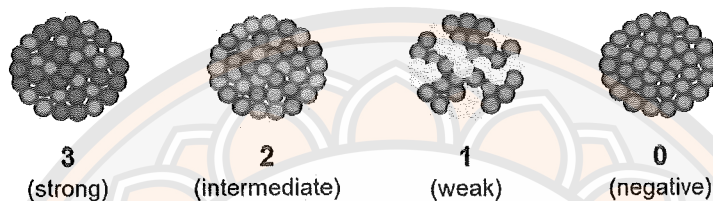
### **Immunohistochemistry**

Immunohistochemistry was performed on both cancer and adjacent non-cancer tissues. Briefly, 4- $\mu$ m-thick tissue sections were incubated in a hot-air oven at 60°C for 1 h, deparaffinized in xylene, and rehydrated in graded series of ethanol/water. Thereafter, the tissue slides were immersed in 0.3% Triton-X in PBS-T (PBS containing 0.3% Tween-20; pH 7.4) for 40 minutes and then washed twice with PBS-T. Antigen retrieval was performed using heat-induced epitope retrieval (HIER) protocol with a buffer containing 10 mM Tris-Base, 1 mM EDTA and 0.05% Tween-20 (pH 8.0) at 97°C for 30 minutes. The tissue slides were then cooled down at 25°C for 20 minutes, washed twice with PBS-T, and incubated with 3% H<sub>2</sub>O<sub>2</sub>/methanol for 10 minutes. Non-specific bindings were blocked with 5% BSA at 25°C for 30 minutes. The sections were incubated with rabbit polyclonal anti-ARID1A antibody (Sigma-Aldrich; St. Louis, MO) (diluted 1:400) at 25°C overnight. The sections were incubated with biotinylated goat anti-rabbit secondary antibody (Dako Corp.; Kyoto, Japan) (diluted 1:200) at 37°C for 2 hours. After washing with PBS-T three times, the sections were incubated with HRP-conjugated streptavidin (Dako Corp.) (diluted 1:200) at 25°C for 1 hour. The immunoreactive protein was colorized with DAB (3, 3'-diaminobenzidine) peroxidase substrate (Vector Laboratories; Burlingame, CA) for 4 minutes. The section stained without primary antibody was used as a negative control, and positive control slide was normal colon sample. The stained sections were observed and photographed under an Olympus BX50 light microscope (Olympus; Tokyo, Japan).

### Quantitative analysis of ARID1A protein expression

Three randomized locales per slide were evaluated by the pathologist and the researcher in a double-blind fashion. Allred scoring is commonly used for quantitative analysis of estrogen/progesterone receptor in breast cancer (Qureshi, & Pervez, 2010). Investigation of ARID1A protein expression was evaluated in cancer and adjacent non-cancer tissues using Allred scoring. Details of Allred scoring were summarized in Figure 25. Briefly, proportional score (PS) is proportion of the ARID1A-stained cells to total cells, and intensity score (IS) is intensity of ARID1A protein. The proportional score ranged from no ARID1A-stained cells to over than 2/3 ARID1A-stained cells (score = 0-5) in each field, whereas the intensity score ranged from negative to strong staining (score = 0-3) (Figures 25A and 25B). Summation of the proportional and intensity scores were finally graded as negative, weak, moderate, and strong expression (Figure 25C). In case of disagreement between two investigators, the scores were reassessed to find out the correct score.

In addition, levels of ARID1A protein expression in various parts of the nephron, including glomerulus (Glom), proximal convoluted tubule (PCT), distal convoluted tubule (DCT) and collecting duct (CD), were evaluated in the adjacent non-cancer areas of ccRCC (grade I) compared to ccRCC (grade II). The intensity of ARID1A was quantitated from at least 100 cells per each part of a nephron using Image J analysis software (<http://fiji.sc/Fiji>). Briefly, picture was adjusted using the color deconvolution algorithm “H DAB” to separate images of hematoxylin and DAB staining. The intensity of ARID1A expression was calculated using DAB image, corresponding to the original figure. Mean gray value of ARID1A expression in all nuclei was calculated to optical density (OD) by the following formula:  $OD = \log_{10} (\text{Max intensity} / \text{Mean intensity})$ , where max intensity = 255 for 8-bit images (<https://imagej.nih.gov/ij/docs/menus/analyze.html>).

**A Proportional score (PS)****B Intensity score (IS)****C**

Allred score = PS + IS (0 – 8)	
Score	Grading
6 - 8	Strong
4 - 5	Moderate
2 - 3	Weak
0 - 1	Negative

**Figure 25** The details of Allred score (A) Proportional score (ranged from 0 to 5). B) Intensity score (ranged from 0 to 3). ARID1A-positive staining is illustrated with shaded brown color, whereas negative staining is indicated with blue color. C) Formulation of Allred score (ranged from negative to strong))

**Source:** Modified from Qureshi, & Pervez, 2010



### **Association of ARID1A protein expression with clinicopathology and progression-free survival**

After grading by the Allred score, expressions of ARID1A protein were categorized into “negative to weak expression” and “moderate to strong expression”. Thereafter, associations of ARID1A expression with clinicopathology and five-year progression-free survival were investigated.

### **Statistical analysis**

All *in vitro* experiments were performed in triplicate for each condition. All quantitative data were presented as mean  $\pm$  SEM unless stated otherwise. Comparisons of the data between the paired samples were done by paired Student's t-test, whereas comparisons of the unpaired samples were done by unpaired Student's t-test or by Mann-Whitney test (when the data did not distribute normally). The association between ARID1A protein expression and clinicopathology was analyzed by Pearson's chi-square and Fisher's exact tests. The association between ARID1A protein expression and progression-free survival was evaluated by Kaplan-Meier analysis and log-rank test. All statistical analyses were done through the SPSS software (version 16.0) (SPSS; Chicago, IL),  $p$  value  $< 0.05$  was considered statistically significant.

## CHAPTER IV

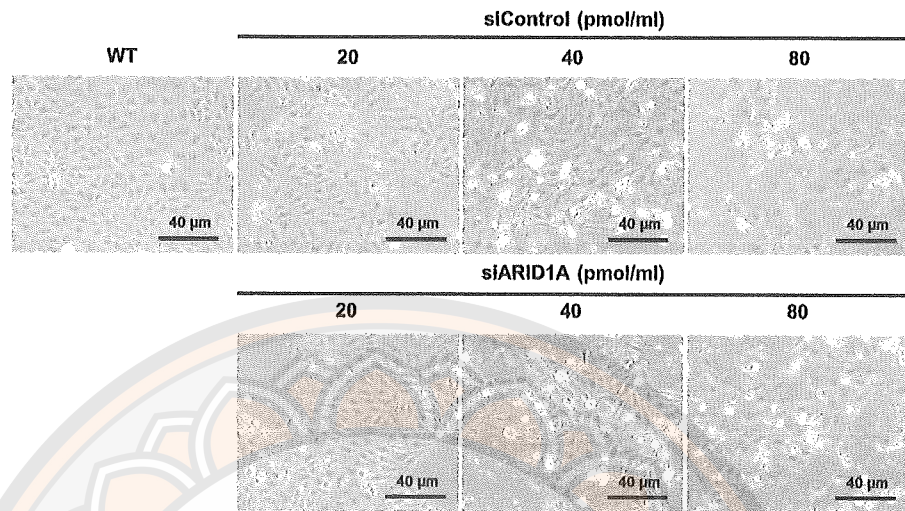
### RESULTS

#### **Determination of optimal dose of siARID1A**

To determine an optimal dose of siARID1A for transfection, we evaluated morphological change, total cell number, cell death and cell viability of MDCK cells with varied doses of siARID1A. Morphology of wild-type MDCK cells at 80% confluent cells was polygonal shape. After transfection with 20 pmol of siControl and siARID1A, the transfected cells were changed from polygonal the spindle shape when compared to wild-type MDCK cells (Figure 26A). The transfected cells were obviously seen spindle shape at 40 pmol of siControl and siARID1A when compared to wild-type cells, but transfected cells were distorted in shape at 80 pmol (Figure 26A). We stained the cells using trypan blue staining and calculated total cell number, cell death and cell viability. The results showed that transfection protocol effects to total cell number, cell death and cell viability when compared to wild-type cells. The total cell number and cell viability were gradually decreased, whereas cell death number was increased at 20, 40, and 80 pmol of siControl and siARID1A, respectively (Figure 26B and 27). All data were represented in Table 12.

These results showed that transfection by 80 pmol of siARID1A had severe cytotoxic effects on cell morphology and cell death, while 20 pmol of siARID1A did not effect to transformation of transfected cells to the mesenchymal phenotype. Therefore, 40 pmol of siARID1A was used in this study for subsequent experiments to investigate the roles of ARID1A on EMT in MDCK cells.

A



B

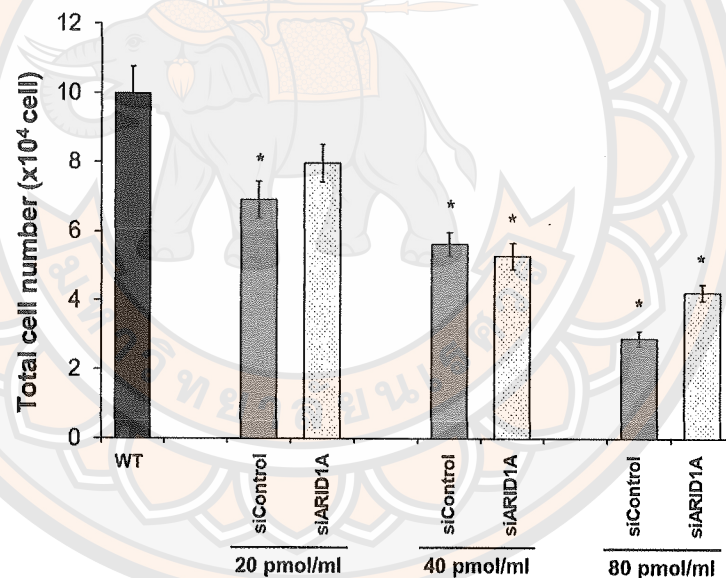
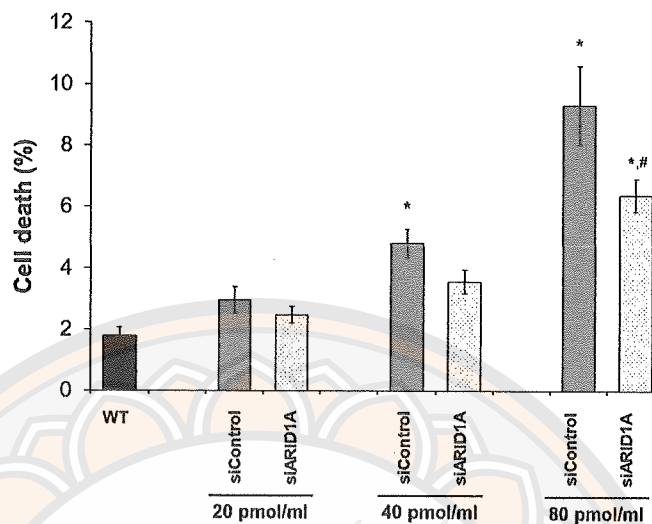


**Figure 26 Morphology and total cell number of MDCK cells after transfection with various doses of siARID1A (A) The transfected cells were obviously seen spindle shape at 40 and 80 pmol of both siControl and siARID1A when compared to wild-type cells. B) The total cell number were gradually decreased at 20, 40, and 80 pmol of siControl and siARID1A when compared to wild-type cells. Each bar was represented as mean  $\pm$  SEM. \* $p$  < 0.05 when compared to wild-type (WT))**

A



B

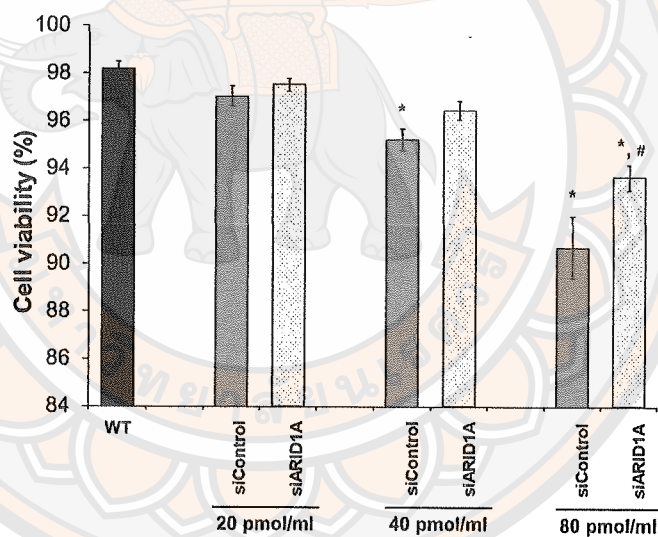


**Figure 27** Percentage of cell death and cell viability of MDCK cells after transfection with various doses of siARID1A (A) Cell death (%) was increased at 20, 40, and 80 pmol of siControl and siARID1A, respectively. B) Cell viability (%) was gradually decreased at 20, 40, and 80 pmol of siControl and siARID1A, respectively. \* $p < 0.05$  when compared to wild-type (WT); # $p < 0.05$  when compared to siControl)

**Table 12 Total cell number, cell death and cell viability of MDCK cells after transfection with various doses of siARID1A**

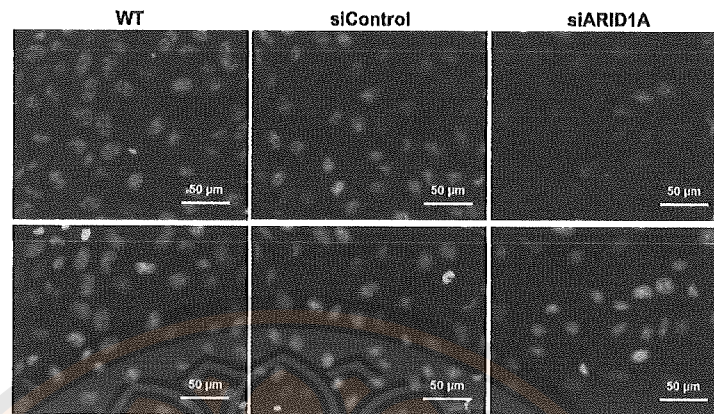
Parameter/ Groups	WT	20 pmol/ml		40 pmol/ml		80 pmol/ml	
		siControl	siARID1A	siControl	siARID1A	siControl	siARID1A
Total cell number ( $\times 10^4$ cell)	9.99 $\pm$ 0.78	6.9 $\pm$ 0.53	7.96 $\pm$ 0.55	5.63 $\pm$ 0.34	5.29 $\pm$ 0.38	2.9 $\pm$ 0.22	4.23 $\pm$ 0.23
Cell death (%)	1.79 $\pm$ 0.27	2.96 $\pm$ 0.43	2.48 $\pm$ 0.27	4.80 $\pm$ 0.47	3.56 $\pm$ 0.39	9.31 $\pm$ 1.30	5.37 $\pm$ 0.54
Cell viability (%)	98.21 $\pm$ 0.27	97.04 $\pm$ 0.43	97.52 $\pm$ 0.27	95.20 $\pm$ 0.47	96.44 $\pm$ 0.39	90.69 $\pm$ 1.30	93.63 $\pm$ 0.54

#### **Efficacy of ARID1A knockdown by siRNA transfection**

To determine efficacy of ARID1A knockdown, MDCK cells were transfected with 40 pmol siARID1A. The fluorescent images showed nuclear loss of ARID1A protein in siARID1A group compared with those in wild-type and siControl groups (Figure 28A and B). The means of fluorescent intensity of ARID1A protein in wild-type, siControl, and siARID1A groups were 27.53 $\pm$ 0.62, 25.68 $\pm$ 0.45, and 15.83 $\pm$ 0.27, respectively. The results showed that intensity of ARID1A protein had a significant decrease in siControl and siARID1A groups compared with those in wild-type group ( $p < 0.05$ ). In addition, intensity of ARID1A expression displayed significant decrease in in siARID1A group compared with those in siControl group ( $p < 0.05$ ) (Figure 29).



A



B

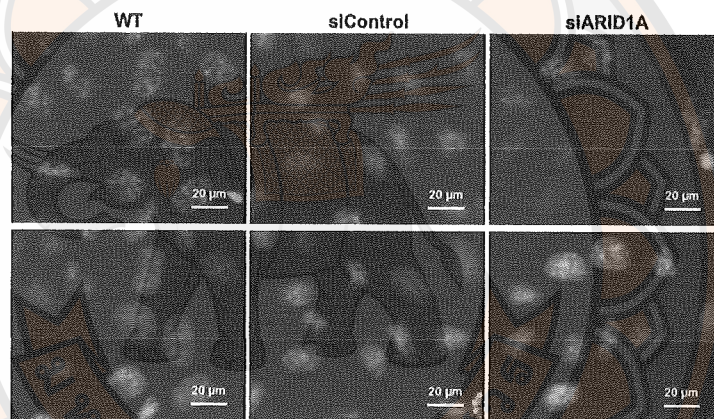


**Figure 28 Immunofluorescent staining of nuclear ARID1A protein (A) The siARID1A group showed nuclear losing of ARID1A protein (green color, upper panel) compared with those in wild-type (WT), and siControl groups. Nuclei of MDCK cells were stained with Hoechst dye (blue color, lower panel) (original magnification,  $\times 200$ ). B) High magnification of fluorescent images (original magnification,  $\times 400$ ))**

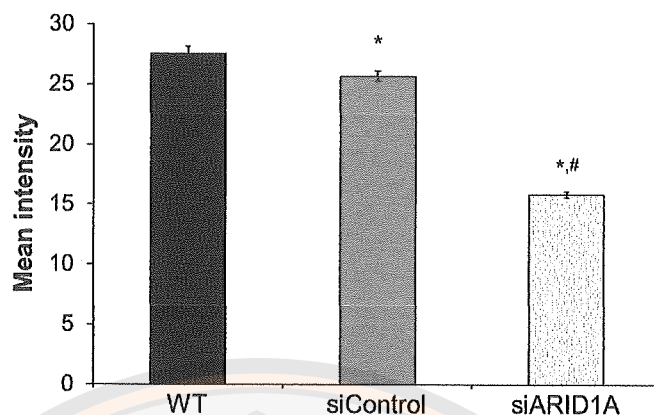


**Figure 29** The quantitative data of fluorescence intensity of the ARID1A expression (Intensity of ARID1A expression showed a significant decrease in siARID1A group compared with those in wild-type and siControl groups. Each bar was represented as mean  $\pm$  SEM (\* $p < 0.05$  when compared to wild-type (WT); # $p < 0.05$  when compared to siControl))

#### **Effects of ARID1A knockdown on total cell number, cell death and cell viability**

We studied effects of ARID1A knockdown on total cell number, cell death and cell viability in MDCK cells by trypan blue staining. Total cell number of the siARID1A group ( $119.7 \pm 5.5$ ) was higher than in wild-type ( $109.2 \pm 6.7$ ) and siControl groups ( $114.7 \pm 1.3$ ). However, there is no statistically significant difference in total cell number among the three groups (Figure 30A). The percentage of cell death showed a significant decrease in siARID1A group ( $10 \pm 0.9\%$ ) compared with the wild-type ( $14 \pm 0.7\%$ ), and siControl groups ( $14 \pm 1.5\%$ ) ( $p < 0.05$ ) (Figure 30B). The percentage of cell viability in the siARID1A group ( $90 \pm 0.9\%$ ) was significant higher than in the wild-type ( $86 \pm 0.7\%$ ), and siControl groups ( $86 \pm 1.5\%$ ) ( $p < 0.05$ ) (Figure 30C).

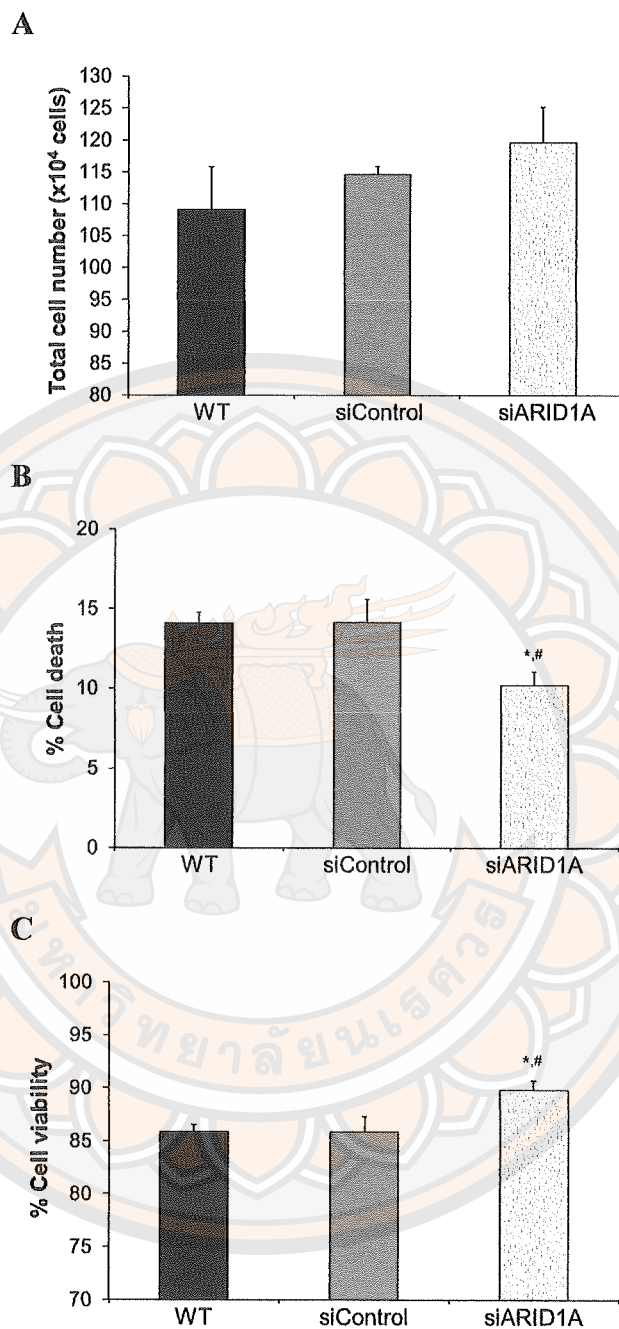


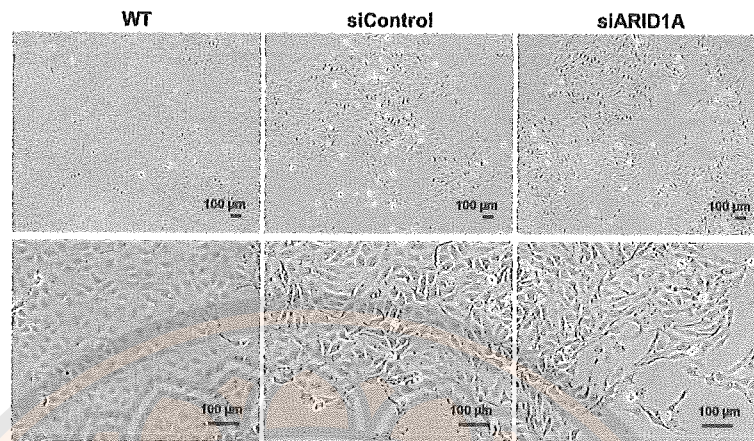
**Figure 30** The quantitative data of total cell number, cell death, and cell viability of MDCK cells after transfection with 40 pmol of siARID1A (A) Total cell number was significantly increased in siARID1A group. B) Cell death (%) was significantly decreased in siARID1A group. C) Cell viability was significantly increased in siARID1A group. Each bar was represented as mean  $\pm$  SEM ( $*p < 0.05$  when compared to wild-type (WT);  $\#p < 0.05$  when compared to siControl))

### Effects of ARID1A knockdown on cell morphology and nuclear size

To determine the effects of ARID1A knockdown on morphological changes, the morphology of MDCK cells was observed under the inverted microscope. Morphology of cells in siARID1A group was mostly found spindle-shaped and finger-like protrusion when compared with those in wild-type and siControl groups (Figure 31A). The spindle index at the end point of siRNA transfection of the siARID1A group ( $4.03 \pm 0.07$ ) was significantly higher than in the wild-type ( $1.67 \pm 0.03$ ) and siControl groups ( $2.41 \pm 0.05$ ) ( $p < 0.05$ ) (Figure 31B). The fluorescent nuclear staining with the Hoechst dye was illustrated and compared among three groups (Figure 32). The nuclear sizes of MDCK cells in siARID1A group were larger than in the other groups. Distributions of nuclear sizes among three groups were reported in Figure 32B and Table 13. Moreover, mean of nuclear size of siARID1A group ( $689.39 \pm 27.43$ ) were significantly higher than in the wild-type ( $380.02 \pm 10.73$ ) and siControl groups ( $431.01 \pm 10.73$ ) ( $p < 0.05$ ) (Figure 32C).



A



B

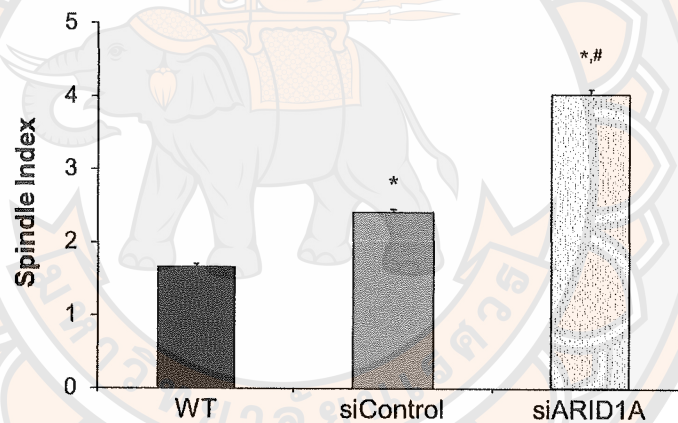
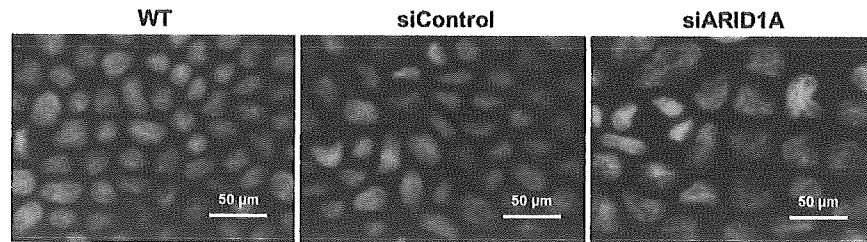


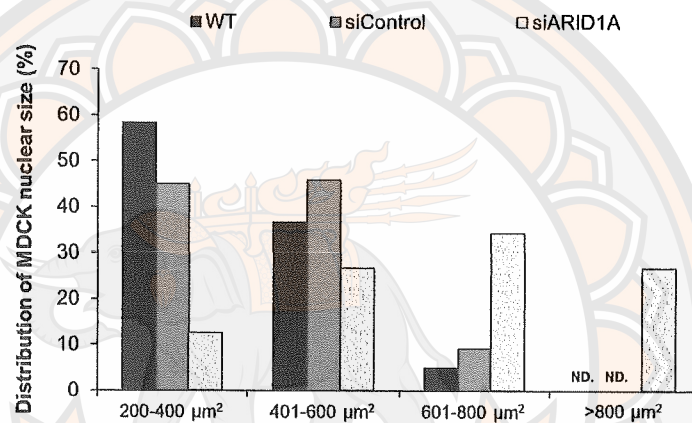
**Figure 31 Effect of ARID1A knockdown on cell morphology (A) Morphology of MDCK cells after 48 hours of siRNA transfection procedure demonstrated abundant of spindle shaped cells in the siARID1A group (original magnification,  $\times 400$ ). B) The quantitative data of spindle index in the siARID1A group showed significant higher than in other groups. Each bar was represented as mean  $\pm$  SEM (\* $p < 0.05$  when compared to wild-type (WT); # $p < 0.05$  when compared to siControl))**



A



B



C

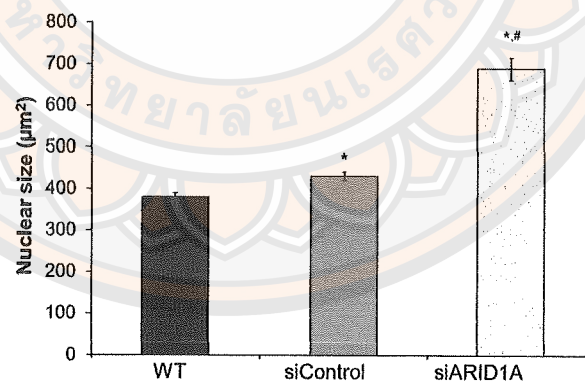


**Figure 32** Effect of ARID1A knockdown on nuclear size (A) The fluorescent images of nuclei staining were compared among three groups. B) Distributions of nuclear sizes of siARID1A group were larger than in other groups (ND., not detected). C) Means of nuclear size in the siARID1A group was significant higher than in other groups. Each bar was represented as mean  $\pm$  SEM (\* $p < 0.05$  when compared to wild-type (WT); # $p < 0.05$  when compared to siControl))

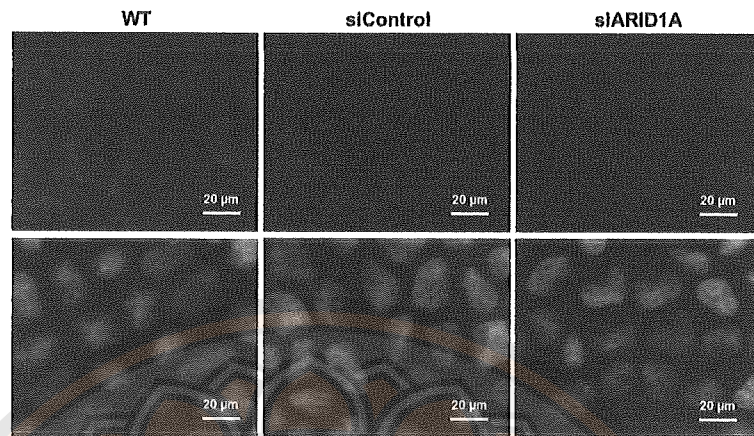
**Table 13 The number and percentage of MDCK nuclei in different nuclear sizes**

Range of nuclear size ( $\mu\text{m}^2$ )	Number of nuclei (no. of cells)			Percentage of nuclei (%)		
	WT	siControl	siARID1A	WT	siControl	siARID1A
200-400	70	54	15	58.3	45.0	12.5
401-600	44	55	32	36.7	45.8	26.7
601-800	6	11	41	5	9.2	34.1
>800	0	0	32	0	0	26.7
Total	120	120	120	100	100	100

**Effects of ARID1A knockdown on expression of EMT-related proteins**

Effects of ARID1A knockdown on expression of EMT-related proteins were assessed by immunofluorescence staining. The epithelial markers included E-cadherin and ZO-1), and the mesenchymal markers included vimentin and fibronectin. The fluorescent images showed that expressions of mesenchymal proteins in siARID1A group were increase, while expressions of epithelial proteins were decrease when compared with those in wild-type and siControl groups (Figure 33-36). Means of fluorescent intensity of E-cadherin and ZO-1 proteins had a significant decrease in siARID1A groups ( $16.13 \pm 0.28$ ,  $8.38 \pm 0.30$ ) compared with those in wild-type ( $17.45 \pm 0.39$ ,  $15.77 \pm 0.49$ ) and siControl groups ( $17.55 \pm 0.29$ ,  $14.40 \pm 0.26$ ) ( $p < 0.05$ ). In addition, Means of fluorescent intensity of vimentin and fibronectin proteins displayed significant decrease in in siARID1A group ( $21.77 \pm 0.77$ ,  $17.45 \pm 0.63$ ) compared those in wild-type ( $13.90 \pm 0.44$ ,  $11.16 \pm 0.14$ ) and siControl groups ( $15.32 \pm 0.71$ ,  $12.58 \pm 0.19$ ) ( $p < 0.05$ ) (Figure 33-36).

A



B

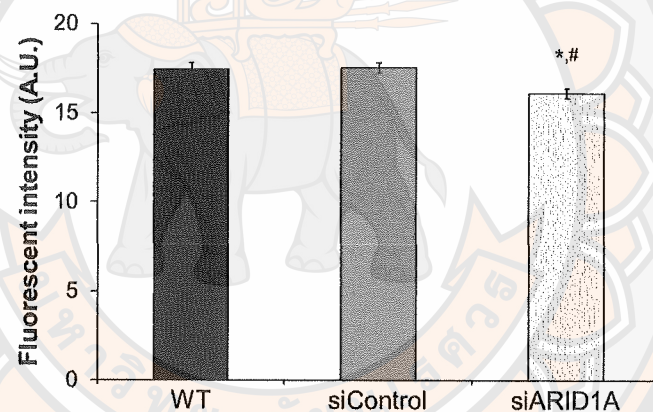
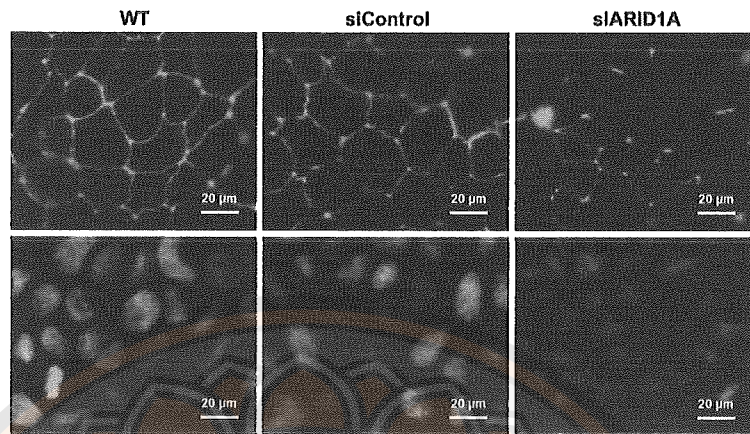


**Figure 33 Effect of ARID1A knockdown on expression of E-cadherin protein (A)** The fluorescent images of E-cadherin protein were stained at cell membrane (red color, upper panel) of MDCK cells. Nuclei of MDCK cells were stained with Hoechst dye (blue color, lower panel). **B)** The quantitative data of fluorescence intensity of E-cadherin protein in siARID1A group was significantly lower than those in wild-type and siControl groups. Each bar was represented as mean  $\pm$  SEM ( $*p < 0.05$  when compared to wild-type (WT);  $\#p < 0.05$  when compared to siControl))



A



B

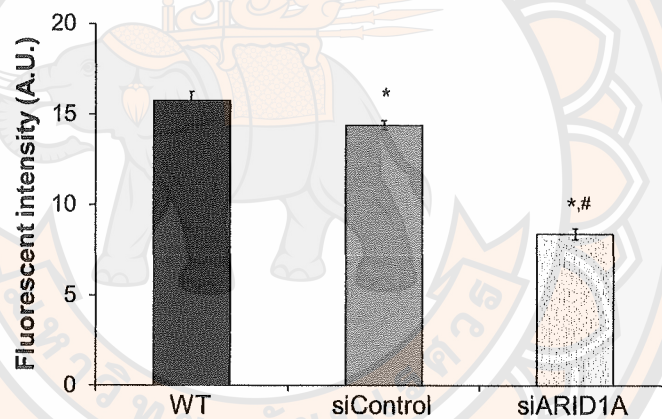
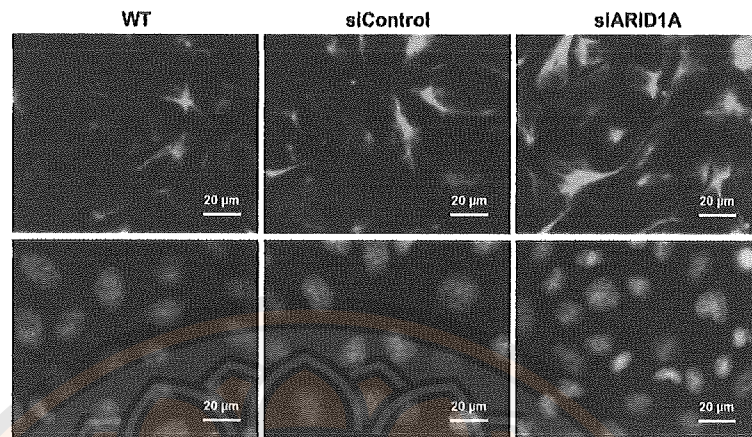


**Figure 34** Effect of ARID1A knockdown on expression of ZO-1 protein (A) The fluorescent images of ZO-1 protein were stained at cell membrane (green color, upper panel) of MDCK cells. Nuclei of MDCK cells were stained with Hoechst dye (blue color, lower panel). B) The quantitative data of fluorescence intensity of ZO-1 protein in siARID1A group was significantly lower than those in wild-type and siControl groups (ZO-1, Zonula occludens-1). Each bar was represented as mean  $\pm$  SEM (\* $p$  < 0.05 when compared to wild-type (WT); # $p$  < 0.05 when compared to siControl))

A



B

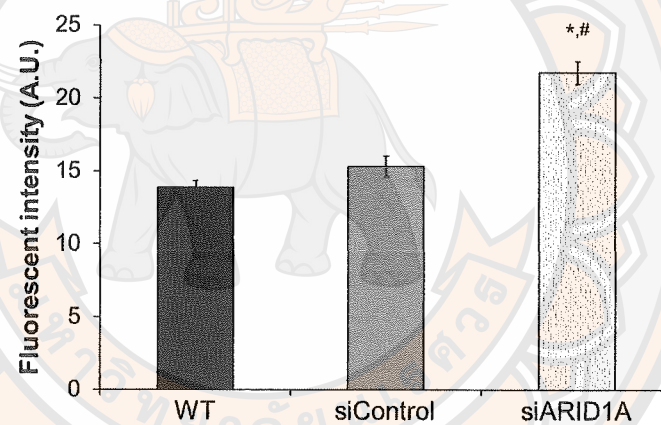
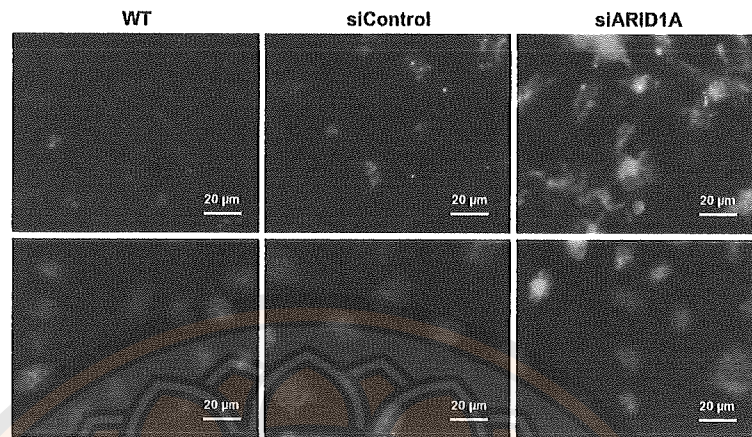


**Figure 35 Effect of ARID1A knockdown on expression of vimentin protein (A)**  
 The fluorescent images of vimentin protein showed diffuse cytoplasmic staining (green color, upper panel) in MDCK cells. Nuclei of MDCK cells were stained with Hoechst dye (blue color, lower panel). **B)** The quantitative data of fluorescence intensity of vimentin protein in siARID1A group was significantly higher than those in wild-type and siControl groups. Each bar was represented as mean  $\pm$  SEM (\* $p$  < 0.05 when compared to wild-type (WT); # $p$  < 0.05 when compared to siControl))



A



B

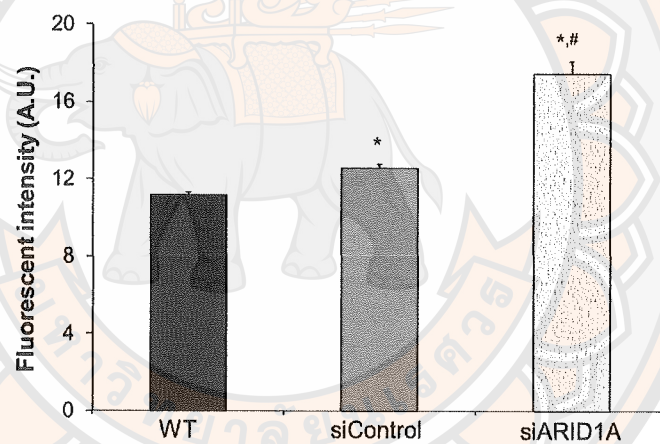


**Figure 36 Effect of ARID1A knockdown on expression of fibronectin protein (A)**

The fluorescent images of fibronectin protein were mostly found at cell surface and between MDCK cells (green color, upper panel) in siARID1A group. Nuclei of MDCK cells were stained with Hoechst dye (blue color, lower panel). B) The quantitative data of fluorescence intensity of fibronectin protein in siARID1A group was significantly higher than those in wild-type and siControl groups. Each bar was represented as mean  $\pm$  SEM (\* $p < 0.05$  when compared to wild-type (WT); # $p < 0.05$  when compared to siControl))

### **Effect of ARID1A knockdown on the expression of SNAI1 transcription factor protein**

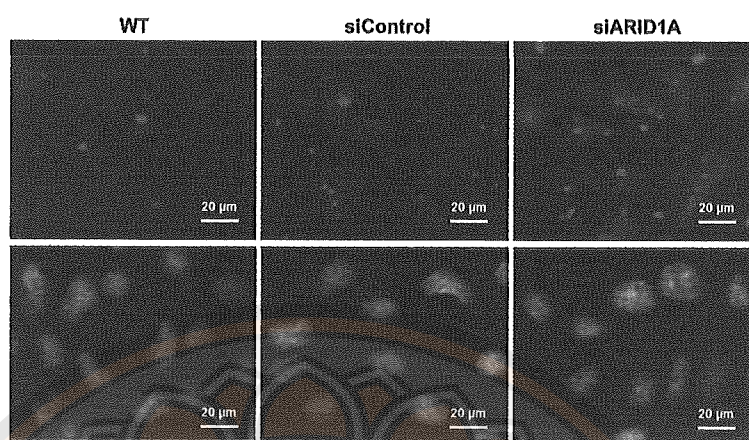
To investigate the interaction of SNAI1 signaling protein and EMT induced by ARID1A knockdown, we performed immunofluorescence staining. The fluorescence images of SNAI1 protein showed strong staining in the siARID1A group when compared with those in wild-type and siControl groups (Figure 37A). Means of fluorescent intensity of SNAI1 protein had a significant increase in siARID1A groups ( $19.58 \pm 0.25$ ) compared with those in wild-type ( $16.29 \pm 0.15$ ) and siControl groups ( $16.81 \pm 0.13$ ) ( $p < 0.05$ ) (Figure 37B).

### **Effects of ARID1A knockdown on cell migrating activity and cell aggregation**

To elucidate the effect of ARID1A knockdown on migrating activity, we performed the scratch wound assay on monolayer of MDCK cells as compared among three groups. Phase contrast pictures of MDCK cells were taken at each timepoint (0, 3, 6, 9, 12 hours) after performing scratch wound assay. Reference dash line indicated the boundary of migrating MDCK cells. The proliferation and migration of MDCK cells in wild-type group were greater than those in the siControl and siARID1A groups at all timepoints, and siARID1A group showed a faster migration rate at 12 hours than in the siControl group (Figure 38). The quantitative results of wound width of the siARID1A group showed a significant decrease, and percentage of cell preparing activity showed a significant increase when compared with the siControl group at the last time point (Figure 39 and 40). This result showed that cell migrating activity of siARID1A group was significantly increased when compared with the siControl group.

The hanging drop assay was performed to investigate size of spheroid formation of MDCK cells after siRNA transfection. As shown in Figure 41, the large spheroid formations were mostly seen in the siARID1A group. It is corresponding to the quantitative results of spheroid diameter and area that was significantly larger than in the siARID1A group ( $50.53 \pm 1.20$ ,  $3,212 \pm 168.75$ ) when compared with the wild-type ( $34.98 \pm 0.91$ ,  $1,036 \pm 59.55$ ) and siControl ( $38.37 \pm 1.2$ ,  $1,287 \pm 89.23$ ) groups (Figure 42A and B).

A



B

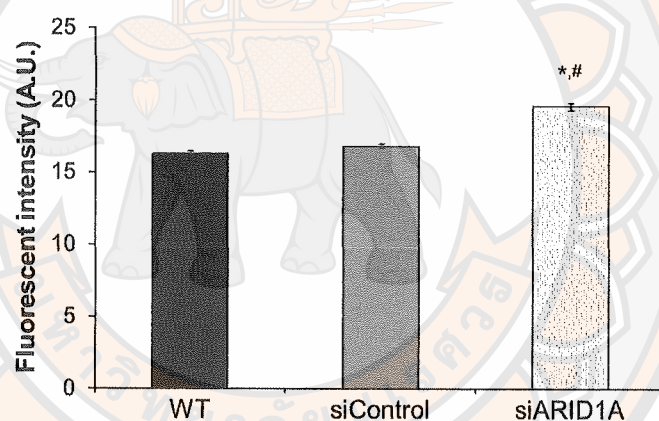


**Figure 37** Effect of ARID1A knockdown on expression of SNAI1 protein (A) The fluorescent images of SNAI1 protein showed nucleocytoplasmic staining in MDCK cells (red color, upper panel) of siARID1A group. Nuclei of MDCK cells were stained with Hoechst dye (blue color, lower panel). B) The quantitative data of fluorescence intensity of SNAI1 protein in siARID1A group was significantly higher than those in wild-type and siControl groups. Each bar was represented as mean  $\pm$  SEM ( $*p < 0.05$  when compared to wild-type (WT);  $\#p < 0.05$  when compared to siControl))



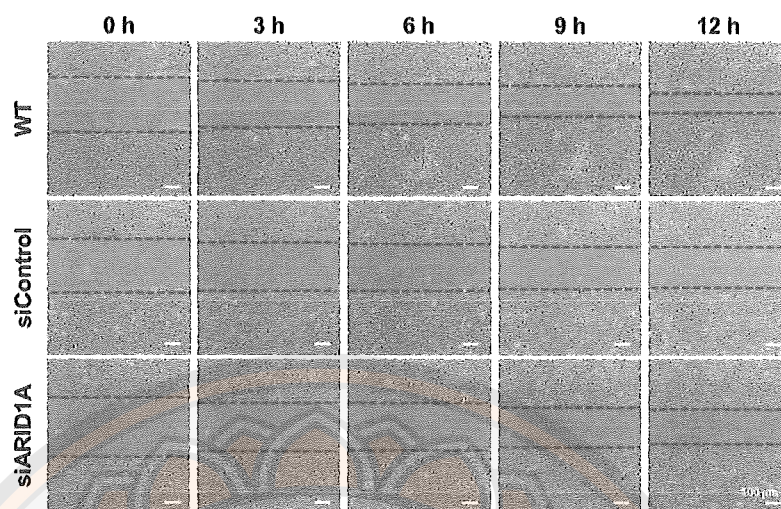


**Figure 38** Effect of ARID1A knockdown on enhancing of migrating activity by using scratch wound assay (Phase contrast images of MDCK cells were taken at each timepoint after performing scratch wound assay. Reference dash line indicated the boundary of migrating MDCK cells as compared among three groups)



**Table 14** The wound width ( $\mu\text{M}$ ) at each timepoint in all three groups

Timepoints (hours)	Wound width ( $\mu\text{M}$ )		
	WT	siControl	siARID1A
0	783.76 $\pm$ 8.72	798.14 $\pm$ 39.07	777.56 $\pm$ 33.41
3	633.95 $\pm$ 15.58	733.09 $\pm$ 42.20	702.45 $\pm$ 39.81
6	484.50 $\pm$ 32.63	691.67 $\pm$ 35.79	646.02 $\pm$ 39.81
9	376.82 $\pm$ 41.36	644.35 $\pm$ 34.53	574.82 $\pm$ 26.15
12	248.08 $\pm$ 32.75	574.85 $\pm$ 25.19	494.23 $\pm$ 23.12

\* Data was represented as mean  $\pm$  SEM.

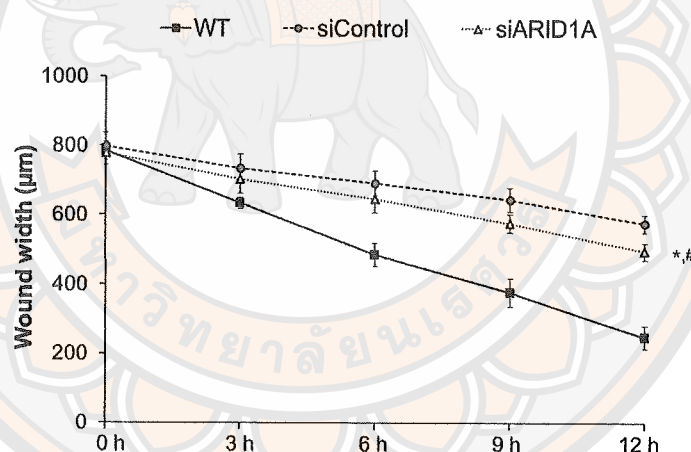


**Figure 39** The quantitative data of wound width as compared among three groups (Wound width of transfected cells in wild-type group was greater than those in other groups at all timepoints. The transfected cells in siARID1A group proliferated and migrated faster than in the siControl group at all timepoints. Data was represented as mean  $\pm$  SEM (\* $p < 0.05$  when compared to wild-type (WT); # $p < 0.05$  when compared to siControl))

**Table 15** The percentage of cell migrating activity at each timepoint in all three groups

Timepoints (hours)	cell migrating activity (%)		
	WT	siControl	siARID1A
3	19.09±1.38	8.11±1.09	9.76±1.42
6	38.21±3.55	13.25±1.93	17.03±1.88
9	51.98±4.82	19.18±2.11	26.04±0.92
12	68.35±4.01	27.85±1.66	36.43±1.95

\* Data was represented as mean ± SEM.

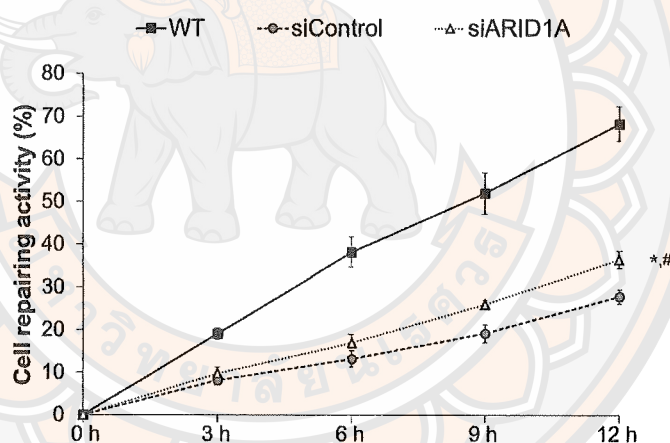


**Figure 40** The quantitative data of cell migrating activity (%) as compared among three groups (Cell migrating activity (%) of transfected cells in wild-type group was greater than those in other groups at all timepoints. Cell migrating activity (%) of transfected cells in siARID1A group was faster than those in siControl group at all timepoints. Data was represented as mean ± SEM (\* $p < 0.05$  when compared to wild-type (WT); # $p < 0.05$  when compared to siControl))

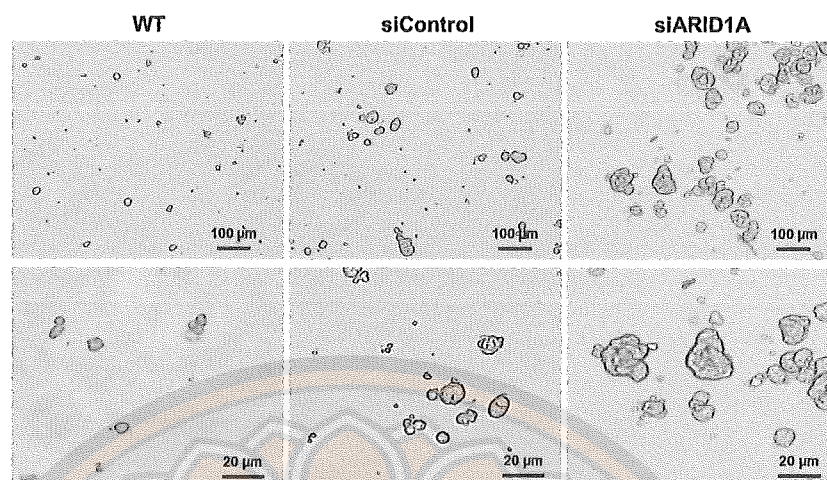
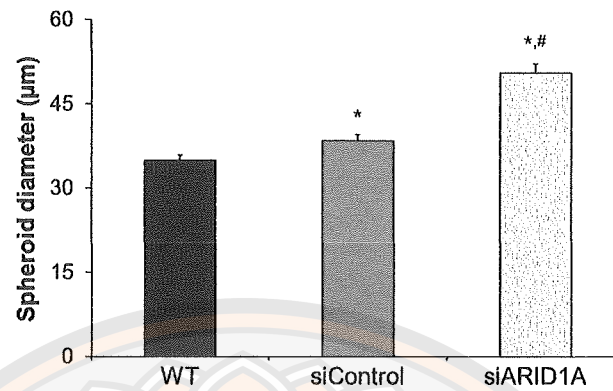


**Figure 41** Effect of ARID1A knockdown on cell aggregation (The representative images of spheroid formation siARID1A group showed larger spheroid formation than in the wild-type and siControl groups (original magnification,  $\times 400$ ))

A



B

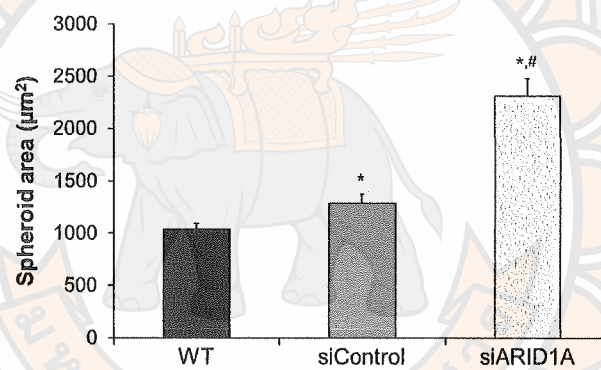


**Figure 42** The quantitative data of ARID1A knockdown on cell aggregation as compared among three groups (The quantitative results of diameter (A) and area (B) of spheroids were significantly increased in the siARID1A group as compared with other groups. Each bar was represented as mean  $\pm$  SEM (\* $p$  < 0.05 when compared to wild-type (WT); # $p$  < 0.05 when compared to siControl))



***ARID1A* was one of the top-ten mutated genes most frequently found in kidney cancers and its mutations were found along its sequence.**

To study bioinformatics of *ARID1A* mutation and others in kidney cancers, we accessed the data of genetic mutation on GDC database. The result of mutated genes in kidney cancers of TCGA projects showed that *ARID1A* was one of the top-ten mutated genes most frequently found in kidney cancers (Figure 4.18A). A total of 32 mutations related to kidney cancers were found in *ARID1A* gene, accounting for 4.03% of all the mutated genes detected in all the affected cases. In addition, these 32 mutations in *ARID1A* gene, including 14 frameshift, 4 stop gained and 14 missense mutations, were found along its protein sequence (Figure 43B). Interestingly, six of these mutations were found in the important domains, including ARID DNA-binding domain (PF01388) and SWI/SNF-like complex subunit BAF250/Osa (PF12031) domains (Figure 43B). The details of mutation types and its consequence in 32 patients were described in the Table 16. Moreover, patients with *ARID1A* mutations had significantly lower survival rate (38%; n=68) comparing to the non-*ARID1A* mutated cases (58%; n=192) (Figure 44).

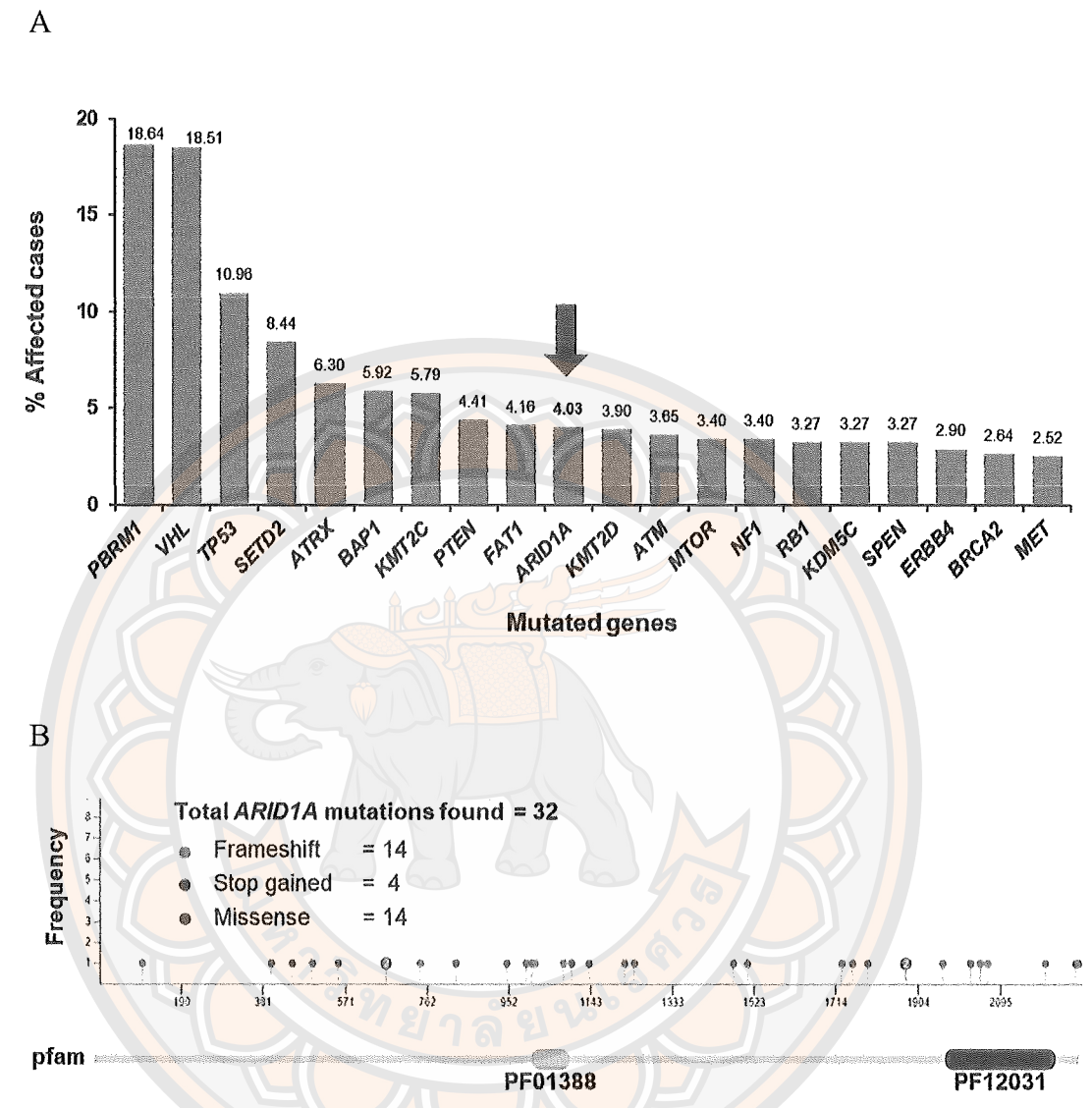


**Figure 43** List of top twenty mutated genes and *ARID1A* mutation profiles in kidney cancers (data from GDC database) (A): The top-20 mutated genes in kidney cancers found. The arrow indicates that *ARID1A* was one of the top-10 mutated genes found. B) Frequency and mapping of frameshift, stop gained, and missense mutations of *ARID1A* gene along its protein sequence and ARID DNA-binding domain (PF01388) and SWI/SNF-like complex subunit BAF250/Osa (PF12031) domains)

**Table 16 Frequent somatic mutations of ARID1A in kidney cancers**

No.	Mutation ID	DNA Change	Type	Consequences
1	0a42f761-3a87-58ae-915e-576d77c894f0	chr1:g.26696698G>T	Substitution	Missense ARID1A D99Y
2	ba521aaf-45dd-509b-9f1f-6b8fd74f64e5	chr1:g.26729710delC	Deletion	Frameshift ARID1A P400Hfs*33
3	32717d4d-4aa2-5830-a1ce-fbbfc0b49559	chr1:g.26729858C>T	Substitution	Stop Gained ARID1A Q449*
4	ce5ef103-70ff-5b64-95da-431e4a0fc28d	chr1:g.26731284C>T	Substitution	Missense ARID1A H495Y
5	7335453d-5b50-5d00-b060-6985744c35b7	chr1:g.26731461delC	Deletion	Frameshift ARID1A P554Hfs*65
6	56770122-b84c-5a0e-acb6-eb595189fdef	chr1:g.26760928delGG	Deletion	Frameshift ARID1A G665Dfs*10
7	efc243d0-7fbe-54b8-9554-1fc12f74bcba	chr1:g.26760929G>C	Substitution	Missense ARID1A G665A
8	3f553648-1c4b-568e-a027-0963b74a542a	chr1:g.26761456G>A	Substitution	Missense ARID1A S745N
9	fc2f4307-d3f4-555c-ac00-6b41c3c1d346	chr1:g.26763034delCATG	Deletion	Frameshift ARID1A M828Hfs*37
10	c538b79c-ef7d-5add-9138-0ef8347665d1	chr1:g.26766324delC	Deletion	Frameshift ARID1A P947Hfs*21
11	54b87c9b-ff4d-5508-bd93-47a72b3a293c	chr1:g.26766551_26766552	Insertion	Frameshift ARID1A E992Kfs*52
12	40df39d8-da47-5e54-a9fb-bd538181f503	chr1:g.26767817G>T	Substitution	Stop Gained ARID1A E1006*
13	0a8f2de7-e93d-5ce9-a611-5fbc372c42db	chr1:g.26767838G>A	Substitution	Missense ARID1A E1013K
14	8aa0dc0a-184f-5a51-bc9e-f6efc7690578	chr1:g.26771156A>T	Substitution	Missense ARID1A N1079I
15	e7b7ec31-598c-50c8-99f0-199be3b790cd	chr1:g.26771212C>T	Substitution	Stop Gained ARID1A Q1098*
16	0dbbbb6f-6b67-5f09-826d-bfe69fbc463a	chr1:g.26772507delAGGA	Deletion	Frameshift ARID1A G1139Lfs*21

Table 16 (cont.)

No.	Mutation ID	DNA Change	Type	Consequences
17	0dcd456e-7538-5817-a2ad-d37cda0943b2	chr1:g.26772934T>G	Substitution	Missense ARID1A M1221R
18	2f1d7a48-d069-5a16-96cc-ca70ceb15fc0	chr1:g.26773361C>A	Substitution	Missense ARID1A P1244H
19	12840a78-b5f3-5f9c-ade7-7d64114f988c	chr1:g.26774652delC	Deletion	Frameshift ARID1A N1475Kfs*6
20	9cbbf445-693e-5d85-8849-40a96bfd9c4	chr1:g.26774750A>G	Substitution	Missense ARID1A Y1508C
21	f15d637d-73fa-5a44-a9cb-de3318f21380	chr1:g.26779078delTC	Deletion	Frameshift ARID1A F1728Wfs*7
22	9aa727ca-81ed-5bbb-bcee-e5b9ab16493a	chr1:g.26779154delG	Deletion	Frameshift ARID1A V1753Cfs*17
23	7d179745-eed2-5387-8ab1-aec0e54d0558	chr1:g.26779260_26779261	Insertion	Frameshift ARID1A I1788Kfs*15
24	2efd1ca7-f50f-5fe2-843a-5797ba226dc1	chr1:g.26779519_26779520insC	Insertion	Frameshift ARID1A P1876Tfs*25
25	915b1024-clac-511f-b0bb-3e6d2353ca3e	chr1:g.26779524delC	Deletion	Frameshift ARID1A P1876Qfs*7
26	98bb2623-92f8-5343-ba3c-675eb3285230	chr1:g.26779780G>A	Substitution	Missense ARID1A S1961N
27	181f1852-80fe-5acf-a545-34fefe2f9ddf	chr1:g.26779969delG	Deletion	Frameshift ARID1A K2025Sfs*5
28	37a3e733-0d1e-5e4f-a335-1d5bb5568d5b	chr1:g.26780037G>A	Substitution	Missense ARID1A E2047K
29	232f62fc-9a30-52b8-b46b-faa11d4d6ef3	chr1:g.26780089T>C	Substitution	Missense ARID1A L2064P
30	441e8ac4-e10e-5286-bb69-a59bec3b5f33	chr1:g.26780491T>C	Substitution	Missense ARID1A F2198S
31	81bf730a-2198-5380-9f86-1c8044de4a41	chr1:g.26780704C>A	Substitution	Stop Gained ARID1A S2269*
32	44709e55-5e4f-50c1-ba57-291df6f3435a	chr1:g.26780722T>C	Substitution	Missense ARID1A I2275T



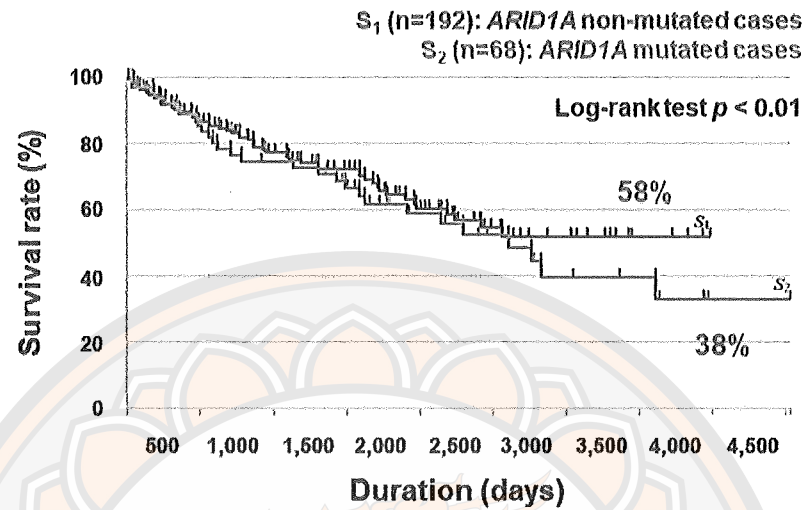


**Figure 44 Overall survival (OS) of patients (The overall survival of *ARID1A* mutated patients (orange line) was significantly shorter than the non-*ARID1A* mutated patients (blue line). Log-Rank Test represents a significant statistical analysis between groups,  $p < 0.01$ )**

### **Histopathology and ARID1A protein expression in cancer vs. adjacent non-cancer areas**

The histopathology of cancer and adjacent non-cancer areas of the paired renal tissues collected from RCC patients, who were admitted at Sawanpracharak Hospital, Nakhon Sawan, Thailand for nephrectomy during 2013-2017, was examined with H&E staining. The subtype and the Fuhrman nuclear grading were then evaluated (Figure 45). From a total of 26 RCC patients recruited, 17 had clear cell RCC (ccRCC) (six with Fuhrman nuclear grade I and 11 with Fuhrman nuclear grade II), six had chromophobe RCC (chRCC), two had papillary RCC (pRCC), and only one had sarcomatoid RCC (sRCC) (Figure 45).

Immunohistochemistry was performed to evaluate ARID1A protein expression in these paired renal tissues (Figure 46). The data showed that ARID1A protein was strongly expressed in the nuclei of lymphocytes, fibroblasts, intraglomerular cells, and tubular epithelial cells of proximal convoluted tubules and distal convoluted tubules in the adjacent non-cancer areas (Figures 46), whereas lighter ARID1A staining were observed in these cells in the cancer area (Figures 46). Quantitative analysis using Allred scoring and grading system (as described with details in “CHAPTER III” and Figure 27) revealed that ARID1A Allred score was significantly decreased in cancer areas of all RCC cases (Figure 47A). Comparing in each subtype of RCC, ARID1A Allred score was markedly decreased in cancer area of ccRCC (grade I), RCC (grade II) and chRCC, whereas there was no significant difference observed in pRCC and sRCC (Figure 47A). Similarly, Allred grading revealed that almost all of the adjacent non-cancer area (25/26 cases) had moderate to strong ARID1A expression, whereas almost all of the cancer area of ccRCC (grade I), ccRCC (grade II) and chRCC (21/23 cases) had negative to weak ARID1A expression (Figure 4.22B). However, the three cases with pRCC and sRCC had moderate to strong ARID1A expression (Figure 47B). The details of proportional score, intensity score, allred score and grading are described as the table 17.

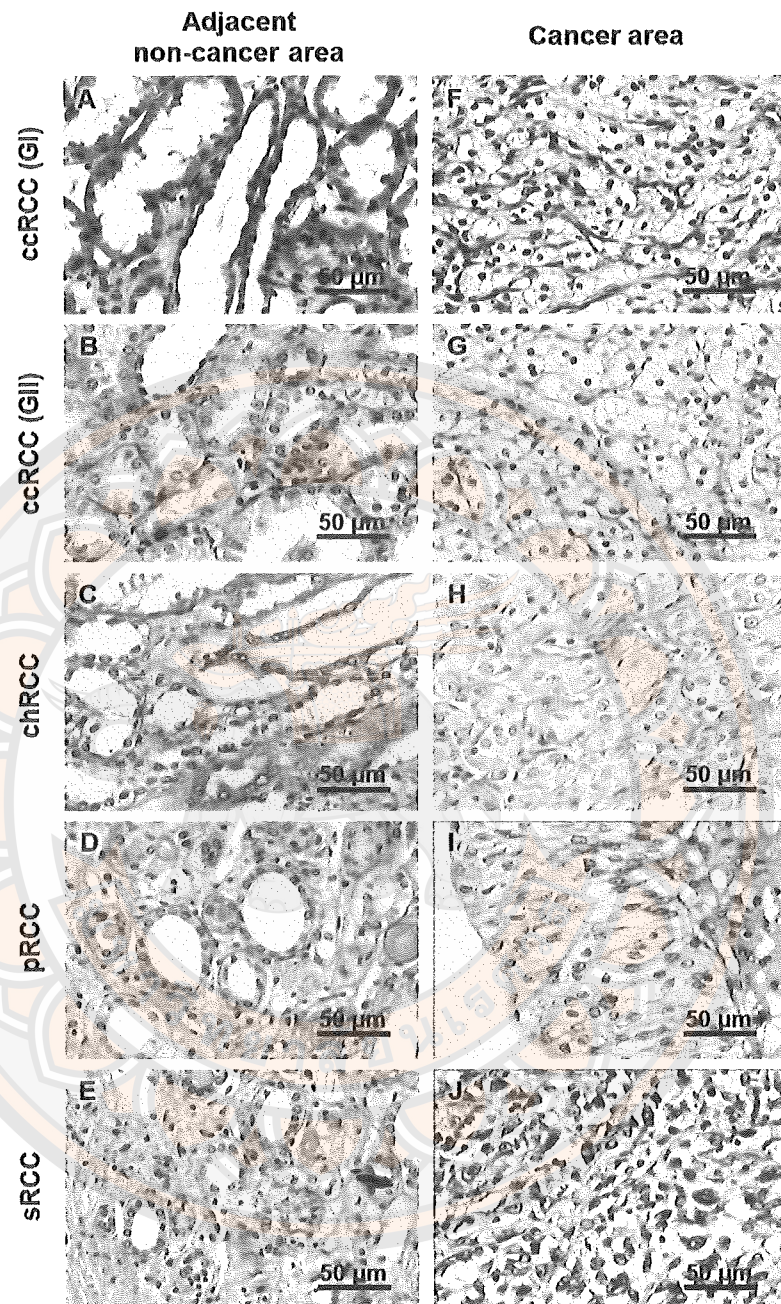


**Figure 45** Histopathology of renal tissues from RCC patients (A-E) H&E staining of the representative adjacent non-cancer area in ccRCC grade I (GI), ccRCC grade II (GII), chRCC, pRCC and sRCC, respectively. F-J) The representative cancer area in ccRCC grade I (GI), ccRCC grade II (GII), chRCC, pRCC and sRCC, respectively, stained by H&E staining. Original magnification power of 400× for all panels)



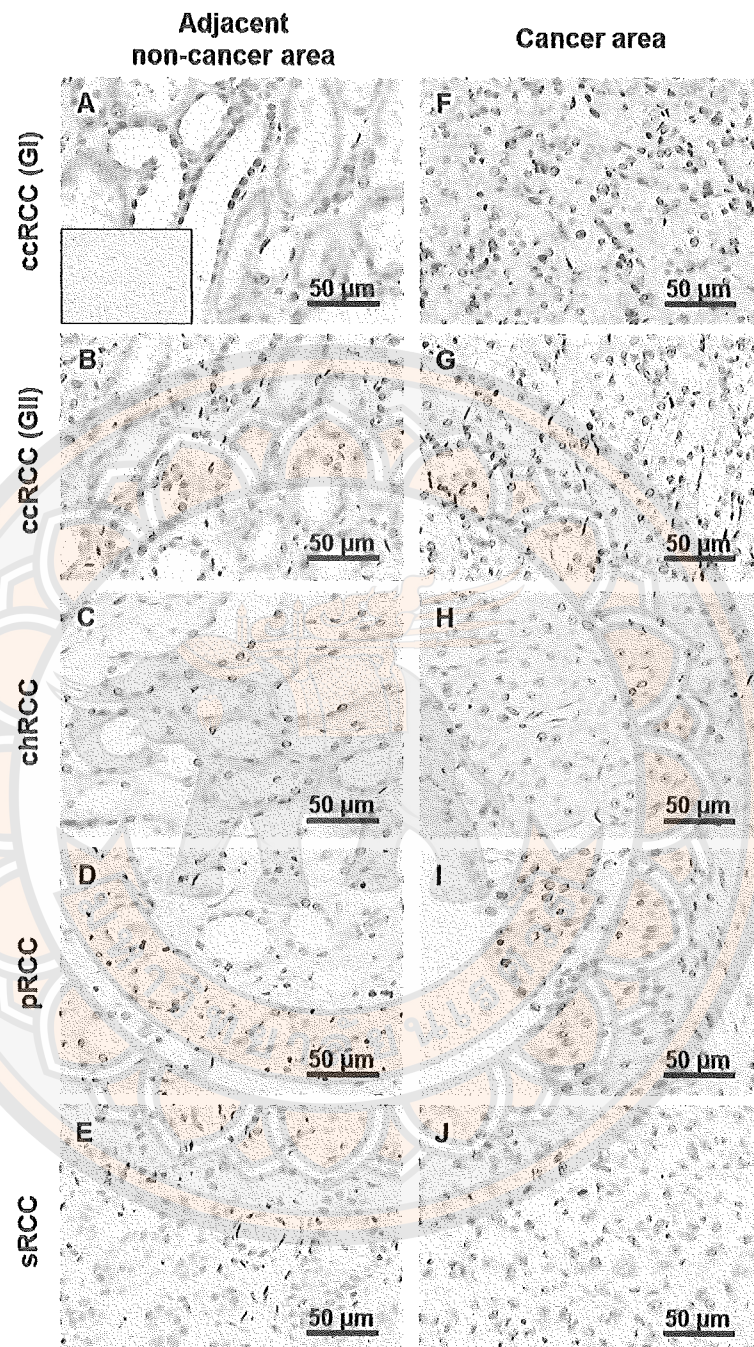
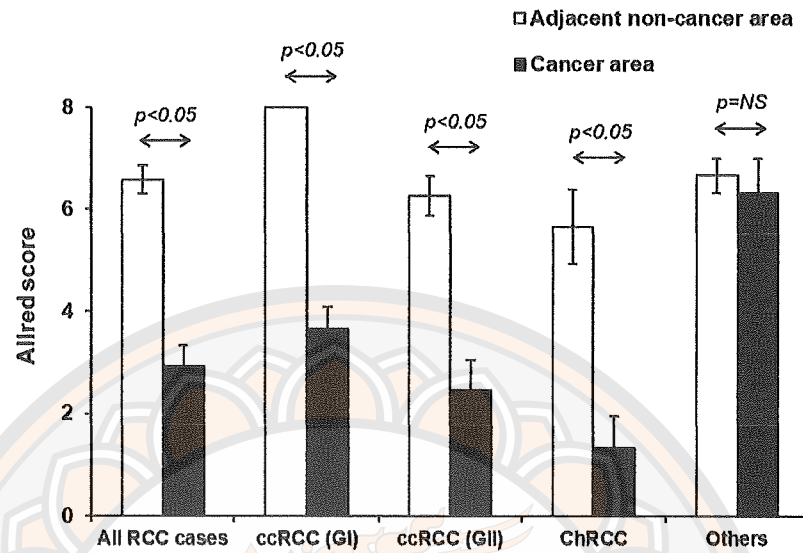


**Figure 46** Expression of ARID1A protein in RCC tissues (A-E) ARID1A IHC of the adjacent non-cancer area in ccRCC grade I (GI), ccRCC grade II (GII), chRCC, pRCC and sRCC, respectively. F-J) ARID1A IHC of the cancer area in ccRCC grade I (GI), ccRCC grade II (GII), chRCC, pRCC and sRCC, respectively. ARID1A staining is observed in brown. An inset in panel A shows the negative control for ARID1A staining. Original magnification power of 400× for all panels)



A



B

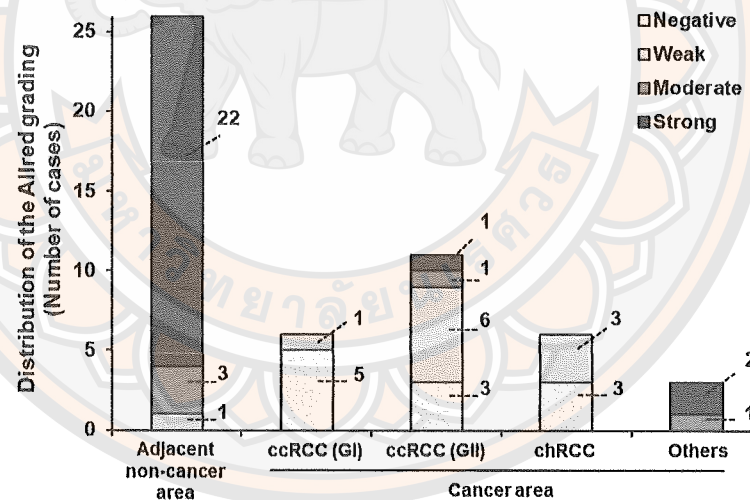


**Figure 47** Quantitative analysis of expression of ARID1A protein (A) Allred score of the adjacent non-cancer area versus cancer area in ccRCC grade I (GI), ccRCC grade II (GII), chRCC, and others (including pRCC and sRCC). The data were presented as mean  $\pm$  SEM ( $p < 0.05$ , NS = no statistical difference). B) Distribution and number of cases with different Allred grades in the adjacent non-cancer and cancer areas)

**Table 17 The details of Allred score and four grading of ARID1A expression in normal and cancer areas of all patients**

Cancer types	Case no.	Normal		Allred score	Grading	Cancer		Allred score	Grading
		PS	IS			PS	IS		
ccRCC (GI)	1	5	3	8	Strong	2	2	4	Moderate
	2	5	3	8	Strong	1	1	2	Weak
	3	5	3	8	Strong	2	2	4	Moderate
	4	5	3	8	Strong	3	1	4	Moderate
	5	5	3	8	Strong	2	1	3	Weak
	6	5	3	8	Strong	3	2	5	Moderate
ccRCC (GII)	7	3	1	4	Moderate	0	0	0	Negative
	8	5	3	8	Strong	2	1	3	Weak
	9	4	2	6	Strong	3	2	5	Moderate
	10	5	3	8	Strong	4	2	6	Strong
	11	3	2	5	Moderate	2	1	3	Weak
	12	4	2	6	Strong	0	0	0	Negative
	13	3	3	6	Strong	1	1	2	Weak
	14	4	2	6	Strong	1	1	2	Weak
	15	4	2	6	Strong	0	0	0	Negative
	16	4	2	6	Strong	2	1	3	Weak
	17	5	3	8	Strong	2	1	3	Weak
chRCC	18	5	2	7	Strong	0	0	0	Negative
	19	5	2	7	Strong	2	1	3	Weak
	20	5	2	7	Strong	1	1	2	Weak
	21	2	1	3	Weak	0	0	0	Negative
	22	4	2	6	Strong	0	0	0	Negative
	23	2	2	4	Moderate	2	1	3	Weak
Others	24	5	2	7	Strong	3	2	5	Moderate
	25	5	2	7	Strong	5	2	7	Strong
	26	4	2	6	Strong	5	2	7	Strong

**Note:** PS, proportional score; IS, intensity score

### **ARID1A protein expression in adjacent non-cancer area in ccRCC (grade I) vs. ccRCC (grade II)**

In addition, we also compared expression of ARID1A protein in the non-cancer area of ccRCC (grade I) to that of ccRCC (grade II). The data demonstrated that level of ARID1A protein was significantly lower in ccRCC (grade II) at all locales, including glomerulus, proximal convoluted tubule, distal convoluted tubule, and collecting duct (Figure 47).

### **Association of ARID1A protein expression with clinicopathology and progression-free survival**

Allred grading was then applied to compare clinicopathology and prognosis (as reflected by progression-free survival) of RCC patients. There were 17 cases with “moderate to strong ARID1A expression” and nine cases with “negative to weak ARID1A expression”. Their mean ages were comparable, whereas tumor mass diameter tended to be larger and progression-free duration tended to be shorter in patients with negative to weak ARID1A protein expression although the statistically significant threshold was not reached (Table 18). Using Fisher’s exact test, patients with negative to weak ARID1A expression had significantly greater number and percentage of ccRCC (grade II) and chRCC cases as compared to those with moderate to strong ARID1A expression (Table 19). However, their elderly (age  $\geq 60$  years), gender, tumor laterality, TNM stage and AJCC stage had no significant differences between the two groups (Table 19). Interestingly, ARID1A protein was undetectable in 3/11 cases with ccRCC (grade II) and 2/6 chRCC cases, all of which had metastasis (to lung, brain, bone, and liver) 1-50 months after surgical removal (Table 20).

Finally, 5-year progression-free survival was analyzed. Interestingly, all 9/9 RCC patients with moderate to strong ARID1A expression had 5-year progression-free survival rate of 100% (Figure 49). Log-rank test revealed a tendency of lower progression-free survival in patients with negative to weak ARID1A expression (n=17) as compared to those with moderate to strong ARID1A expression (n=9) but the *p* value did not reach the statistically significant threshold (Figure 49).

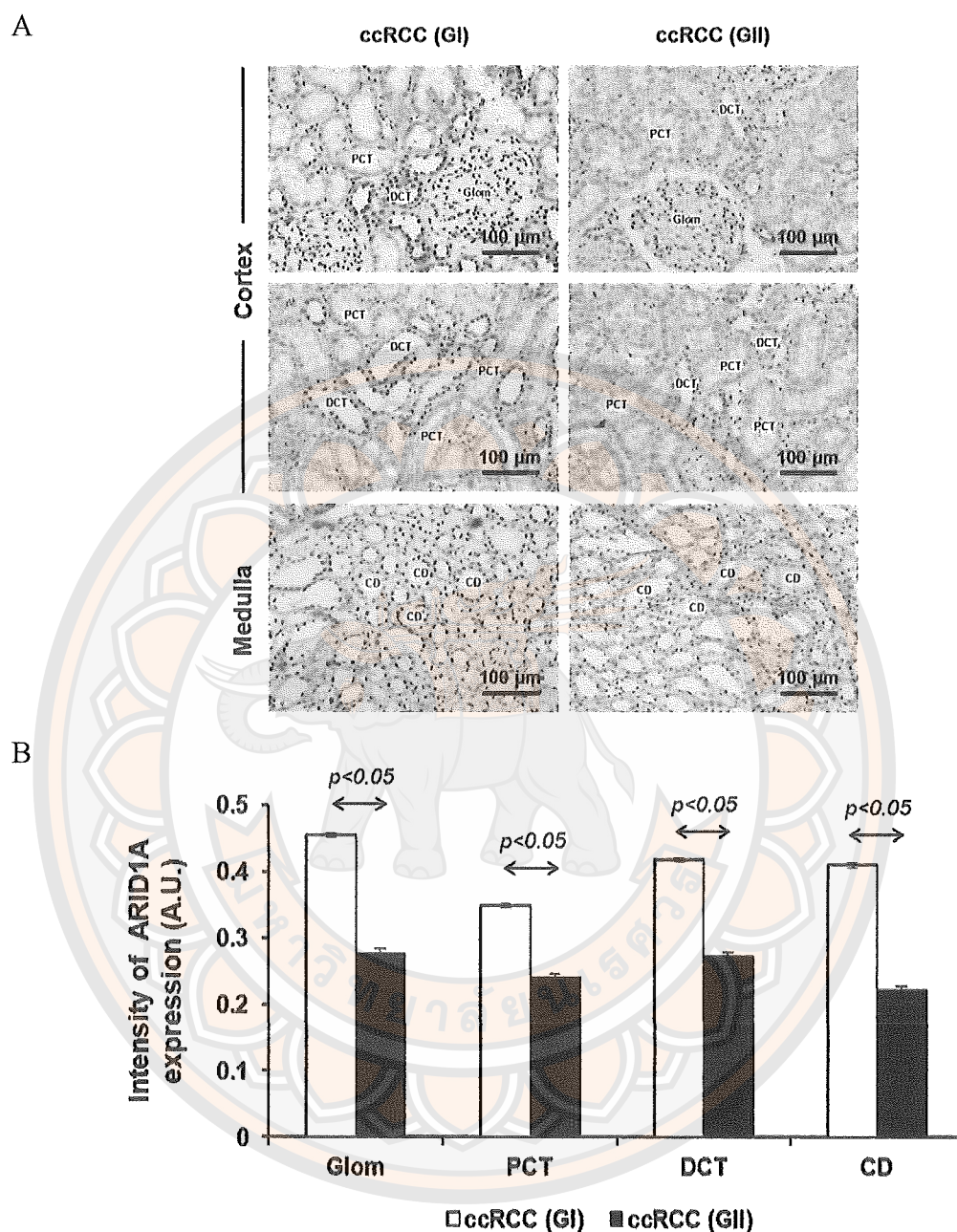


**Figure 48** Expression of ARID1A protein in adjacent non-cancer area in ccRCC grade I (GI) versus ccRCC grade II (GII) (A) ARID1A immunohistochemistry of the adjacent non-cancer area from cases with ccRCC (GI) (left column) versus ccRCC (GII) (right column) in both cortex and medulla. B) Quantitative analysis of ARID1A protein expression in each locale of the renal tissues. Abbreviations used: Glom, glomerulus; PCT, proximal convoluted tubule; DCT, distal convoluted tubule; CD, collecting duct; A.U., arbitrary unit)



**Table 18 Clinical data of RCC patients (total n = 26; moderate to strong ARID1A expression = 9 cases; negative to weak ARID1A expression = 17 cases)**

<b>Clinical data</b>	<b>Mean <math>\pm</math> SEM</b>	<b><i>p</i>-value</b>
<b>Age (year)</b>	61.00 $\pm$ 1.94	
Moderate to strong ARID1A expression	61.00 $\pm$ 3.91	0.75 <sup>a</sup>
Negative to weak ARID1A expression	60.88 $\pm$ 2.17	
<b>Tumor mass diameter (cm)</b>	7.91 $\pm$ 0.61	
Moderate to strong ARID1A expression	6.23 $\pm$ 1.17	0.07 <sup>b</sup>
Negative to weak ARID1A expression	8.60 $\pm$ 0.66	
<b>Progression-free duration (month)</b>	52.65 $\pm$ 3.35	
Moderate to strong ARID1A expression	60.00 $\pm$ 0.00	0.24 <sup>a</sup>
Negative to weak ARID1A expression	48.82 $\pm$ 4.91	

<sup>a</sup> By Mann-Whitney U test; <sup>b</sup> By unpaired Student's t-test.

**Table 19 Association of ARID1A expression with clinicopathology of RCC patients (total n=26)**

Parameters	n (%)	ARID1A expression		p-value <sup>c</sup>
		Moderate to strong n (%)	Negative to weak n (%)	
Elderly				
≥ 60 years old	13 (50.0)	3 (11.5)	10 (38.5)	0.41
< 60 years old	13 (50.0)	6 (23.1)	7 (26.9)	
Gender				
Male	21 (80.8)	7 (26.9)	14 (53.8)	1.00
Female	5 (19.2)	2 (7.7)	3 (11.5)	
Tumor laterality				
Right	17 (65.4)	5 (19.2)	12 (46.2)	0.67
Left	9 (34.6)	4 (15.4)	5 (19.2)	
Pathological types				
ccRCC (grade I)	6 (23.1)	4 (15.4)	2 (7.7)	0.03*
ccRCC (grade II)	11 (42.3)	2 (7.7)	9 (34.6)	
chRCC	6 (23.1)	0 (0)	6 (23.1)	
Others	3 (11.5)	3 (11.5)	0 (0)	
T stage				
T1	7 (26.9)	3 (11.5)	4 (15.4)	0.66
T2-4	19 (73.1)	6 (23.1)	13 (50)	
N stage				
N0	22 (84.6)	7 (26.9)	15 (57.7)	0.59
N1	4 (15.4)	2 (7.7)	2 (7.7)	
M stage				
M0	24 (92.3)	9 (34.6)	15 (57.7)	0.53
M1	2 (7.7)	0 (0)	2 (7.7)	
AJCC stage				
Stage I	7 (26.9)	3 (11.5)	4 (15.4)	0.66
Stage II-IV	19 (73.1)	6 (23.1)	13 (50.0)	

<sup>c</sup> By Fisher's exact test.

\*  $p < 0.05$

**Table 20 The clinicopathology and outcome of patients with negative ARID1A expression**

Pt. no.	ARID1A expression	Age	Gender	Laterality	Pathologica l subtypes (Fuhrman grade)	Tumor mass diameter (cm)	Description	Staging at diagnosis				Metastasis (months after surgery)	Comorbidity
								T	N	M	AJCC		
014	Negative	67	Male	Right	ccRCC (grade II)	8.0	The tumor invaded renal capsule and the mass protruded renal pelvis.	T3	N0	M0	3	Lung metastasis (1 month)	Hypertension, pneumonia, and adrenal insufficiency
015	Negative	52	Male	Left	ccRCC (grade II)	11.5	The tumor invaded renal pelvis and calyces.	T3	N1	M0	2	Brain and bone metastasis (8 months)	Hypertension, CKD, kidney stone, and brain hemorrhage
016	Negative	65	Male	Right	ccRCC (grade II)	5.0	The tumor was confined within the renal capsule.	T1b	N0	M0	1	Brain metastasis (24 months)	Type 2 diabetes, hypertension, and liver cirrhosis
020	Negative	65	Male	Right	chRCC	9.0	Renal vein was invaded.	T3a	N0	M0	3	Liver metastasis (50 months)	Hypertension and hematuria
022	Negative	49	Male	Right	chRCC	12.5	The tumor pushed renal capsule and invaded renal vein.	T3a	N1	M0	3	Liver metastasis (27 months)	Type 2 diabetes and hypertension

Abbreviations used: Pt. no., patient number; T, tumor; N, lymph node; M, metastasis; CKD, chronic kidney disease

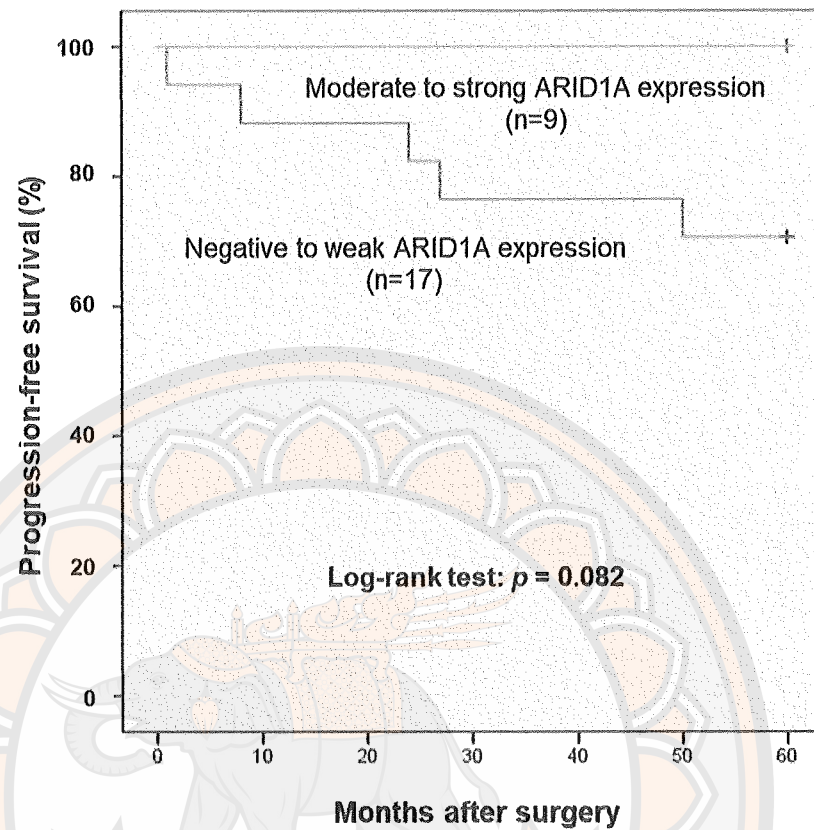


**Figure 49** The 5-year progression-free survival of patients (The 5-year progression-free survival of patients with negative to weak ARID1A expression (blue line) was significantly shorter than those in moderate to strong ARID1A expression (green line). Log-Rank Test was no significant difference between groups ( $p = 0.08$ ,  $n=26$ ))



## CHAPTER V

### DISCUSSION

The present study, we aimed to investigate functional role of ARID1A in carcinogenesis of renal cells. Our study confirmed that down-regulation of ARID1A mRNA can induce carcinogenic features of renal cells. The siARID1A-transfected cells had a significantly decrease in percentage of cell death, while number of total cells, and cell viability were significantly increased. These results were consistent with the previous reports in liver cancer cells, breast cancer cells, ovarian cancer cells, and gastric cancer cells. These studies showed that deficiency of ARID1A protein decreased apoptosis whereas cell proliferation, invasion, and migration were increased (He et al., 2015; Mamo et al., 2011). Role of ARID1A protein was concomitant in PI3K/(AKT) pathway to control cell proliferation (Ibarrola-Villava et al., 2015; Yamamoto, Tsuda, Takano, Tamai, & Matsubara, 2012; Y. Yang et al., 2019). On the other hand, regulation of ARID1A in apoptosis evasion remains unclear but may involve inhibition of Fas-mediated cell death, which was suggested by a previous study. The suppression of ARID1A by short-hairpin RNA (shRNA) inhibited both Fas-Ab-induced caspase-8 cleavage and mitochondrial potential reduction (Luo et al., 2008). Moreover, there is evidence demonstrating that ARID1A mutation caused dysfunction of histone H2B ubiquitination and restoration of nuclear histone H2B resulted in an aberration of chromatin remodeling proteins, which led to apoptosis evasion (Shigetomi et al., 2011).

Epithelial-mesenchymal transition (EMT) is involved in several biological processes including embryogenesis, organ fibrosis, and invasion-metastasis cascade of cancer cells (Kalluri, & Weinberg, 2009; Kanlaya, Khamchun, Kapincharanon, & Thongboonkerd, 2016). EMT is accompanied with several changes of epithelial cells, including acquisition of mesenchymal morphology and loss of polarity, resulting in detachment and elongation of the cells (Lee, Dedhar, Kalluri, & Thompson, 2006; Q. C. Zhu, Gao, Wu, & Qin, 2013). In addition, the cells undergoing EMT exhibit down-regulation of epithelial markers (e.g., E-cadherin, ZO-1, claudins, and cytokeratins)

and up-regulation of mesenchymal markers (e.g., vimentin, fibronectin, and  $\alpha$ -smooth muscle actin) (Lee et al., 2006; Q. C. Zhu et al., 2013). Activation of EMT process has been studied in pancreatic and gastric cancers, the ARID1A-mutant/knockdown cancer cells had increased mesenchymal features, decreased epithelial phenotypes, and increased migrating activity (Ibarrola-Villava et al., 2015; W. Wang et al., 2019; Yan et al., 2014). Our results were consistent with those in previous studies demonstrating that the siARID1A-transfected MDCK cells exhibited morphological changes (spindle-shape, finger-like protrusion, increased spindle index) and increased expression of mesenchymal markers (vimentin and fibronectin). These data indicate that decreased ARID1A expression in renal epithelial cells can trigger EMT process.

Moreover, the siARID1A-transfected MDCK cells also showed enlargement of nuclei and multicellular spheroids, it is consistent with the features of polyploid giant cancer cells (PGCCs) (S. Zhang et al., 2014). Previous study reported that PGCC have been considered as the cancer stem cells, which can metastases in a model of human ovarian cancer (L. Zhang et al., 2014). Clonal of PGCCs showed association with the expression of stem cell markers, including octamer-binding transcription factor 4 (OCT4), SRY (sex determining region Y)-box 2, also known as SOX2, and stage-specific embryonic antigen-1 (SSEA-1) (Niu, Mercado-Urbe, & Liu, 2017). Moreover, PGCCs could also produce daughter cells, which were obviously resistant to chemotherapy (i.e., paclitaxel) (Chen et al., 2017). Spheroid formation was propose of metastatic cancer cells shedding from the primary tumor site, which spheroids had resistance to radiation or common therapeutic drugs (Shield, Ackland, Ahmed, & Rice, 2009). Our result showed that siARID1A-transfected MDCK cells generated the large spheroid formation. It is consistent with the previous study that the shARID1A 9090 SAS cells (squamous cell carcinoma cell line of the oral tongue) exhibited large spheroid formation as compared with the shControl cells, and showed up-regulation of OCT4 and Sox2 stem cell proteins (Lu et al., 2016).

Interestingly, activation of specific transcription factors, including SNAI1, SNAI2 (Slug), zinc finger E-box-binding homeobox 1/2 (ZEB1/2), and Twist-related protein 1/2 (Twist1/2), is common in the cells undergoing EMT and carcinogenesis (Lee et al., 2006; Q. C. Zhu et al., 2013). Clinically, SNAI1 expression showed a strong correlation with tumor recurrence, metastasis, and resistance to therapy (Chen et al., 2017). Expression of SNAI1 protein was focused in our model. The result confirmed that SNAI1 signaling pathway was turned on in the siARID1A-transfected MDCK cells which is consistent with evidence in several cell lines, highlighting the roles of SNAI1 in EMT process, invasion, metastasis, and therapeutic resistance (Jia et al., 2018; Noman, Van Moer, Marani, & Gemmill, 2018; S. Wang et al., 2018; Y. Zhu et al., 2018)

Furthermore, mutations of *ARID1A* gene in kidney cancers were accessed from the Genome Data Commons (GDC). The results showed that mutation of *ARID1A* gene was one of the top-ten mutated genes in kidney cancers together with *PBRM1* (*Polybromo 1*), *VHL* (*von Hippel-Lindau*), *TP53* (*tumor suppressor 53*), *SETD2* (*SET domain-containing protein 2*), etc. Among these genes, mutations of *PBRM1* and *VHL* are common of ccRCC subtype (Cairns, 2011; Lindgren, Sjolund, & Axelson, 2018). Mutation of *MET* proto-oncogene and inactivation of *SWI/SNF* chromatin/histone modifiers are common in pRCC type I, whereas mutations of *FH* (*fumarate hydratase*), *SETD2*, and *CDKN2A* (*cyclin dependent kinase inhibitor 2A*) are more common in pRCC type II (Cairns, 2011; Lindgren et al., 2018). Chromophobe RCC is associated with mutations of *PTEN* (*phosphatase and tensin homolog*), *TP53*, and *TERT* (*telomerase reverse transcriptase*) mitochondrial genes (Cairns, 2011; Lindgren et al., 2018). Consistent with our study, a recent study by Ricketts et al. showed that mutations of *SWI/SNF* complex genes, including *PBRM1*, *ARID1A* and *SMARCA4*, were found notably in ccRCC (47.1%), pRCC (53.0%) and chRCC (14.9%), respectively (Ricketts et al., 2018). There was thus plausible that mutation of *ARID1A* might be involved in development and/or progression of RCC.

Mutation profiles of *ARID1A* gene in patients with kidney cancers were also investigated. From a total of 32 mutations found, the majority came from frameshift mutations (14/32) and missense mutations (14/32), whereas only 4 had stop-gained mutations. The mutation profiles occurred along the protein sequence of ARID1A,

including the two conserved domains (ARID DNA-binding domain and SWI/SNF-like complex subunit BAF250/Osa domain on the C-terminus) of the Pfam structure. Human ARID1A protein, also known as BAF250a, comprises 2,285 amino acids with a molecular mass of approximately 250 kDa. ARID1A protein is a component of the SWI/SNF chromatin remodeling complex that regulates gene transcription (Nie et al., 2000). The ARID DNA-binding domain (at residues 1019-1104) involved in selective binding to AT-rich sites of DNA and assembly of polymorphic BRG-/BRM-associated factor (BAF) and polybromo-associated BAF (PBAF) complexes (Sandhya, Maulik, Giri, & Singh, 2018). The C-terminal domain of ARID1A (at residues 1976-2231) is essential for stimulating glucocorticoid receptor (GR)-mediated transcriptional activation (Nie et al., 2000). Structural modeling has shown that ARID1A mediates GR interaction via the SWI/SNF complex that facilitates the transcriptional activation by GR (Muratcioglu et al., 2015). Recurrent mutation and protein loss of *ARID1A* gene are most frequently found in ovarian clear cell carcinoma (mutation = 46-57 % and protein loss = 41-59 %) and endometrial endometrioid carcinoma (mutation = 39-44 % and protein loss = 19-34 %) (Wiegand et al., 2010; R.-C. Wu, Wang, & Shih, 2014; 2014). Due to these mutations found in *ARID1A*, the structural and functional complexes of ARID1A protein and SWI/SNF would be expected to be affected in cancer patients. Further analysis showed that the patients with mutated *ARID1A* had a shorter survival than those without *ARID1A* mutations. Consistently, several studies have also reported that patients with either mutation or loss of ARID1A expression had a shorter disease-free survival and/or poorer overall outcome/survival (He et al., 2015; Katagiri et al., 2011; L. Yang et al., 2016). Our results were in concordance with those reported previously indicating that *ARID1A* is an important tumor suppressor gene in RCC and may also serve as a prognostic biomarker in RCC patients.

Globally, most of the RCC cases are affected by three main RCC subtypes, including ccRCC (75%), pRCC (15%), and chRCC (5%) (Banumathy, & Cairns, 2010). Sarcomatoid differentiation is distinct in a high-grade and poorly differentiated components and is found in only 5% of RCC (Corti et al., 2006). In this present study, we recruited a variety of RCC subtypes and grades, including ccRCC (grade I), ccRCC (grade II), chRCC, pRCC and sRCC from patients with age of >45 years



following the recent classification system and histopathological descriptions (Zhou, & He). To our knowledge, this is the first evidence demonstrating ARID1A protein expression in sRCC.

Our histopathological data showed that ARID1A localized mainly in the nuclei of lymphocytes, fibroblasts, intraglomerular cells and renal tubular epithelial cells in the adjacent non-cancer tissues. By contrast, nuclear ARID1A expression was diminished in the cancer cells, especially in ccRCC and chRCC. However, no significant changes were observed in pRCC and sRCC. Consistent with the recent studies, ARID1A protein was generally expressed in the nuclei of the stromal cells—such as lymphocytes, fibroblasts and endothelial cells, which is frequently used as a positive control to compare with that in the cancer cells (Agaimy et al., 2017; Takao et al., 2017; L. Zhang et al., 2018). In our study, the loss/decrease of ARID1A expression was commonly found in the nuclei of the cancer cells, especially in ccRCC and chRCC, when compared with the paired adjacent non-cancer tissues. Such loss or decrease could be explained by mutations and molecular/epigenetic variations because the majority of the *ARID1A* mutations were the inactivation by nonsense and frameshift mutations throughout the gene that could lead to the loss of ARID1A expression (J. N. Wu, & Roberts, 2013; R.-C. Wu et al., 2014). Alternatively, in-frame indel (insertion-deletion) mutations of *ARID1A* affecting the nuclear export signal could disturb the stability of ARID1A protein expression, like nonsense and frameshift mutations. Degradation of abnormal nuclear ARID1A is regulated by the nuclear ubiquitin-proteasome system (Guan, Gao, Wu, Wang, & Shih Ie, 2012). On the other hand, epigenetic silencing might be also involved (X. Zhang et al., 2013). *ARID1A* gene promoter hypermethylation is the main etiologic factor for the decreasing *ARID1A* mRNA expression that is also controlled by a repressive histone modification in invasive breast cancers (X. Zhang et al., 2013).

Currently, there is no clearly specific method for investigating ARID1A protein expression although some interpretation systems, such as the three staining grades (Agaimy et al., 2017) and Histo-score (Numata et al., 2013), had been used. In this study, we employed the Allred scoring and grading system to quantify ARID1A protein expression in the renal tissues. This strategy was also applied in a recent study evaluating ARID1A expression in breast cancer tissues (Takao et al., 2017).

The Allred scores of ARID1A protein expression in cancer tissues, particularly ccRCC (grade I), ccRCC (grade II) and chRCC, were significantly lower than in the paired non-cancer tissues, whereas those of pRCC and sRCC subtypes had no significant changes. Interestingly, a previous report has shown a similar results indicating that ARID1A protein expression was significantly decreased mostly in ccRCC (Lichner et al., 2013). In addition, the four-grade system allowed us to discriminate the RCC patients with negative to weak expression from those with moderate to strong expression. As a result, the RCC patients with negative to weak ARID1A expression tended to have lower progression-free survival, consistent with another study in cervical cancer demonstrating that the patients with ARID1A loss had significantly lower survival (Cho et al., 2013).

In summary, the role of ARID1A on EMT inducing carcinogenesis in nonmalignant MDCK renal cells has been reported in our study. Knockdown of ARID1A protein increases in cell proliferation, cell viability, mesenchymal phenotypes, migratory activity, nuclear enlargement, multicellular spheroid formation. The mechanism could be driven through TGF- $\beta$ 1/SNAI1 signaling pathway. Additionally, we have shown herein that *ARID1A* was one among the most common mutated genes found in kidney cancers. The down-regulation of ARID1A protein expression could be confirmed in human RCC tissues, especially in ccRCC and chRCC. Level of ARID1A protein expression in the adjacent non-cancer renal tissues was significantly lower in ccRCC (grade II) than in ccRCC (grade I). Moreover, all of the RCC cases with negative ARID1A protein expression (3/11 cases with ccRCC (grade II) and 2/6 chRCC cases) had metastasis 1–50 months after the surgical removal. Five-year progression-free survival tended to be shorter in RCC patients with negative to weak ARID1A expression. Taken together, these data implicate that the defect/loss of ARID1A expression is associated with poor prognosis and metastasis of RCC and thus may serve as the prognostic marker of RCC, particularly ccRCC and chRCC subtypes.

## CHAPTER VI

### CONCLUSION

We concluded that down-regulation of ARID1A in non-malignant renal cells promoted carcinogenesis features, including increases in cell viability, EMT, migratory activity, nuclear enlargement, multicellular spheroid formation. These features were most likely driven through TGF- $\beta$ 1/SNAI1 signaling pathway. The Genomic Data Commons (GDC) database showed that *ARID1A* gene was one of the top-ten mutated genes found in kidney cancers and its mutations were found along crucial sequences. By immunohistochemistry, expression level of ARID1A protein is particularly decreased in clear cell RCC (ccRCC) and chromophobe RCC (chRCC) as compared to the adjacent non-cancer tissues. Patients with negative to weak ARID1A expression tended to have short 5-year progression-free survival and cancer metastasis. Taken together, these results implicate that ARID1A plays important roles in carcinogenesis and cancer progression by triggering EMT in renal cells. The defect/loss of ARID1A expression is associated with poor prognosis and metastasis of RCC and thus may serve as the prognostic marker of RCC, particularly ccRCC and chRCC subtypes.



## REFERENCES



## REFERENCES

- Agaimy, A., Cheng, L., Egevad, L., Feyerabend, B., Hes, O., & Keck, B. (2017). Rhabdoid and undifferentiated phenotype in renal cell carcinoma: analysis of 32 cases indicating a distinctive common pathway of dedifferentiation frequently associated with SWI/SNF complex deficiency. *The American Journal of Surgical Pathology*, 41(2), 253-262.
- Al-Ahmadie, H. A., Alden, D., Fine, S. W., Gopalan, A., Touijer, K. A., & Russo, P. (2011). Role of immunohistochemistry in the evaluation of needle core biopsies in adult renal cortical tumors: an ex vivo study. *The American Journal of Surgical Pathology*, 35(7), 949-961.
- Albadine, R., Schultz, L., Illei, P., Ertoy, D., Hicks, J., & Sharma, R. (2010). PAX8 (+)/p63 (-) immunostaining pattern in renal collecting duct carcinoma (CDC): a useful immunoprofile in the differential diagnosis of CDC versus urothelial carcinoma of upper urinary tract. *The American Journal of Surgical Pathology*, 34(7), 965-969.
- Aluksanasuwan, S., Sueksakit, K., Fong-Ngern, K., & Thongboonkerd, V. (2017). Role of HSP60 (HSPD1) in diabetes-induced renal tubular dysfunction: regulation of intracellular protein aggregation, ATP production, and oxidative stress. *FASEB J*, 31(5), 2157-2167.
- Aplin, J. D., Haigh, T., Vicovac, L., Church, H. J., & Jones, C. J. (1998). Anchorage in the developing placenta: an overlooked determinant of pregnancy outcome?. *Human Fertility (Cambridge, England)*, 1(1), 75-79.
- Ata-ur-Rehman, R., Ashraf, S., Rahim, J., Hussain, N., Jamil, M. N., & Tahir, M. M. (2015). Clinical presentation of renal cell carcinoma. *Journal of Ayub Medical College Abbottabad*, 27(2), 326-328.
- Aufderheide, E., Chiquet-Ehrismann, R., & Ekblom, P. (1987). Epithelial-mesenchymal interactions in the developing kidney lead to expression of tenascin in the mesenchyme. *Journal of Cell Biology*, 105(1), 599-608.
- Bagchi, A., & Mills, A. A. (2008). The quest for the 1p36 tumor suppressor. *Cancer Research*, 68(8), 2551.

- Bansal, R. K., Tanguay, S., Finelli, A., Rendon, R., Moore, R. B., & Breau, R. H. (2017). Positive surgical margins during partial nephrectomy for renal cell carcinoma: Results from Canadian Kidney Cancer information system (CKCis) collaborative. *Canadian Urological Association Journal*, 11(6), 182-187.
- Banumathy, G., & Cairns, P. (2010). Signaling pathways in renal cell carcinoma. *Cancer Biology & Therapy*, 10(7), 658-664.
- Bassal, M., C Mertens, A., Taylor, L., P Neglia, J., S Greffe, B., & Hammond, S. (2006). Risk of selected subsequent carcinomas in survivors of childhood cancer: A report from the childhood cancer survivor study. *Journal of Clinical Oncology: official journal of the American Society of Clinical Oncology*, 24(3), 476-483.
- Beisland, C., Johannesen, T. B., Klepp, O., Axcrone, U., Torgersen, K. M., & Kowalski, J. (2017). Overall survival in renal cell carcinoma after introduction of targeted therapies: a Norwegian population-based study. *OncoTargets and Therapy*, 10, 371-385.
- Bianchi, M., Sun, M., Jeldres, C., Shariat, S. F., Trinh, Q. D., & Briganti, A. (2012). Distribution of metastatic sites in renal cell carcinoma: a population-based analysis. *Annals of Oncology*, 23(4), 973-980.
- Bitler, B. G., Fatkhutdinov, N., & Zhang, R. (2015). Potential therapeutic targets in ARID1A-mutated cancers. *Expert Opinion on Therapeutic Targets*, 19(11), 1419-1422.
- Bonsib, S. M. (2009). Renal cystic diseases and renal neoplasms: a mini-review. *Clinical Journal of the American Society of Nephrology*, 4(12), 1998-2007.
- Bürgesser, M. V., Riva, V., Ojeda, S. M., Muñoz Morales, D., Calafat, P., & Diller, A. (2014). Expression of VEGF-A, HIF-1 A, CD34 and Ki67 in clear cell renal cell carcinomas and their relationship with conventional prognostic markers. *Revista de la Facultad de Ciencias Médicas (Córdoba, Argentina)*, 71(1), 7-15.
- Butnor, K. J., & Ordonez, N. G. (2008). Uroplakin is not a reliable immunohistochemical marker for malignant mesothelioma of the pleura. *Applied Immunohistochemistry & Molecular Morphology*, 16(4), 326-328.

- Cairns, P. (2011). Renal cell carcinoma. *Cancer Biomarkers*, 9(1-6), 461-473.
- Cao, H., Xu, E., Liu, H., Wan, L., & Lai, M. (2015). Epithelial-mesenchymal transition in colorectal cancer metastasis: A system review. *Pathology Research and Practice*, 211(8), 557-569.
- Capitanio, U., & Montorsi, F. (2016). Renal cancer. *The Lancet*, 387(10021), 894-906.
- Chen, Y., Lu, L., Feng, B., Han, S., Cui, S., & Chu, X. (2017). Non-coding RNAs as emerging regulators of epithelial to mesenchymal transition in non-small cell lung cancer. *Oncotarget*, 8(22), 36787-36799.
- Cho, H., Kim, J. S. Y., Chung, H., Perry, C., Lee, H., & Kim, J. H. (2013). Loss of ARID1A/BAF250a expression is linked to tumor progression and adverse prognosis in cervical cancer. *Human Pathology*, 44(7), 1365-1374.
- Chow, W. H., Gridley, G., Fraumeni, J. F., Jr., & Jarvholm, B. (2000). Obesity, hypertension, and the risk of kidney cancer in men. *The New England Journal of Medicine*, 343(18), 1305-1311.
- Chow, W.-H., Dong, L. M., & Devesa, S. S. (2010). Epidemiology and risk factors for kidney cancer. *Nature Reviews Urology*, 7(5), 245-257.
- Clague, J., Shao, L., Lin, J., Chang, S., Zhu, Y., & Wang, W. (2009). Sensitivity to NNKOAc is associated with renal cancer risk. *Carcinogenesis*, 30(4), 706-710.
- Corti, B., Zucchini, N., Fabbrizio, B., Martorana, G., Schiavina, R., & Grigioni, A. D. E. (2006). Pathology and molecular pathogenesis of renal cell carcinoma. *European Urology Supplements*, 5(8), 573-579.
- de Peralta-Venturina, M., Moch, H., Amin, M., Tamboli, P., Hailemariam, S., & Mihatsch, M. (2001). Sarcomatoid differentiation in renal cell carcinoma: A study of 101 cases. *The American Journal of Surgical Pathology*, 25(3), 275-284.
- Eble, J. N., S. G., Epstein, J. I., & Sesterhenn, I. A. (2004). *Pathology and genetics, tumors of the urinary system and male genital organs*. Lyon: IAPC.
- Edge, S. B., & Compton, C. C. (2010). The American Joint Committee on Cancer: the 7th Edition of the AJCC cancer staging manual and the future of TNM. *Annals of Surgical Oncology*, 17(6), 1471-1474.

- Ferlay, J., Soerjomataram, I., Dikshit, R., Eser, S., Mathers, C., & Rebelo, M. (2015). Cancer incidence and mortality worldwide: sources, methods and major patterns in GLOBOCAN 2012. *International Journal of Cancer*, 136(5), E359-386.
- Flanigan, R. C., Salmon, S. E., Blumenstein, B. A., Bearman, S. I., Roy, V., & McGrath, P. C. (2001). Nephrectomy followed by interferon alfa-2b compared with interferon alfa-2b alone for metastatic renal-cell cancer. *The New England Journal of Medicine*, 345(23), 1655-1659.
- Flores-Alcantar, A., Gonzalez-Sandoval, A., Escalante-Alcalde, D., & Lomeli, H. (2011). Dynamics of expression of ARID1A and ARID1B subunits in mouse embryos and in cells during the cell cycle. *Cell and Tissue Research*, 345(1), 137-148.
- Foty R. (2011). A simple hanging drop cell culture protocol for generation of 3D spheroids. *Journal of Visualized Experiments: JoVE*, 51, 2720.
- Fuhrman, S. A., Lasky, L. C., & Limas, C. (1982). Prognostic significance of morphologic parameters in renal cell carcinoma. *The American Journal of Surgical Pathology*, 6(7), 655-663.
- Gago-Dominguez, M., Castelao, J. E., Yuan, J. M., Ross, R. K., & Yu, M. C. (2002). Lipid peroxidation: a novel and unifying concept of the etiology of renal cell carcinoma (United States). *Cancer Causes & Control*, 13(3), 287-293.
- Gershman, B., Moreira, D. M., Thompson, R. H., Boorjian, S. A., Lohse, C. M., & Costello, B. A. (2017). Renal cell carcinoma with isolated lymph node involvement: Long-term natural history and predictors of oncologic outcomes following surgical resection. *European Urology*, 72(2), 300-306.
- Gnemmi, V., Bouillez, A., Gaudelot, K., Hémon, B., Ringot, B., & Pottier, N. (2014). MUC1 drives epithelial-mesenchymal transition in renal carcinoma through Wnt/ $\beta$ -catenin pathway and interaction with SNAIL promoter. *Cancer Letters*, 346(2), 225-236.



- Group, U. S. C. S. W. (2017). *United States cancer statistics: 1999-2014 Incidence and mortality web-based report*. Atlanta: U.S. Department of Health and Human Services. Retrieved January 15, 2018, from Centers for Disease Control and Prevention and National Cancer Institute  
[https://nccd.cdc.gov/uscs/topten\\_cancers.aspx](https://nccd.cdc.gov/uscs/topten_cancers.aspx)
- Guan, B., Gao, M., Wu, C. H., Wang, T. L., & Shih Ie, M. (2012). Functional analysis of in-frame indel ARID1A mutations reveals new regulatory mechanisms of its tumor suppressor functions. *Neoplasia*, 14(10), 986-993.
- Guan, B., Mao, T. L., Panuganti, P. K., Kuhn, E., Kurman, R. J., Maeda, D., et al. (2011). Mutation and loss of expression of ARID1A in uterine low-grade endometrioid carcinoma. *The American Journal of Surgical Pathology*, 35(5), 625-632.
- Hay, E. D. (2005). The mesenchymal cell, its role in the embryo, and the remarkable signaling mechanisms that create it. *Developmental Dynamics*, 233(3), 706-720.
- He, F., Li, J., Xu, J., Zhang, S., Xu, Y., & Zhao, W. (2015). Decreased expression of ARID1A associates with poor prognosis and promotes metastases of hepatocellular carcinoma. *Journal of Experimental & Clinical Cancer Research*, 34, 47.
- Helming, K. C., Wang, X., Wilson, B. G., Vazquez, F., Haswell, J. R., & Manchester, H. E. (2014). ARID1B is a specific vulnerability in ARID1A-mutant cancers. *Nature Medicine*, 20(3), 251-254.
- Hoeben, A., Landuyt, B., Highley, M. S., Wildiers, H., Van Oosterom, A. T., & De Bruijn, E. A. (2004). Vascular endothelial growth factor and angiogenesis. *Pharmacological reviews*, 56(4), 549-580.
- Ibarrola-Villava, M., Llorca-Cardenosa, M. J., Tarazona, N., Mongort, C., Fleitas, T., & Perez-Fidalgo, J. A. (2015). Deregulation of ARID1A, CDH1, cMET and PIK3CA and target-related microRNA expression in gastric cancer. *Oncotarget*, 6(29), 26935-26945.

- Ibragimova, I., Maradeo, M. E., Dulaimi, E., & Cairns, P. (2013). Aberrant promoter hypermethylation of PBRM1, BAP1, SETD2, KDM6A and other chromatin-modifying genes is absent or rare in clear cell RCC. *Epigenetics*, 8(5), 486-493.
- Ivanova, L., Butt, M. J., & Matsell, D. G. (2008). Mesenchymal transition in kidney collecting duct epithelial cells. *American journal of physiology. Renal physiology*, 294(5), F1238-1248.
- Jia, Z., Wang, M., Li, S., Li, X., Bai, X. Y., & Xu, Z. (2018). U-box ubiquitin ligase PPIL2 suppresses breast cancer invasion and metastasis by altering cell morphology and promoting SNAIL ubiquitination and degradation. *Cell Death and Disease*, 9(2), 63.
- Jonasch, E., Gao, J., & Rathmell, W. K. (2014). Renal cell carcinoma. *BMJ*, 10(349), g4797.
- Jones, S., Wang, T. L., Shih Ie, M., Mao, T. L., Nakayama, K., & Roden, R. (2010). Frequent mutations of chromatin remodeling gene ARID1A in ovarian clear cell carcinoma. *Science (New York, N.Y.)*, 330(6001), 228–231.
- Kabat, G. C., Silvera, S. A. N., Miller, A. B., & Rohan, T. E. (2007). A cohort study of reproductive and hormonal factors and renal cell cancer risk in women. *British Journal of Cancer*, 96(5), 845-849.
- Kadoch, C., & Crabtree, G. R. (2015). Mammalian SWI/SNF chromatin remodeling complexes and cancer: Mechanistic insights gained from human genomics. *Science Advances*, 1(5), e1500447.
- Kalluri, R., & Weinberg, R. A. (2009). The basics of epithelial-mesenchymal transition. *The Journal of Clinical Investigation*, 119(6), 1420-1428.
- Kanlaya, R., Khamchun, S., Kapincharanon, C., & Thongboonkerd, V. (2016). Protective effect of epigallocatechin-3-gallate (EGCG) via Nrf2 pathway against oxalate-induced epithelial mesenchymal transition (EMT) of renal tubular cells. *Scientific Reports*, 6, 30233.

- Katagiri, A., Nakayama, K., Rahman, M. T., Rahman, M., Katagiri, H., & Nakayama, N. (2011). Loss of ARID1A expression is related to shorter progression-free survival and chemoresistance in ovarian clear cell carcinoma. *Modern Pathology*, 25, 282.
- Kim, K. K., Kugler, M. C., Wolters, P. J., Robillard, L., Galvez, M. G., & Brumwell, A. N. (2006). Alveolar epithelial cell mesenchymal transition develops in vivo during pulmonary fibrosis and is regulated by the extracellular matrix. *Proceedings of the National Academy of Sciences of the United States of America*, 103(35), 13180-13185.
- Klatte, T., Seitz, C., Waldert, M., de Martino, M., Kikic, Z., & Bohmig, G. A. (2010). Features and outcomes of renal cell carcinoma of native kidneys in renal transplant recipients. *BJU International*, 105(9), 1260-1265.
- Kumar, V., & Robbins, S. L. 1. (2007). *Robbins basic pathology* (8th ed.). Philadelphia, PA: Saunders/Elsevier.
- Lambe, M., Lindblad, P., Wu, J., Remler, R., & Hsieh, C. C. (2002). Pregnancy and risk of renal cell cancer: a population-based study in Sweden. *British Journal Of Cancer*, 86(9), 1425-1429.
- Landolt, L., Eikrem, Ø., Strauss, P., Scherer, A., Lovett, D. H., & Beisland, C. (2017). Clear cell renal cell carcinoma is linked to epithelial-to-mesenchymal transition and to fibrosis. *Physiological Reports*, 5(11), e13305.
- Lang, H., & Jacqmin, D. (2003). Prognostic factors in renal cell carcinoma. *EAU update series*, 1(4), 215-219.
- Lee, J. E., Hankinson, S. E., & Cho, E. (2009). Reproductive factors and risk of renal cell cancer: The Nurses' health study. *American journal of epidemiology*, 169(10), 1243-1250.
- Lee, J. E., Hunter, D. J., Spiegelman, D., Adami, H. O., Albanes, D., & Bernstein, L. (2007). Alcohol intake and renal cell cancer in a pooled analysis of 12 prospective studies. *Journal of the National Cancer Institute*, 99(10), 801-810.
- Lee, J. M., Dedhar, S., Kalluri, R., & Thompson, E. W. (2006). The epithelial-mesenchymal transition: new insights in signaling, development, and disease. *Journal of Cell Biology*, 172(7), 973-981.

- Li, L., & Kalantar-Zadeh, K. (2013). Obesity that makes kidney cancer more likely but helps fight it more strongly. *Journal of the National Cancer Institute*, 105(24), 1848-1849.
- Lichner, Z., Scorilas, A., White, N. M., Girgis, A. H., Rotstein, L., & Wiegand, K. C. (2013). The chromatin remodeling gene ARID1A is a new prognostic marker in clear cell renal cell carcinoma. *The American Journal of Pathology*, 182(4), 1163-1170.
- Lindgren, D., Sjolund, J., & Axelson, H. (2018). Tracing renal cell carcinomas back to the nephron. *Trends Cancer*, 4(7), 472-484.
- Liu, P., Wakamiya, M., Shea, M. J., Albrecht, U., Behringer, R. R., & Bradley, A. (1999). Requirement for Wnt3 in vertebrate axis formation. *Nature Genetics*, 22(4), 361-365.
- Ljungberg, B. (2007). Prognostic markers in renal cell carcinoma. *Current Opinion in Urology*, 17(5), 303-308.
- Ljungberg, B., Bensalah, K., Canfield, S., Dabestani, S., Hofmann, F., Hora, M. (2015). EAU guidelines on renal cell carcinoma: 2014 update. *European Urology*, 67(5), 913-924.
- Ljungberg, B., Cowan, N. C., Hanbury, D. C., Hora, M., Kuczyk, M. A., & Merseburger, A. S. (2010). EAU guidelines on renal cell carcinoma: 2010 update. *European Urology*, 58(3), 398-406.
- Lojanapiwat, B. (2015). Urologic cancer in Thailand. *Japanese Journal of Clinical Oncology*, 45(11), 1007-1015.
- Lu, W.-C., Liu, C.-J., Tu, H.-F., Chung, Y.-T., Yang, C.-C., & Kao, S.-Y. (2016). miR-31 targets ARID1A and enhances the oncogenicity and stemness of head and neck squamous cell carcinoma. *Oncotarget*, 7(35), 57254-57267.
- Luo, B., Cheung, H. W., Subramanian, A., Sharifnia, T., Okamoto, M., & Yang, X. (2008). Highly parallel identification of essential genes in cancer cells. *Proceedings of the National Academy of Sciences*, 105(51), 20380-20385.
- Malir, F., Ostry, V., Pfohl-Leszkowicz, A., & Novotna, E. (2013). Ochratoxin A: developmental and reproductive toxicity-an overview. *Birth Defects Research. Part B, Developmental and Reproductive Toxicology*, 98(6), 493-502.



- Mamo, A., Cavallone, L., Tuzmen, S., Chabot, C., Ferrario, C., & Hassan, S. (2011). An integrated genomic approach identifies ARID1A as a candidate tumor-suppressor gene in breast cancer. *Oncogene*, 31, 2090.
- Mamo, A., Cavallone, L., Tuzmen, S., Chabot, C., Ferrario, C., & Hassan, S. (2011). An integrated genomic approach identifies ARID1A as a candidate tumor-suppressor gene in breast cancer. *Oncogene*, 31, 2090.
- Manissorn, J., Khamchun, S., Vinaiphath, A., & Thongboonkerd, V. (2016). Alpha-tubulin enhanced renal tubular cell proliferation and tissue repair but reduced cell death and cell-crystal adhesion. *Scientific reports*, 6(1), 28808.
- Mathur, R., Alver, B. H., San Roman, A. K., Wilson, B. G., Wang, X., & Agoston, A. T. (2017). ARID1A loss impairs enhancer-mediated gene regulation and drives colon cancer in mice. *Nature genetics*, 49(2), 296-302.
- Mikami, S., Katsube, K., Oya, M., Ishida, M., Kosaka, T., & Mizuno, R. (2011). Expression of Snail and Slug in renal cell carcinoma: E-cadherin repressor Snail is associated with cancer invasion and prognosis. *Laboratory investigation*, 91(10), 1443-1458.
- Moore, K. L., Persaud, T. V. N., & Torchia, M. G. (2015). *The developing human: Clinically oriented embryology* (10<sup>th</sup> ed.). Philadelphia: Elsevier.
- Muratcioglu, S., Presman, Diego M., Pooley, John R., Grøntved, L., Hager, Gordon L., & Nussinov, R. (2015). Structural modeling of GR interactions with the SWI/SNF chromatin remodeling complex and C/EBP. *Biophysical Journal*, 109(6), 1227-1239.
- Murphy WM, G. D., & Perlman, E. J. (2004). Kidney tumors in adults. Tumors of the kidney, bladder, and related urinary structures. *AFIP Atlas of Tumor Pathology*, 2004, 185-187.
- Nawshad, A., Lagamba, D., Polad, A., & Hay, E. D. (2005). Transforming growth factor-beta signaling during epithelial-mesenchymal transformation: implications for embryogenesis and tumor metastasis. *Cells Tissues Organs*, 179(1-2), 11-23.

- Ni, D., Ma, X., Li, H.-Z., Gao, Y., Li, X.-T., & Zhang, Y. (2014). Downregulation of FOXO3a promotes tumor metastasis and is associated with metastasis-free survival of patients with clear cell renal cell carcinoma. *Clinical Cancer Research*, 20(7), 1779.
- Nie, Z., Xue, Y., Yang, D., Zhou, S., Deroo, B. J., & Archer, T. K. (2000). A specificity and targeting subunit of a human SWI/SNF family-related chromatin-remodeling complex. *Molecular and Cellular Biology*, 20(23), 8879-8888.
- Niu, N., Mercado-Urbe, I., & Liu, J. (2017). Dedifferentiation into blastomere-like cancer stem cells via formation of polyploid giant cancer cells. *Oncogene*, 36(34), 4887-4900.
- Noman, M. Z., Van Moer, K., Marani, V., & Gemmill, R. M. (2018). CD47 is a direct target of SNAI1 and ZEB1 and its blockade activates the phagocytosis of breast cancer cells undergoing EMT. *Oncoimmunology*, 7(4), e1345415.
- Numata, M., Morinaga, S., Watanabe, T., Tamagawa, H., Yamamoto, N., & Shiozawa, M. (2013). The clinical significance of SWI/SNF complex in pancreatic cancer. *International Journal of Oncology Research*, 42(2), 403-410.
- Nuovo, A. J., Garofalo, M., Mikhail, A., Nicol, A. F., Vianna-Andrade, C., & Nuovo, G. J. (2013). The effect of aging of formalin-fixed paraffin-embedded tissues on the in situ hybridization and immunohistochemistry signals in cervical lesions. *Diagnostic Molecular Pathology*, 22(3), 164-173.
- Pal, S. K., Sonpavde, G., Agarwal, N., Vogelzang, N. J., Srinivas, S., & Haas, N. B. (2017). Evolution of circulating tumor DNA profile from first-line to subsequent therapy in metastatic renal cell carcinoma. *European Urology*, 72(4), 557-564.
- Pantuck, A. J., Belldegrun, A. S., & Figlin, R. A. (2007). Cytoreductive nephrectomy for metastatic renal cell carcinoma: is it still imperative in the era of targeted therapy?. *Clinical Cancer Research*, 13(2 Pt 2), 693s-696s.
- Park, J. H., Lee, C., Suh, J. H., Chae, J. Y., Kim, H. W., & Moon, K. C. (2015). Decreased ARID1A expression correlates with poor prognosis of clear cell renal cell carcinoma. *Human Pathology*, 46(3), 454-460.

- Patard, J. J., Leray, E., Rodriguez, A., Rioux-Leclercq, N., Guille, F., & Lobel, B. (2003). Correlation between symptom graduation, tumor characteristics and survival in renal cell carcinoma. *European Urology*, 44(2), 226-232.
- Patsialou, A., Wilsker, D., & Moran, E. (2005). DNA-binding properties of ARID family proteins. *Nucleic Acids Research*, 33(1), 66-80.
- Peerapen, P., Chaiyarit, S., & Thongboonkerd, V. (2018). Protein network analysis and functional studies of calcium oxalate crystal-induced cytotoxicity in renal tubular epithelial cells. *Proteomics*, 18(8), e1800008.
- Petejova, N., & Martinek, A. (2016). Review of etiology, pathophysiology and risk factors. *Biomedical Papers of the Medical Faculty of the University Palacky, Olomouc, Czechoslovakia*, 160(2), 183-194.
- Pfohl-Leszkowicz, A. (2009). Ochratoxin A and Aristolochic Acid involvement in nephropathies and associated urothelial tract tumours. *Archives of Industrial Hygiene and Toxicology*, 60(4), 465-83.
- Pialoux, V., Brown, A. D., Leigh, R., Friedenreich, C. M., & Poulin, M. J. (2009). Effect of cardiorespiratory fitness on vascular regulation and oxidative stress in postmenopausal women. *Hypertension*, 54(5), 1014-1020.
- Piva, F., Giulietti, M., Santoni, M., Occhipinti, G., Scarpelli, M., & Lopez-Beltran, A. (2016). Epithelial to mesenchymal transition in renal cell carcinoma: Implications for cancer therapy. *Molecular Diagnosis & Therapy*, 20(2), 111-117.
- Popperl, H., Schmidt, C., Wilson, V., Hume, C. R., Dodd, J., & Krumlauf, R. (1997). Misexpression of Cwnt8C in the mouse induces an ectopic embryonic axis and causes a truncation of the anterior neuroectoderm. *Development*, 124(15), 2997-3005.
- Potenta, S., Zeisberg, E., & Kalluri, R. (2008). The role of endothelial-to-mesenchymal transition in cancer progression. *British Journal of Cancer*, 99(9), 1375-1379.
- Protzel, C., Maruschke, M., & Hakenberg, O. W. (2012). Epidemiology, aetiology, and pathogenesis of renal cell carcinoma. *European Urology Supplements*, 11(3), 52-59.

- Qureshi, A., & Pervez, S. (2010). Allred scoring for ER reporting and its impact in clearly distinguishing ER negative from ER positive breast cancers. *The Journal of the Pakistan Medical Association*, 60(5), 350-353.
- Rao, Q., Xia, Q. Y., Shen, Q., Shi, S. S., Tu, P., & Shi, Q. L. (2014). Coexistent loss of INI1 and BRG1 expression in a rhabdoid renal cell carcinoma (RCC): implications for a possible role of SWI/SNF complex in the pathogenesis of RCC. *International journal of clinical and experimental pathology*, 7(4), 1782-1787.
- Renehan, A. G., Tyson, M., Egger, M., Heller, R. F., & Zwahlen, M. (2008). Body-mass index and incidence of cancer: a systematic review and meta-analysis of prospective observational studies. *Lancet*, 371(9612), 569-578.
- Richardson, C. R., Newton, T. L., Abraham, J. J., Sen, A., Jimbo, M., & Swartz, A. M. (2008). A meta-analysis of pedometer-based walking interventions and weight loss. *Annals of Family Medicine*, 6(1), 69-77.
- Ricketts, C. J., De Cubas, A. A., Fan, H., Smith, C. C., Lang, M., & Reznik, E. (2018). The Cancer Genome Atlas comprehensive molecular characterization of renal cell carcinoma. *Cell Reports*, 23(1), 313-326.e315.
- Rini, B. I., Campbell, S. C., & Escudier, B. (2009). Renal cell carcinoma. *Lancet*, 373(9669), 1119-1132.
- Ruijtenberg, S., & van den Heuvel, S. (2016). Coordinating cell proliferation and differentiation: Antagonism between cell cycle regulators and cell type-specific gene expression. *Cell Cycle*, 15(2), 196-212.
- Samartzis, E. P., Gutsche, K., Dedes, K. J., Fink, D., Stucki, M., & Imesch, P. (2014). Loss of ARID1A expression sensitizes cancer cells to PI3K- and AKT-inhibition. *Oncotarget*, 5(14), 5295-5303.
- Sandhya, S., Maulik, A., Giri, M., & Singh, M. (2018). Domain architecture of BAF250a reveals the ARID and ARM-repeat domains with implication in function and assembly of the BAF remodeling complex. *PLOS ONE*, 13(10), e0205267.
- Sharifi, N., & Farrar, W. L. (2006). Perturbations in hypoxia detection: a shared link between hereditary and sporadic tumor formation?. *Medical hypotheses*, 66(4), 732-735.



- Shen, S. S., Truong, L. D., Scarpelli, M., & Lopez-Beltran, A. (2012). Role of immunohistochemistry in diagnosing renal neoplasms: When is it really useful?. *The Archives of Pathology & Laboratory Medicine*, 136(4), 410-417.
- Shephard, E., Neal, R., Rose, P., Walter, F., & Hamilton, W. T. (2013). Clinical features of kidney cancer in primary care: a case-control study using primary care records. *The British Journal of General Practice*, 63(609), e250-255.
- Shield, K., Ackland, M. L., Ahmed, N., & Rice, G. E. (2009). Multicellular spheroids in ovarian cancer metastases: Biology and pathology. *Gynecologic oncology*, 113(1), 143-148.
- Shigetomi, H., Oonogi, A., Tsunemi, T., Tanase, Y., Yamada, Y., & Kajihara, H. (2011). The role of components of the chromatin modification machinery in carcinogenesis of clear cell carcinoma of the ovary (Review). *Oncology Letters*, 2(4), 591-597.
- Shuch, B., Vourganti, S., Ricketts, C. J., Middleton, L., Peterson, J., & Merino, M. J. (2014). Defining early-onset kidney cancer: Implications for germline and somatic mutation testing and clinical management. *Journal of Clinical Oncology*, 32(5), 431-437.
- Skromne, I., & Stern, C. D. (2001). Interactions between Wnt and Vg1 signalling pathways initiate primitive streak formation in the chick embryo. *Development*, 128(15), 2915-2927.
- Solomon, T. P. J., Haus, J. M., Kelly, K. R., Cook, M. D., Riccardi, M., & Rocco, M. (2009). Randomized trial on the effects of a 7-d low-glycemic diet and exercise intervention on insulin resistance in older obese humans. *The American Journal of Clinical Nutrition*, 90(5), 1222-1229.
- Takao, C., Morikawa, A., Ohkubo, H., Kito, Y., Saigo, C., & Sakuratani, T. (2017). Downregulation of ARID1A, a component of the SWI/SNF chromatin remodeling complex, in breast cancer. *Journal of Cancer*, 8(1), 1-8.
- Takeda, T., Banno, K., Okawa, R., Yanokura, M., Iijima, M., & Irie-Kunitomi, H. (2016). ARID1A gene mutation in ovarian and endometrial cancers (review). *Oncology Reports*, 35(2), 607-613.

- Takeshima, H., Niwa, T., Takahashi, T., Wakabayashi, M., Yamashita, S., & Ando, T. (2015). Frequent involvement of chromatin remodeler alterations in gastric field cancerization. *Cancer Letters*, 357(1), 328-338.
- Taştekin, E., Puyan, F., Kaplan, M., Tokuç, B., Caloglu, V.Y., & Ozyilmaz, F. (2012). The Relationship of Fuhrman Nuclear Grade, Tumor Stage and Sarcomatoid Differentiation with Survival in Renal Cell Carcinomas. *Balkan Medical Journal*, 2012, 14-20.
- Thanomkitti, K., Fong-Ngern, K., Sueksakit, K., Thuangtong, R., & Thongboonkerd, V. (2018). Molecular functional analyses revealed essential roles of HSP90 and lamin A/C in growth, migration, and self-aggregation of dermal papilla cells. *Cell Death Discovery*, 4, 53.
- The Cancer Genome Atlas Research, N. (2013). Comprehensive molecular characterization of clear cell renal cell carcinoma. *Nature*, 499, 43.
- Thiery, J. P., & Sleeman, J. P. (2006). Complex networks orchestrate epithelial-mesenchymal transitions. *Nature reviews. Molecular cell biology*, 7(2), 131-142.
- Thomas, P., Brickman, J. M., Popperl, H., Krumlauf, R., & Beddington, R. S. (1997). Axis duplication and anterior identity in the mouse embryo. *Cold Spring Harbor symposia on quantitative biology*, 62, 115-125.
- Toret, C. P., D'Ambrosio, M. V., Vale, R. D., Simon, M. A., & Nelson, W. J. (2014). A genome-wide screen identifies conserved protein hubs required for cadherin-mediated cell–cell adhesion. *Journal of Cell Biology*, 204(2), 265-279.
- Tornqvist, M. (2005). Acrylamide in food: the discovery and its implications: A historical perspective. *Advances in Experimental Medicine and Biology*, 561, 1-19.
- Tse, J. C., & Kalluri, R. (2007). Mechanisms of metastasis: epithelial-to-mesenchymal transition and contribution of tumor microenvironment. *Journal of Cellular Biochemistry*, 101(4), 816-829.
- Vandin, F., Upfal, E., & Raphael, B. J. (2011). Algorithms for detecting significantly mutated pathways in cancer. *Journal of Computational Biology*, 18(3), 507-522.

- Virk-Baker, M. K., Nagy, T. R., Barnes, S., & Groopman, J. (2014). Dietary acrylamide and human cancer: A systematic review of literature. *Nutrition and Cancer*, 66(5), 774-790.
- Wang, S., Li, J., Xie, J., Liu, F., Duan, Y., & Wu, Y. (2018). Programmed death ligand 1 promotes lymph node metastasis and glucose metabolism in cervical cancer by activating integrin  $\beta 4$ /SNAI1/SIRT3 signaling pathway. *Oncogene*, 37(30), 4164-4180.
- Wang, W., Friedland, S. C., Guo, B., O'Dell, M. R., Alexander, W. B., & Whitney-Miller, C. L. (2019). ARID1A, a SWI/SNF subunit, is critical to acinar cell homeostasis and regeneration and is a barrier to transformation and epithelial-mesenchymal transition in the pancreas. *Gut*, 68(7), 1245-1258.
- Wang, X., Nagl, N. G., Jr., Flowers, S., Zweitzig, D., Dallas, P. B., & Moran, E. (2004). Expression of p270 (ARID1A), a component of human SWI/SNF complexes, in human tumors. *The International Journal of Cancer*, 112(4), 636.
- Weikert, S., Boeing, H., Pischon, T., Weikert, C., Olsen, A., & Tjønneland, A. (2008). Blood pressure and risk of renal cell carcinoma in the European prospective investigation into cancer and nutrition. *American Journal of Epidemiology*, 167(4), 438-446.
- Wiegand, K. C., Shah, S. P., Al-Agha, O. M., Zhao, Y., Tse, K., & Zeng, T. (2010). ARID1A mutations in endometriosis-associated ovarian carcinomas. *The New England Journal of Medicine*, 363(16), 1532-1543.
- Wiklund, F., Tretli, S., Choueiri, T. K., Signoretti, S., Fall, K., & Adami, H. O. (2009). Risk of bilateral renal cell cancer. *Journal of Clinical Oncology*, 27(23), 3737-3741.
- Wong, M. C. S., Goggins, W. B., Yip, B. H. K., Fung, F. D. H., Leung, C., & Fang, Y. (2017). Incidence and mortality of kidney cancer: temporal patterns and global trends in 39 countries. *Scientific Reports*, 7(1), 15698.
- Wu, J. N., & Roberts, C. W. (2013). ARID1A mutations in cancer: another epigenetic tumor suppressor?. *Cancer Discovery*, 3(1), 35-43.
- Wu, R. C., Wang, T. L., & Shih, I. M. (2014). The emerging roles of ARID1A in tumor suppression. *Cancer Biology & Therapy*, 15(6), 655-664.

- Yamamoto, S., Tsuda, H., Takano, M., Tamai, S., & Matsubara, O. (2012). PIK3CA mutations and loss of ARID1A protein expression are early events in the development of cystic ovarian clear cell adenocarcinoma. *Virchows Archiv: European Journal of Pathology*, 460(1), 77-87.
- Yan, H. B., Wang, X. F., Zhang, Q., Tang, Z. Q., Jiang, Y. H., & Fan, H. Z. (2014). Reduced expression of the chromatin remodeling gene ARID1A enhances gastric cancer cell migration and invasion via downregulation of E-cadherin transcription. *Carcinogenesis*, 35(4), 867-876.
- Yang, J., & Weinberg, R. A. (2008). Epithelial-mesenchymal transition: at the crossroads of development and tumor metastasis. *Developmental Cell*, 14(6), 818-829.
- Yang, L., Wei, S., Zhao, R., Wu, Y., Qiu, H., & Xiong, H. (2016). Loss of ARID1A expression predicts poor survival prognosis in gastric cancer: a systematic meta-analysis from 14 studies. *Scientific Reports*, 6, 28919-28919.
- Yang, Y., Wang, X., Yang, J., Duan, J., Wu, Z., & Yang, F. (2019). Loss of ARID1A promotes proliferation, migration and invasion via the Akt signaling pathway in NPC. *Cancer management and research*, 11, 4931-4946.
- Zeisberg, E. M., Tarnavski, O., Zeisberg, M., Dorfman, A. L., McMullen, J. R., & Gustafsson, E. (2007). Endothelial-to-mesenchymal transition contributes to cardiac fibrosis. *Nature Medicine*, 13(8), 952-961.
- Zeisberg, M., & Neilson, E. G. (2009). Biomarkers for epithelial-mesenchymal transitions. *The Journal of Clinical Investigation*, 119(6), 1429-1437.
- Zeisberg, M., Yang, C., Martino, M., Duncan, M. B., Rieder, F., Tanjore, H., & Kalluri, R. (2007). Fibroblasts derive from hepatocytes in liver fibrosis via epithelial to mesenchymal transition. *The Journal of Biological Chemistry*, 282(32), 23337-23347.
- Zhang, G.M., Zhu, Y., & Ye, D.W. (2014). Metabolic syndrome and renal cell carcinoma. *World Journal of Surgical Oncology*, 12, 236-236.
- Zhang, L., Ding, P., Lv, H., Zhang, D., Liu, G., & Yang, Z. (2014). Number of polyploid giant cancer cells and expression of EZH2 are associated with VM formation and tumor grade in human ovarian tumor. *BioMed Research International*, 2014, 9.



- Zhang, L., Wang, C., Yu, S., Jia, C., Yan, J., Lu, Z., & Chen, J. (2018). Loss of ARID1A expression correlates with tumor differentiation and tumor progression stage in pancreatic ductal adenocarcinoma. *Technology in Cancer Research & Treatment*, 17, 1533034618754475.
- Zhang, S., Mercado-Urbe, I., Xing, Z., Sun, B., Kuang, J., & Liu, J. (2014). Generation of cancer stem-like cells through the formation of polyploid giant cancer cells. *Oncogene*, 33(1), 116-128.
- Zhang, X., Sun, Q., Shan, M., Niu, M., Liu, T., & Xia, B. (2013). Promoter hypermethylation of ARID1A gene is responsible for its low mRNA expression in many invasive breast cancers. *PLOS ONE*, 8(1), e53931.
- Zhang, Z. M., Xiao, S., Sun, G. Y., Liu, Y. P., Zhang, F. H., & Yang, H. F. (2014). The clinicopathologic significance of the loss of BAF250a (ARID1A) expression in endometrial carcinoma. *International Journal of Gynecological Cancer*, 24(3), 534-540.
- Zhou, M., & He, H. (2013). Pathology of Renal Cell Carcinoma. In Campbell SC, & Rini BI (Editors), *Renal cell carcinoma: Clinical management, current clinical urology* (pp. 23-41). New York: Springer Science+Business Media.
- Zhu, Q. C., Gao, R. Y., Wu, W., & Qin, H. L. (2013). Epithelial-mesenchymal transition and its role in the pathogenesis of colorectal cancer. *Asian Pacific Journal of Cancer Prevention*, 14(5), 2689-2698.
- Zhu, Y., Horikawa, Y., Yang, H., Wood, C. G., Habuchi, T., & Wu, X. (2008). BPDE-induced lymphocytic chromosome 3p deletions may predict renal cell carcinoma risk. *The Journal of urology*, 179(6), 2416-2421.
- Zhu, Y., Wang, C., Becker, S. A., Hurst, K., Nogueira, L. M., Findlay, V. J., & Camp, E. R. (2018). miR-145 antagonizes SNAI1-mediated stemness and radiation resistance in colorectal cancer. *Molecular Therapy*, 26(3), 744-754.



## Chemicals

1. Trypan blue solution 0.4% (Gibco, USA)
2. 3, 3'-diaminobenzidine (DAB) powder (BIO-RAD, CA)
3. Absolute ethanol ( $C_2H_5OH$ ) (BDH Laboratory Supplies, UK)
4. Bovine serum albumin (BSA) (Sigma, USA)
5. Charcoal activated powder
6. Di-sodium hydrogen phosphate anhydrous ( $Na_2HPO_4$ ) (Merck, Germany)
7. Minimal essential medium (MEM)(Gibco, USA)
8. Ethanol (RCI labscan, Thailand)
9. Ethylenediaminetetraacetic acid disodium salt, dihydrate ( $EDTA.Na_2.2H_2O$ ) (USA)
10. Fetal bovine serum (FBS) (Gibco, USA)
11. Fuchsin basic (Himedia laboratories Pvt. Ltd., India)
12. Glycerol (BDH, USA)
13. Hematoxylin and eosin dye (C.V. Laboratories CO., LTD., Thailand)
14. Hoechst dye (MilliporeSigma)
15. Hydrochloric acid (HCl) (Merck, Germany)
16. L-glutmine (Sigma, USA)
17. Madin-Darby canine kidney (MDCK) (American Type Culture Collection, ATCC, USA)
18. Minimal essential medium (Gibco, USA)
19. OPTI-MEM (Gibco, USA)
20. Paraformaldehyde (Sigma, USA)
21. Penicillin G (Sigma, USA)
22. Periodic acid solution (Himedia laboratories Pvt. Ltd., India)
23. Permout (Fisher Scientific)
24. Potassium chloride (KCl)
25. Potassium dihydrogen phosphate ( $KH_2PO_4$ ) (Merck, Germany)
26. Potassium metabisulphite
27. siRNA Transfection Reagent (Santa Cruz)

28. Sodium chloride (NaCl) (Merck, Germany)
29. Sodium dodecyl sulfate or SDS ( $C_{12}H_{25}O_4SNa$ ) (Sigma, USA)
30. Sodium hydroxide (NaOH) (Merck, Germany)
31. Streptomycin sulfate (Sigma, USA)
32. Triton X-100 (Sigma, USA)
33. Triton-X (BIO-RAD, CA)
34. Trypsin (Gibco, USA)
35. Tween (BIO-RAD, CA)
36. Tween-20 (Sigma, USA)
37. Xylene (RCI labscan, Thailand)

### **Instruments**

1. 2-digits electronic analytical balance (Sartorius ED 822-CW, Sartorius AG, Germany)
2. 4-digits electronic analytical balance (Denver Instrument TP-214, Denver Instrument, NY)
3. Autoclave (TOMY SX-500, Tomy Kogyo Co Ltd, Japan)
4. Biological safety cabinet (Labconco Purifier Logic Class II, Labconco Corp, MO)
5. BioStation CT (Nikon)
6. CO<sub>2</sub> incubator (Forma Steri-Cycle, Thermo Fisher Scientific, OH)
7. Deep freezer (-80°C) (Forma 906, Thermo Fisher Scientific, OH)
8. Fluorescent microscope (Nikon ECLIPSE 80i, Nikon Corp., Japan)
9. Freezer (-20°C) (Sanyo SF-C1497 (GYN), Sanyo Commercial Co Ltd, Thailand)
10. Fume hood (Purair P5-48-XT, Air science USA LLC, Fort Myers, FL)
11. Hemacytometer
12. Hot air oven (Binder FED115, Binder GmbH, Germany)
13. Hot air oven UN55 (Mettler Co. Ltd., Shanghai, China).
14. Inverted light microscope (Olympus CKX41, Olympus Co Ltd, Japan)



15. Magnetic stirrers (Stuart CB162, Bibby scientific Ltd, UK)
16. Microplate reader (Anthos Fluido2, Anthos Labtec Instruments, Austria)
17. Nikon Eclipse 80i fluorescence microscope (Nikon, Tokyo, Japan),
18. Nikon Eclipse Ti inverted microscope (Nikon)
19. Nikon Eclipse Ti inverted phase-contrast microscope (Nikon)
20. NIS-Elements D v.4.11 (Nikon)
21. Olympus BX50 microscope (Olympus; Tokyo, Japan).
22. pH meter (Denver Instrument 215, Denver Instrument, NY)
23. Refrigerated centrifuge (CAX-370 Hybrid Refrigerated Centrifuge, Tomy Kogyo Co Ltd, Japan)
24. Refrigerated centrifuge (Sorvall legend micro 21R, Thermo Scientific, OH)
25. Tarosoft Image framework v.0.9.6 (Nikon)
26. Ultracentrifuge (Sorvall WX80 Ultracentrifuge, Thermo Fisher Scientific, NC)
27. Ultrapure water purification system (Milli-Q plus, Millipore Corp, MA)
28. Vortex mixer (Scientific Industries, NY)

## Reagents

### Reagents for cell culture

#### 1. Minimal essential medium (MEM)

- |                        |       |      |
|------------------------|-------|------|
| 1.1 MEM powder         | 1     | pack |
| 1.2 Sodium bicarbonate | 2.2   | g    |
| 1.3 Add DW to          | 1,000 | ml   |

\* sterilized by filtration through 0.2  $\mu$ m cellulose acetate membrane filter and kept at 4°C.

#### 2. Heat-inactivated fetal bovine serum (FBS)

FBS was inactivated by incubation at 56°C for 30 min and kept at 4°C.

#### 3. 200 mM L-glutamine

- |                 |      |    |
|-----------------|------|----|
| 3.1 L-glutamine | 1.46 | g  |
| 3.2 Add DW to   | 50   | ml |

\* sterilized by filtration through 0.2  $\mu\text{m}$  cellulose acetate membrane filter and kept at 4°C.

#### 4. Penicillin G/Streptomycin solution

4.1 Penicillin G	310.81	g
4.2 Streptomycin sulfate	500.00	mg

\* dissolved in normal salt saline solution to a final volume of 50 ml

\* sterilized by filtration through 0.2  $\mu\text{m}$  cellulose acetate membrane filter and kept at 4°C.

#### 5. Phosphate buffer saline (PBS) (pH 7.4)

(342.5 mM NaCl, 6.75 mM KCl, 25 mM  $\text{Na}_2\text{HPO}_4$ , and 5 mM  $\text{KH}_2\text{PO}_4$ )

5.1 NaCl	8.00	g
5.2 KCl	0.20	g
5.3 $\text{Na}_2\text{HPO}_4$	1.44	g
5.4 $\text{KH}_2\text{PO}_4$	0.20	g
5.5 DW	1,000	ml

\* mixed on a magnetic stirrer until completely dissolved

\* sterilized by autoclave at 121°C for 15 min and kept at room temperature

#### 6. Complete growth medium

(MEM supplemented with 10% heat-inactivated FBS, 1.2% Penicillin G/Streptomycin, and 2 mM L-glutamine)

6.1 Heat-inactivated FBS	10.0	ml
6.2 200 mM L-glutamine	1.0	ml
6.3 Penicillin G/Streptomycin solution	1.2	ml

\* mixed with MEM and make a final volume of 100 ml under sterile condition

\* kept at 4°C under sterile condition.

#### 7. 2.5 mM EDTA/PBS solution

7.1 EDTA	0.4653	g
7.2 dissolved in PBS to a final volume of 500 ml		

\* sterilized by autoclave at 121°C for 15 min and kept at room temperature.

#### 8. Trypsin solution (10% trypsin in 2.5 mM EDTA/PBS solution)

8.1 Trypsin	2	g
8.2 dissolved in 2.5 mM EDTA/PBS solution to a final volume of 20 ml		

\* sterilized by filtration through 0.2  $\mu\text{m}$  cellulose acetate membrane filter and kept at 4°C.

## 9. Working trypsin solution (0.1% trypsin in 2.5 mM EDTA/PBS solution)

9.1 dilute trypsin solution in 2.5 mM EDTA/PBS solution to make a final concentration of 0.1% trypsin under sterile condition.

9.2 Working trypsin solution was kept at 4°C.

## Reagents for immunofluorescence staining

### 10. Membrane preserving buffer

(PBS containing 1 mM  $\text{MgCl}_2$  and 0.1 mM  $\text{CaCl}_2$ )

10.1 1 M  $\text{MgCl}_2$  100  $\mu\text{l}$

10.2 1 M  $\text{CaCl}_2$  10  $\mu\text{l}$

\* mixed with PBS and make a final volume of 100 ml.

### 11. 3.7% Paraformaldehyde

11.1 paraformaldehyde powder 3.7 g

11.2 Add PBS to 80 ml

\* heating at 60°C and then add 1 N NaOH until clear solution was obtained

\* wait until temperature is equally to the room temperature

\* Adjust pH to 6.9 using diluted HCl and add PBS to make a final volume of 100 ml

### 12. 0.1% Triton X-100

12.1 Triton X-100 1 ml

12.2 PBS to a final volume of 100 ml.

## Reagents for immunohistochemistry

### 13. 0.1 M phosphate buffer, pH 7.4

13.1 DW 800 ml

13.2  $\text{Na}_2\text{HPO}_4$  12.25 g

13.3  $\text{NaH}_2\text{PO}_4$  3.68 g

13.4 Adjust pH to 7.4 with HCl

13.5 Add DW to 1,000 ml

\* mixed on a magnetic stirrer until completely dissolved

**14. 10X PBS (Phosphate buffered saline) pH 7.4: stock solution**

14.1 DW	800	ml
14.2 NaCl	80	g
14.3 Na <sub>2</sub> HPO <sub>4</sub> . (2H <sub>2</sub> O)	14.4	g
14.4 KH <sub>2</sub> PO <sub>4</sub>	2	g
14.5 Adjust pH to	7.4 with HCl	
14.6 Add DW to	1,000	ml

\* kept at 4°C

**15. 1X (Phosphate buffered saline) pH 7.4: working solution**

15.1 10X PBS	100	ml
15.2 DW	900	ml

**16. 0.3% Triton-X in PBS**

16.1 Triton-X	30	ml
16.2 PBS	1,000	ml

**17. 0.3% H<sub>2</sub>O<sub>2</sub> in methanol**

17.1 H <sub>2</sub> O <sub>2</sub>	30	ml
17.2 Methanol	1,000	ml

**18. DAB (working solution)**

18.1 Tris-HCL	10	ul
18.2 H <sub>2</sub> O <sub>2</sub>	10	ul
18.3 DAB	1-2	ug

**19. 50 mM Tris-HCL (working solution)**

19.1 NH <sub>2</sub> (CH <sub>2</sub> OH) <sub>3</sub> · HCL	6.057	g
19.2 DW	1,000	ml

**20. Tris-buffer saline (TBS)**

20.1 Tris-HCL	12.11	g
20.2 DW	900	ml
* adjust pH 7.5		
20.3 NaCl	9	g

\* dilute to 1 L with DW



**21. Tris-buffer saline-Tween (TBS-T)**

21.1 TBS	1,000 ml
21.2 0.1%Tween-20	0.01 ml

**22. Tris-EDTA buffer**

(10mM Tris Base, 1mM EDTA Solution, 0.05% Tween 20, pH = 8.0)

22.1 Tris Base	1.21 g
22.2 EDTA	0.37 g
22.3 DW	1,000 ml

\*Adjust the pH to 9.0 with 1N sodium hydroxide

\*and then add 0.5 ml of Tween 20

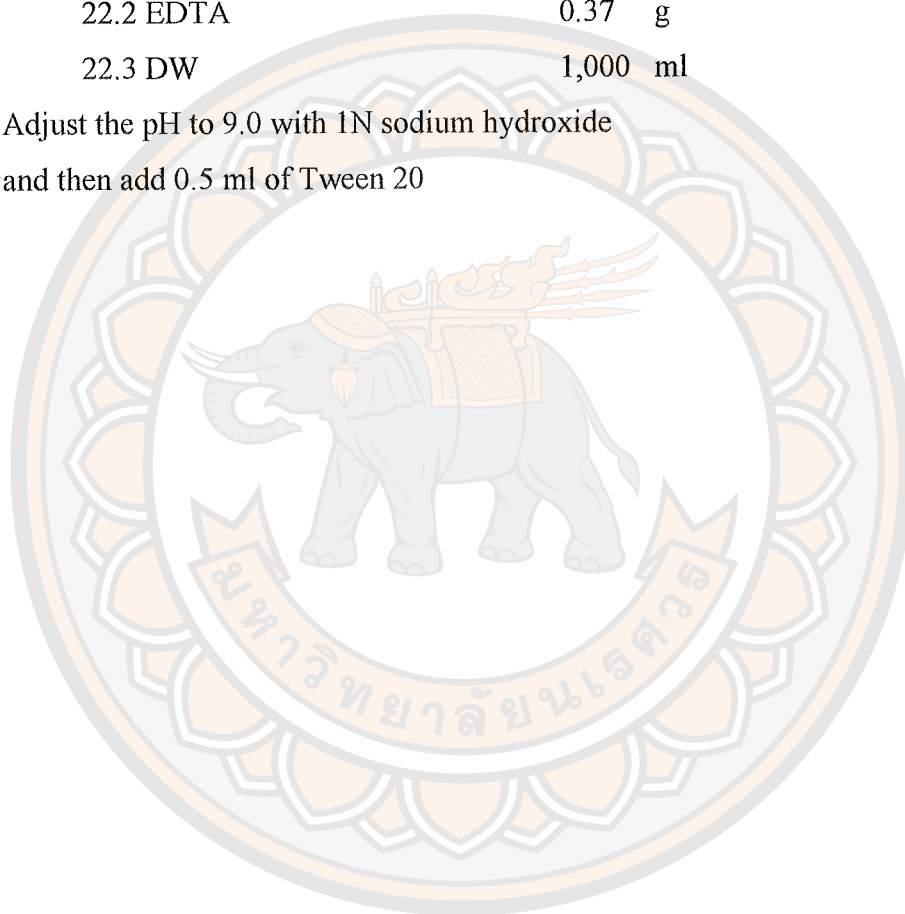


Table A1 Clinical and pathological data of all patients

Pt No.	ARID1A expression	Age	Gender	Laterality	Pathological grade	T stage	cm.	Description	N stage	M stage	AJCC stage	Metastatic recurrence (months after surgery)	Comorbidity
001	Positive	59	Male	Right	ccRCC (G1)	T3	11	Tumor invades the perinephric fat.	NO	MO	3	no	
002	Negative	76	Male	Right	ccRCC (G1)	T3a	10	Tumor invades the perinephric fat.	NO	MO	3	no	no
003	Positive	53	Male	Right	ccRCC (G1)	T1	3	Tumor is confined within the renal capsule.	NO	MO	1	no	Mild fatty liver/gall stone/acute cholecystitis
004	Positive	91	Male	Right	ccRCC (G1)	T1	4.3	Tumor is confined within the renal capsule.	NO	MO	1	no	no
005	Negative	50	Male	Right	ccRCC (G1)	T1	5.8	Tumor is confined within the renal capsule.	NO	MO	1	no	no
006	Positive	56	Female	Left	ccRCC (G1)	T1b	5	Fibrous adhesion and congested perinephric fat	NO	MO	1	no	HT
007	Negative	69	Female	Right	ccRCC (G2)	T1b	5.2	Tumor is confined within the renal capsule.	NO	MO	1	no	no
008	Negative	64	Male	Right	ccRCC (G2)	T2a	8.5	Tumor is confined within the renal capsule.	NO	MO	2	no	HT, hyperlipidemia, cystic kidney disease
009	Positive	56	Female	Left	ccRCC (G2)	T3a	UN	Tumor extends to perinephric fat and no definite renal vein invasion seen	NO	MO	3	no	no
010	Positive	61	Male	Left	ccRCC (G2)	T4	6.3	Tumor extends thought the renal capsule with renal vein invasion c hemorrhage adrenal gland	NO	MO	4	no	no

Table A1 (cont.)

Pt No.	ARID1A expression	Age	Gender	Laterality	Pathological grade	T stage	cm.	Description	N stage	M stage	AJCC stage	Metastatic recurrence (months after surgery)	Comorbidity
011	Negative	51	Male	Left	ccRCC (G2)	T3	6.3	The tumor extends through the renal capsule into perinephric fat.	NO	MO	4	no	Gall stone/Arteriosclerosis of aorta
012	Negative	65	Male	Right	ccRCC (G2)	T3b	7	The tumor extends through the renal capsule into perinephric fat. Tumor invades grossly into the renal vein and, invades to vascular lumen	NO	M1	3	no	no
013	Negative	64	Male	Left	ccRCC (G2)	T3c	8	The tumor invades into perinephric fat. Ureteral and renal vein margins are positive for tumor. Present of renal vein invasion. IVC consists of seven irregular pieces of dark brown soft and rubbery tissue.	NO	MO	3	no	DM type2, hyperkalemia, HT, disorder of lipoprotein
014	Negative	67	Male	Right	ccRCC (G2)	T3	8	Tumor against to the renal capsule. Mass protrude to renal pelvis.	NO	MO	3	Metastasis (1 month)/Dead	Hyperkalemia, phuenomia, adrenal insufficiency
015	Negative	52	Male	Left	ccRCC (G2)	T3	11.5	The renal pelvis and calyces are invading by a mass.	N1	MO	2	Brain and bone metastasis (8 months)	HT, CKD at LK, stone at RK, RCC at RK, hemorrhage brain
016	Negative	65	Male	Right	ccRCC (G2)	T1b	5	Tumor is confined within the renal capsule.	NO	MO	1	Brain metastasis (24 months)	DM type II, HT, liver cirrhosis

Table A1 (cont.)

Pt No.	ARD1A expression	Age	Gender	Laterality	Pathological grade	T stage	cm.	Description	N stage	M stage	AJCC stage	Metastatic recurrence (months after surgery)	Comorbidity
017	Negative	56	Female	Left	ccRCC (G2)	T2	10	Tumor is confined within the renal capsule.	NO	MO	2	no	HT, ischemic heart disease, inflammatory liver disease, mild fatty liver without mass lesion
018	Negative	75	Male	Right	chRCC	T1b	5.7	Tumor is confined within the renal capsule.	NO	MO	1	no	DM, HT, Hepatitis B virus, fatty liver
019	Negative	65	Male	Right	chRCC	T4	13	Tumor invades the renal capsule and shows nodular renal cortex.	NO	MO	4	no	no
020	Negative	65	Male	Right	chRCC	T3a	9	Present renal vein invasion	NO	MO	3	Liver metastasis and retroperitoneal recurrence (50 months)	HT, hematuria
021	Negative	53	Female	Right	chRCC	T2a	9	Tumor is defined within the renal capsule.	NO	MO	2	no	no
022	Negative	49	Male	Right	chRCC	T3a	12.5	The mass pushes the renal capsule. Tumor invades renal vein.	N1	MO	3	Liver metastasis (27 months)	DM type 2, HT
023	Negative	49	Male	Left	chRCC	T3a	4	Present renal vein invasion	NO	MO	4	no	Hematuria
024	Positive	53	Male	Right	pRCC	T4	UN	Tumor extends into perinephric tissue with gerota's fascia	N1	M1	4	no	Disorder of fluid electrolyte balance
025	Positive	64	Male	Right	pRCC	T3a	4	Tumor extends to perinephric fat. Soft tissue margin positive for tumor.	NO	MO	3	no	no
026	Positive	58	Male	Left	sRCC	T3a	10	Tumor invades renal vein, renal pelvis, renal capsule and perinephric fat.	N1	MO	3	no	no

**Note:** Abbreviation: Pt no., patient number; UN, unknown; T, tumor; N, lymphnode; M, metastasis; HT, hypertension; DM, diabetes mellitus; CKD; chronic kidney disease; LK, left kidney; RK, right kidney



<b>งานวิจัยและวารสาร</b>	
เลขที่รับ	196
วันที่	14 มิ.ย. 60
เวลา	4.1.10

<b>กลุ่มงานพัฒนาทรัพยากรบุคคล</b>	
งานวิจัยและสื่อแบบบุคลากร	
เลขที่รับ	03155
รับวันที่	14 มิ.ย. 2550
เวลา	10.15

<b>โรงพยาบาลสุราษฎร์ธานี</b>	
คำถึงที่	15414
วันที่	14 มิ.ย. 2550
เวลา	9.31



ที่ ศธ ๐๕๒๗.๑๖/๐๕๒๖

คณะวิทยาศาสตร์การแพทย์  
มหาวิทยาลัยนเรศวร  
อำเภอเมืองพิษณุโลก  
จังหวัดพิษณุโลก ๖๕๐๐๐

๕ พฤศจิกายน ๒๕๕๐

เรื่อง ขอความร่วมมือการทำวิจัยและเก็บตัวอย่างชิ้นเนื้อผู้ป่วยมะเร็งเซลล์ไต  
เรียน ผู้อำนวยการโรงพยาบาลสุราษฎร์ธานี

<b>กลุ่มงานพัฒนาระบบบริหารงาน</b>	
เลขที่	๒๕๕
วันที่	17 มิ.ย. 2550
เวลา	๑๕.๐๐

ตามที่ผู้ช่วยศาสตราจารย์ ดร.ณัฐธิดา สดกุลศักดิ์ ตำแหน่งอาจารย์ สังกัดภาควิชากายวิภาคศาสตร์ คณะวิทยาศาสตร์การแพทย์ มหาวิทยาลัยนเรศวร ได้จัดทำโครงการวิจัย เรื่อง (ภาษาไทย) แบบแผนการแสดงออกของ ARID1A ที่ใช้เป็นตัวบ่งชี้ทางชีวภาพใหม่ในการวินิจฉัยโรคมะเร็งไตในระยะต่างๆ (ภาษาอังกฤษ) The ARID1A expression patterns as a new biomarker for renal cell carcinoma diagnosis in various stages โดยในงานวิจัยโครงการดังกล่าวได้รับความร่วมมือจาก แพทย์หญิงเจริญรัตน์ สามีต สังกัดกลุ่มงานพยาธิวิทยาภาควิชาพยาธิวิทยา โรงพยาบาลสุราษฎร์ธานี

ในการนี้ คณะวิทยาศาสตร์การแพทย์ มหาวิทยาลัยนเรศวร จึงใคร่ขอความอนุเคราะห์บุคลากรในสังกัดของท่าน คือ แพทย์หญิงเจริญรัตน์ สามีต เข้าร่วมเป็นผู้วิจัยร่วมในโครงการดังกล่าว และขอความอนุเคราะห์ในการเก็บชิ้นเนื้อทางพยาธิที่ทำการตรวจวินิจฉัยเสร็จสิ้นแล้ว โดยทางคณะผู้วิจัยขอรับรองว่าข้อมูลของผู้ป่วยทั้งหมดถือเป็นความลับจะได้รับการปกปิดเป็นอย่างดีตามประกาศสิทธิผู้ป่วย และหวังเป็นอย่างยิ่งว่าการทำวิจัยในครั้งนี้จะมีส่วนสนับสนุนให้เกิดความร่วมมือทางด้านการวิจัยในอนาคตต่อไป

จึงเรียนมาเพื่อโปรดพิจารณา

เรียน ผอ.รพ.สุราษฎร์ธานี

- ร.น.นพ.วิมล วัฒนวิทย์ และคณะ ขอแสดงความนับถือ

- ร.น.นพ.วิมล วัฒนวิทย์ และคณะ

- ร.น.นพ.วิมล วัฒนวิทย์ และคณะ

- ร.น.นพ.วิมล วัฒนวิทย์ และคณะ

(รองศาสตราจารย์ ดร.เลมอ ถาน้อย)

คณบดีคณะวิทยาศาสตร์การแพทย์

คณบดี

สำนักงานเลขานุการคณะวิทยาศาสตร์การแพทย์

โทร. ๐ ๕๕๔๖ ๔๖๔๕, ๐ ๕๕๔๖ ๔๗๐๕

โทรสาร ๐ ๕๕๔๖ ๔๗๗๐

- งานการประชาสัมพันธ์ การวิจัย แล้ว

- ร.น.นพ.วิมล วัฒนวิทย์

- ร.น.นพ.วิมล วัฒนวิทย์ และคณะ

(แพทย์หญิงณัฐธิดา พัฒนศักดิ์กัญญา)

รองผู้อำนวยการศูนย์วิจัยและพัฒนาแบบแผนการ  
และสนับสนุนการวิจัย การปฏิบัติโครงการงาน  
ศูนย์วิจัยและพัฒนาแบบแผนการวิจัย จังหวัดนเรศวร

๑ ๕ มิ.ย. ๖๐

ที่ ศธ ๐๕๒๗.๑๖/๐๕๑๗



คณะวิทยาศาสตร์การแพทย์  
มหาวิทยาลัยอัสสัมชัญ  
ย่านเมืองพิษณุโลก  
จังหวัดพิษณุโลก ๖๕๐๐๐

๗ พฤศจิกายน ๒๕๖๐

เรื่อง ขอความร่วมมือการให้วิจัยและเก็บตัวอย่างชิ้นเนื้อผู้ป่วยผู้ป่วยมะเร็งเซลล์ไต  
เรื้อรัง หัวหน้ากลุ่มงานพยาธิวิทยาภาค โรงพยาบาลสวรรค์ประชารักษ์

ตามที่ผู้ช่วยศาสตราจารย์ ดร.ณัฐริยา สกุศลศักดิ์ ตำแหน่งอาจารย์ สังกัดภาควิชากายวิภาคศาสตร์ คณะวิทยาศาสตร์การแพทย์ ได้จัดทำโครงการวิจัย เรื่อง (ภาษาไทย) แบบแผนการแสดงออกของ ARID1A ที่ใช้เป็นตัวบ่งชี้ทางชีวภาพใหม่ในการวินิจฉัยโรคมะเร็งไตในระยะต่างๆ (ภาษาอังกฤษ) The ARID1A expression patterns as a new biomarker for renal cell carcinoma diagnosis in various stages โดยในงานวิจัยโครงการดังกล่าวได้รับความร่วมมือจาก แพทย์หญิงศิริรัตน์ สามล หัวหน้ากลุ่มงานพยาธิวิทยาภาค โรงพยาบาลสวรรค์ประชารักษ์

ในการนี้ คณะวิทยาศาสตร์การแพทย์ มหาวิทยาลัยอัสสัมชัญ จึงใคร่ขอความอนุเคราะห์บุคลากรในสังกัดของท่าน คือ แพทย์หญิงศิริรัตน์ สามล เข้าร่วมเป็นผู้วิจัยร่วมในโครงการดังกล่าว และขอความอนุเคราะห์ในการเก็บชิ้นเนื้อทางพยาธิวิทยาการตรวจวินิจฉัยเสร็จสิ้นแล้ว โดยทางคณะผู้วิจัยขอรับรองว่าข้อมูลของผู้ป่วยทั้งหมดถือเป็นความลับจะได้รับการปกปิดเป็นอย่างดีตามประกาศสิทธิผู้ป่วย และหวังเป็นอย่างยิ่งว่าการพิจารณาในครั้งนี้จะช่วยให้เกิดความร่วมมือทางด้านการวิจัยในโอกาสต่อไป

จึงเรียนมาเพื่อโปรดพิจารณา

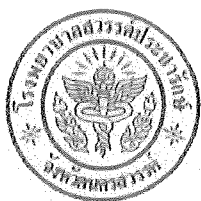
ขอแสดงความนับถือ

(รองศาสตราจารย์ ดร.เดเมอ ดาณ้อย)  
คณบดีคณะวิทยาศาสตร์การแพทย์

สำนักงานเลขานุการคณะวิทยาศาสตร์การแพทย์

โทร. ๐ ๕๕๔๖ ๔๖๔๕, ๐ ๕๕๔๖ ๔๗๐๕

โทรสาร ๐ ๕๕๔๖ ๔๗๗๐



งานวิจัยและวารสาร โรงพยาบาลสุราษฎร์ธานี  
 ๕๑ ถนนบรรณวิถี ตำบลปากน้ำโพ อำเภอเมือง จังหวัดนครศรีธรรมราช  
 โทรศัพท์ ๐๕๖-๒๑๑๙๙๙ ต่อ ๒๖๐๔

แบบรายงานผลการพิจารณาจริยธรรมการวิจัยในคน  
 โรงพยาบาลสุราษฎร์ธานี

เลขที่ ๔๗/ ๒๕๖๐

ชื่อโครงการวิจัย : แบบแผนการแสดงออกของ ARID1A ที่ใช้เป็นตัวบ่งชี้ทางชีวภาพใหม่ในการวินิจฉัยโรคมะเร็งไตในระยะต่างๆ

ภาษาอังกฤษ : The ARID1A expression patterns as a new biomarker for renal cell carcinoma diagnosis in various stages

ชื่อหัวหน้าโครงการ : ศศ.ดร.ณัฐธิดา สุกอศักดิ์

ผู้วิจัยร่วม : แพทย์หญิงณัฐรัตน์ สามล

นางสาวกীরดีการ สมส่วน

หน่วยงานที่สังกัด : มหาวิทยาลัยนเรศวร

ผลการพิจารณาของคณะกรรมการจริยธรรมการวิจัยในคน โรงพยาบาลสุราษฎร์ธานี คณะกรรมการฯ ได้พิจารณารายละเอียดโครงการวิจัยเรื่องดังกล่าวข้างต้นแล้วในประเด็นเกี่ยวกับ

- ๑) การเคารพในศักดิ์ศรี และสิทธิของมนุษย์ที่ใช้เป็นตัวอย่างการวิจัย
- ๒) วิธีการที่เหมาะสมในการได้รับความยินยอมจากกลุ่มตัวอย่างก่อนเข้าร่วมโครงการวิจัย รวมทั้งการปกป้องสิทธิประโยชน์และรักษาความลับของกลุ่มตัวอย่าง
- ๓) การดำเนินการวิจัยอย่างเหมาะสม เพื่อไม่ให้เกิดความเสียหายต่อสิ่งมีชีวิตการวิจัย

คณะกรรมการจริยธรรมการวิจัยในคนเห็นชอบ รับรองโครงการวิจัย

วันที่ ที่ให้การรับรอง ๒๕ ธันวาคม ๒๕๖๐

(แพทย์หญิงณัฐธิดา พัฒนศักดิ์กัญญา)

ประธานคณะกรรมการจริยธรรมการวิจัยในคน